DRAG COEFFICIENTS OF SPHERES IN TURBULENT, NON-STEADY FLOW.

A thesis presented for the
degree of Doctor of Philosophy in Mechanical Engineering
in the University of Canterbury,
Christchurch, New Zealand.

by

D.J. PAINTER.

1969

ACKNOWLEDGEMENTS.

Dr A.J. Sutherland of the Civil Engineering Department supervised this project in all but its early stages. His interest in all aspects, especially his scrupulous examination and criticism of the thesis in preparation, have been invaluable.

The project began under the supervision of Professor F.M. Henderson (now of Newcastle University, Australia) and E.P. Giddens, Civil Engineering Department; their encouragement and advice are gratefully remembered, especially as the latter has retained his interest throughout the project.

Many members of the academic and technical staff of Mechanical, Civil, Chemical and Electrical Engineering and other University departments, the Computer Centre and the Engineering and Science departmental libraries, have provided help and advice; especially H.J. Anink, G.F. Archer, P.C. Dawson, E. Retallick and R.I. Stewart. Equipment has been made available by all the engineering departments.

Consecutive scholarships from the New Zealand University Grants Committee and the New Zealand Agricultural Engineering Institute provided the writer with financial support.

My fellow post-graduate students and Mrs N. Newman

of the Mechanical Engineering Department have contributed in many indirect ways during the course of this project.

My wife has displayed great care, perseverance and ingenuity in typing almost the entire thesis under trying circumstances; some of the experimental work and all of the tedious reduction of photographic measurements were shared by her. Her encouragement at all times, and sacrifice at some, has far exceeded wifely duty.

ABSTRACT.

A re-derivation of the equation of non-steady motion of a sphere in viscous, incompressible fluid at very low Reynolds numbers is presented. The emphasis is on completeness to show clearly the limitations of the mathematical description. With this analytical treatment as basis, the non-steady, higher Reynolds number motion of a sphere in turbulent ambient flow is examined using dimensional and physical arguments. The parameters suggested as important in determining the drag coefficients are : particle Reynolds number; acceleration number; turbulence intensity and scale relative to particle slip speed and diameter, respectively; and particle-fluid density ratio.

The development of a new method of measuring drag coefficients is described. A diffuser is used to provide an inertial field in which particles slip with respect to an ambient, turbulent flow of water. The experimental results show that drag coefficients, for the parameter ranges investigated, depend at least upon particle Reynolds number, acceleration number and turbulence intensity. The ranges on turbulence scale and density ratio were insufficient to establish the variation in drag coefficient, if any, caused by these parameters, although the method is capable of determining this.

Some previous methods of solids-in-gas drag coefficients made by a quite different method (Torobin and Gauvin (1961c)) are compared with the present results. They are shown to depend on the same parameters as in this study, and in a similar manner.

These results suggest that the discrepancies between results of previous workers could have been caused by different averaging processes and by neglect of important parameters. Some parameters have a small effect for certain ranges on the other parameters, but a large effect for different ranges.

CONTENTS.

LIST OF FIGURES.

LIST OF COMMONLY OCCURRING SYMBOLS.

(Some of these are temporarily defined to have other meanings in certain sections; all symbols are defined where they first occur).

a	sphere radius
Ac	dimensionless acceleration number $\frac{a\frac{dv_p}{dt}}{v_p^2}$ or $\frac{a\left[\frac{dv_p}{dt}-\frac{dv}{dt}\right]}{(v_p-v)^2}$
b(r)	function describing initial conditions, (2-46)
c	expoment in (4-9)
C_D	steady drag coefficient
C_{DA}	non-steady drag coefficient
d	particle diameter
D	drag force
D_c	steady drag force
e	anemometer bridge voltage, see 5.4
E(n)	1-dimensional energy spectrum function, see 4.6
f	spatial correlation coefficient (longitudinal), see 4.6
f(s)	Laplace transform of $v_r(t)$
f(r,t)	function defined by (2-18)
F_i	functions related to C_{DA}, see (3-4,5,8,9)
g	gravitational acceleration
h(s)	Laplace transform of v(t)

$h(r,t)$ solution to the 1-dimensional heat flow equation defined by (2-35)

H operator, $\frac{d^2}{dr^2} - \frac{2}{r^2}$

Hi dimensionless "history" number, see 3.2

H_m jet pump driving static pressure (p.s.i.g.)

I fluid turbulence intensity, $\frac{\sqrt{\overline{v'^2}}}{v}$

Ir particle relative turbulence intensity, $\frac{\sqrt{\overline{v'^2}}}{v_p - v}$

L Laplace transform symbol

L turbulence scale (general)

L_d diffuser direct length

L_e Eulerian integral scale of turbulence (longitudinal), (4-17)

m fluid dynamic viscosity

n fluid kinematic viscosity, $\frac{m}{\rho}$

n frequency, cycles per second (Hz)

p fluid pressure

Q_d circuit discharge flow rate ($ft^3 sec^{-1}$)

r radial coordinate direction (spherical coordinates)

Re_c "critical" Reynolds number, see 3.31

Re_d discharge Reynolds number, $\frac{Q_d}{2y_i n}$

Re_p particle Reynolds number, $\frac{2a|v_p|}{n}$ or $\frac{2a|v_p - v|}{n}$

Re_{pt}	Re_p corresponding to terminal speed of a particle in still fluid
s	Laplace variable in transforms
s	relative density, $\frac{\rho_s}{\rho}$
t	time
Ti	dimensionless time parameter, see 3.2
u,v,w	fluid velocity components in x,y,z directions
u_r, u_θ, u_ϕ	fluid velocity components in r,θ,ϕ directions
$\underline{u}$	absolute fluid velocity vector
v	fluid mean speed (Chapter 3 onwards)
v_m	local central axis value of fluid mean speed in the flow circuit
v_{max}	v_m at entrance to the diffuser ($\frac{x}{L_d} = 0$)
v_p	particle mean speed
v_r	sphere relative speed (Chapter 2)
v_s	particle settling speed in still fluid
$\overline{v'^2}(n)$	turbulence fluctuation energy per unit mass of fluid recorded via a band-pass filter, central frequency n
$\overline{v'^2}$	total $\overline{v'^2}(n)$ from all frequencies
x,y,z	coordinate directions
x	downstream distance from the diffuser entrance
y	horizontal distance from the flow section central axis perpendicular to the flow

z vertical distance from the flow section central axis (perpendicular to the flow)

y_i diffuser inlet half-width (equals the half-height)

y_m, z_m half-width and half-height of the flow section at given downstream position $\frac{x}{L_d}$

X, Y, Z (coordinate directions, Chapter 2), grid positions, see Figure 5-16

X scalar force potential (Chapter 2)

∇^2 Laplacian operator, $\frac{d^2}{dx^2} + \frac{d^2}{dy^2} + \frac{d^2}{dz^2}$

$\underline{\nabla}\cdot$ divergence

$\underline{\nabla}\times$ curl

Λ turbulence microscale (longitudinal), (4-20)

θ, ϕ (spherical) coordinate directions (Chapter 2)

2θ diffuser included angle

ρ fluid density

ρ_s particle density

Ψ stream function

$\dot{A}$ is sometimes used to mean $\frac{dA}{dt}$, where A may be replaced by v_p, v etc.

$\overline{A}$ is used to mean $\frac{1}{T}\int_{t-\frac{T}{2}}^{t+\frac{T}{2}} A(t)\,dt$, where T is a period long compared to the times of turbulent fluctuations. The convention $v = \overline{v} + v'$ is used only where confusion would otherwise be caused

"If I were asked to name the areas in fluid mechanics which are most frustrating from an all-round point of view, that is, taking account of the conceptual, experimental and analytical difficulties, I should put high on the list first the general problem of turbulence, and second the Lagrangian aspects of fluid flow. Both these areas are involved in the motion of small particles in turbulent flow and consequently this is not a popular subject for research. Only a few results, either experimental or theoretical, of a fundamental nature are available, and the treatment of the relevant practical problems, such as sediment transport, is largely empirical. Such a subject does not allow a survey in which theory is built up brick-by-brick into a well-rounded edifice. But for those who regard a subject in a messy and undeveloped state, especially one which has been that way for more than half a century, as a challenge and a stimulus, consideration of the motion of particles in turbulent flow has its own pleasures."

Professor G.K. Batchelor (1966).

CHAPTER ONE.

1. INTRODUCTION.

1.1 Historical review.

At the end of the nineteenth century the subject of a sphere in slow, non-steady motion in a viscous, incompressible fluid was regarded as an interesting, unsolved problem in hydrodynamics. Papers appearing in the literature as recently as the mid-nineteen-sixties show that confusion about the first derivation and integration of the integro-differential equation concerned still persist. Many English-speaking authors attribute both firsts to London barrister and hydrodynamicist, A.B. Basset. Other authors refer to the equation of motion (2-64) as the Basset-Boussinesq-Oseen equation, thus acknowledging French and German interests. Careful perusal of several of the early papers suggest that the sequence of events was as outlined below.

Study of the problem had been stimulated by work such as that of Navier (1823) and Stokes (1845,1851), Stokes having obtained the well-known formula for the resistance to a sphere in steady motion, and that for a sphere in oscillating (pendulum) motion. Boussinesq (1885 a,b) derived the resistance terms in the equation of motion for a sphere in slow, non-steady motion. That this is the

difficult part, is shown in Chapter 2. Basset (1888) also derived the resistance terms and completed the equation of motion, apparently unaware of Boussinesq's contribution. Picciati (1907a,b,c,d) improved Basset's derivation, making it unnecessary to "first solve the problem when the velocity is constant and then derive therefrom the solution when the velocity is variable" (Basset), and Boggio (1907) succeeded in integrating the equation directly. Basset (1910) modified his previous work according to these Italian results but was unhappy with the integrated solution, thinking that it predicted oscillatory motion for some density ratios and not others. This misunderstanding persisted until satisfactorily explained by Hjelmfelt and Mockros (1967). Rayleigh (1911) showed how the integro-differential equation could be derived very simply from Stokes' result for oscillating motion. Oseen (1927) attributes the derivation of the resistance to Boussinesq, as does Villat (1943).

It appears, then, that the integro-differential equation of motion should most fairly bear the names of both Boussinesq and Basset and that credit for its integration be given to Boggio.

The mathematical problems encountered when the motion of the sphere was not "slow", prevented any extension of the analytical treatment to higher particle Reynolds numbers.

Rayleigh (1892, 1899, 1904, 1909) suggested the use of this dimensionless grouping, Re_p, since universally used, to correlate experimental results for steady drag.

During the last twenty years, interest in the non-steady drag problem has revived as practical situations which involve it come under study. Meteorology, oceanography, sediment transport, hydraulic and pneumatic conveying are fields in which further knowledge of the dependence of drag upon acceleration, turbulence, previous history of the motion and density ratio as well as the more usual parameters of roughness, shape and Reynolds number, would be of great benefit.

Rather little has been added to theoretical knowledge of the problem although numerical solution of the Navier-Stokes equations using large-memory computers is providing new insights. Worthwhile contributions to the subject were made when Tchen (1947) and Lumley (1947) published theses. Tchen showed that the equation of motion could be extended to the case of a sphere in relative motion in a moving fluid (see 2.71). Liu (1956) used the equation to examine dispersion of particles in a stationary field of isotropic turbulence. Brush, Hau-wong Ho and Ben-chie Yen (1964) integrated the Boussinesq-Basset equation using Laplace transforms (a more direct method than the Boggio-Basset integration, see 2.6) and they and Hjelmfelt and

Mockros (1967) presented the integrated solution in more readily usable forms. Hjelmfelt and Mockros (1966) also examined the validity of certain oft-employed simplifications of the equation of motion. Hinze (1959) and Soo (1967) are two of only a few text-book authors who consider the problem.

Recent experimental work up to the present (1969) is examined in Chapter 3, where the emphasis is on higher particle Reynolds number situations. It is sufficient to state here that only in the last ten years have workers begun to measure all the parameters influencing the non-steady drag on a sphere in relative motion in a turbulent fluid. A comprehensive review has been given by Torobin and Gauvin (1959 a,b,c; 1960 a,b; 1961 a).

1.2 Purpose and scope of this thesis.

The main purposes of this thesis are:

1. To make available a clear derivation of the equation for non-steady motion of a sphere in a viscous incompressible fluid at low particle Reynolds numbers, in such a way that the physical meaning and limitations of the derivation are shown (Chapter 2).

2. To review what is known of the dependence of drag upon particle and flow parameters when particle Reynolds numbers greatly exceed unity and the fluid is in turbulent flow, and to examine the physical situation to ascertain

the relative importance of the various parameters (Chapter 3).

3. To present a new method of determining turbulent, non-steady drag coefficients for spheres which is both experimentally straightforward and has a clear similarity to flow situations in sediment transport and hydraulic or pneumatic conveying, two fields of particular interest to engineers.(Chapters 4 and 5).

4. To demonstrate the feasibility of this method by making trial measurements of drag coefficients, and comparing them with other results (Chapters 6 and 7).

5. To use the trial measurements, and the results of other workers, to make preliminary predictions about the dependence of drag coefficients upon their parameters, in the ranges of the experimental variables covered.(Chapters 6 and 7).

The scope of this thesis is suggested by the purposes. The low Reynolds number case is treated as a preliminary to elucidate the higher Reynolds number case. Particle shapes other than spherical are rarely mentioned herein, except where work on cylinders is relevant, and inter-particle or particle-boundary interactions are not considered.

CHAPTER TWO.

2. THEORY OF PARTICLE MOTION; LOW REYNOLDS NUMBERS.

2.1 Synopsis.

Only at particle Reynolds numbers small compared to unity is it at present possible to solve the Navier-Stokes equations for the drag on a spherical particle in non-steady, rectilinear motion through a viscous, incompressible fluid. Such Reynolds numbers ensure that viscous forces predominate and allow convective terms in the equations to be neglected. Although it is not necessary for the fluid to be at rest, any motion of the fluid as a whole must be laminar. It is necessary to suppose that the body of fluid is large compared with the dimensions of the sphere, no slipping between fluid and sphere occurs at their interface and that the motion is "slow" in a way which will be defined.

Most of the basic results in this chapter are known; the Basset-Boussinesq equation (2-64) was presented in 1885 by Boussinesq, and by Basset in 1887, but this writer has not found a complete and clear derivation in English in the literature. The importance of the topic and the frequency with which it is used as a basis for further work demand that implications and shortcomings of the derivation be understood and to that end it is presented

here. This derivation makes major use of the French text by Villat (1943), the order of treatment and some of the mathematical methods being changed for directness and simplicity without loss of rigour. A Laplace transform method suggested by Brush, Hau-wong Ho and Ben-chie Yen (1964) is used to integrate the equation in the gravitational case and some further results are given.

2.11 Rectangular Coordinate systems for the slow motion.

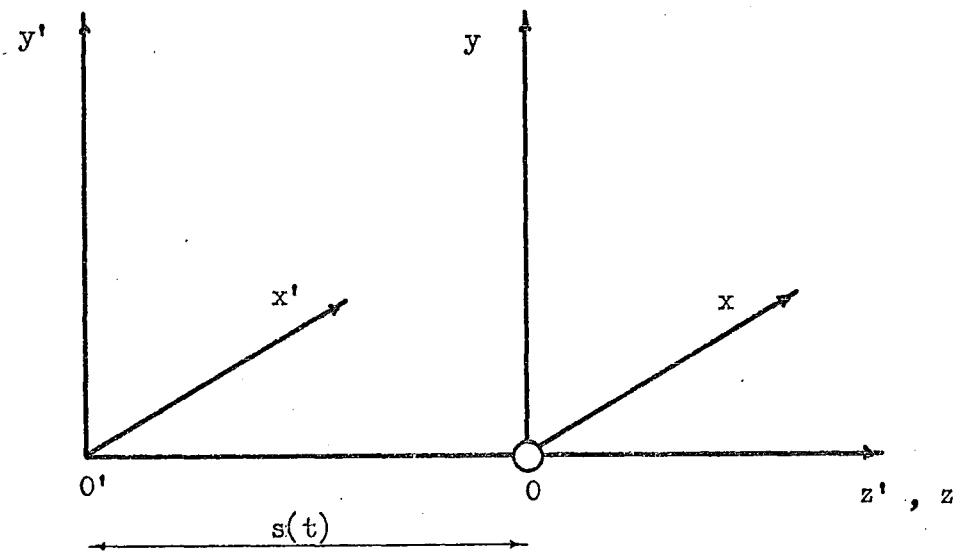

Figure 2-1. Rectangular coordinate systems.

Consider a rigid sphere, radius a, in rectilinear motion in a region of viscous, incompressible fluid whose nearest boundary (if any) is distant D from the sphere, where $\frac{D}{a}$ tends to ∞. The fluid is at rest at distances from the sphere of order D.

The sphere is at the origin of rectangular axes Oxyz which move with the sphere at a speed $v_r'(t) = \frac{ds(t)}{dt}$ relative to axes O'x'y'z', fixed in space with Oz, O'z' aligned in the direction of motion, Figure 2-1. Obviously

$$x' = x, \quad y' = y, \quad z' = z + s. \tag{2-1}$$

$\underline{u}$ is the absolute fluid velocity vector with x',y',z' components u'(x',y',z',t), v'(x',y',z',t), w'(x',y',z',t). Referred to Oxyz the components of $\underline{u}$ are

$$u(x,y,z,t), \quad v(x,y,z,t), \quad w(x,y,z,t).$$

Consider the x component only of $\underline{u}$, and from (2-1)

$$u'(x',y',z',t) = u(x,y,z,t) = u(x',y',z'-s,t), \tag{2-2}$$

and, differentiating (2-2) with respect to t

$$\frac{du'}{dt} = \frac{du'}{dt} + \frac{du'}{dx'}\frac{dx'}{dt} + \frac{du'}{dy'}\frac{dy'}{dt} + \frac{du'}{dz'}\frac{dz'}{dt},$$

$$\frac{du'}{dt} = \frac{du}{dt} = \frac{du}{dt} + \frac{du}{dx}\frac{dx}{dt} + \frac{du}{dy}\frac{dy}{dt} + \frac{du}{dz}\frac{dz}{dt}.$$

In view of (2-1)

$$\frac{du}{dt} = \frac{du}{dt} + u\frac{du}{dx} + v\frac{du}{dy} + (w-\frac{ds}{dt})\frac{du}{dz}. \tag{2-3}$$

The Navier-Stokes equations to be used are intractable while non-linear terms like $B\frac{dC}{db}$ are present, where B, C

are velocity components in b, c directions.

To proceed, put

$$\frac{\frac{du}{dt}}{u\frac{du}{dx} + v\frac{du}{dy} + w\frac{du}{dz}} = L_u$$

and

$$\frac{\frac{du}{dt}}{\frac{ds}{dt}\frac{du}{dz}} = M_u$$

and assume

(a) convective accelerations are sufficiently small compared to local accelerations,

(b) the motion of the sphere is sufficiently slow so L_u, M_u become such large numbers that to sufficient accuracy (2-3) may be written

$$\frac{du'}{dt} = \frac{du}{dt} = \frac{du}{dt} = \frac{du'}{dt}. \tag{2-4}$$

By similar reasoning,

$$\left.\begin{aligned} \frac{dv'}{dt} &= \frac{dv'}{dt} = \frac{dv}{dt}, \\ \frac{dw'}{dt} &= \frac{dw'}{dt} = \frac{dw}{dt}. \end{aligned}\right\} \tag{2-5}$$

Also in view of (2-1)

$$\left.\frac{d^2u'}{dx'^2} + \frac{d^2u'}{dy'^2} + \frac{d^2u'}{dz'^2} = \frac{d^2u}{dx^2} + \frac{d^2u}{dy^2} + \frac{d^2u}{dz^2} = \nabla^2 u\right\} \tag{2-6}$$

and similarly $\nabla^2 v$, $\nabla^2 w$;

and

$$\frac{du'}{dx'} + \frac{dv'}{dy'} + \frac{dw'}{dz'} = \frac{du}{dx} + \frac{dv}{dy} + \frac{dw}{dz} \quad . \qquad (2\text{-}7)$$

(2-1,4,5,6,7) ensure that for the motion specified, equations of motion of the same form apply whether the velocity components are considered relative to the fixed or moving axes.

2.12 Spherical coordinate system.

Spherical coordinates moving with the sphere are adopted (Figure 2-2):

$$\left.\begin{aligned} x &= r \sin\theta \cos\phi \\ y &= r \sin\theta \sin\phi \\ z &= r \cos\theta \end{aligned}\right\} \qquad \left.\begin{aligned} 0 \le \theta \le \pi \\ 0 \le \phi \le 2\pi \end{aligned}\right\} \qquad (2\text{-}8)$$

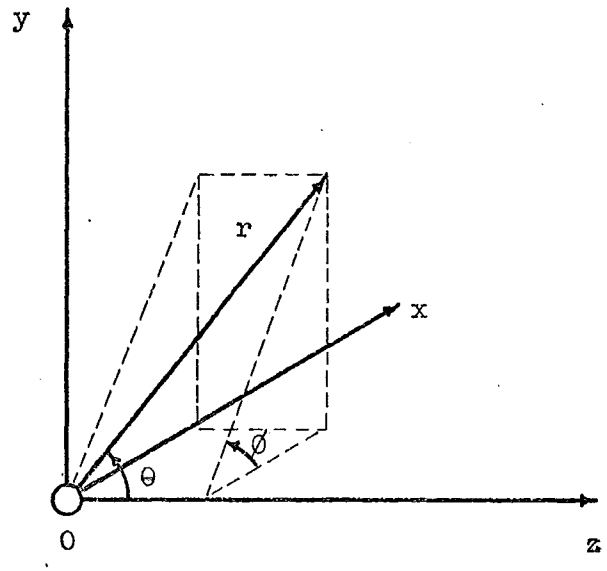

Figure 2-2. The spherical coordinate system.

The appropriate components of the absolute fluid velocity vector are u_r, u_θ, u_ϕ, but u_ϕ is specified zero under the further assumption

(c) There is axial symmetry of the motion about Oz with $\frac{d}{d\phi} = 0$, and $u_\phi = 0$.

2.2 Navier-Stokes equations.

As the main object of this chapter is to determine the resistance experienced by the moving sphere, the velocity components must now be related to the fluid pressure and viscous forces. For a viscous, incompressible fluid the Navier-Stokes equation of motion and equation of continuity are (e.g. page 208, Rouse (1959))

$$\left.\begin{aligned} \frac{du'}{dt} = & -\frac{dX}{dx'} - \frac{1}{\rho}\frac{dp}{dx'} + \frac{m}{\rho}\left[\frac{d^2u'}{dx'^2} + \frac{d^2u'}{dy'^2} + \frac{d^2u'}{dz'^2}\right] \end{aligned}\right\} \qquad (2\text{-}9)$$

and similarly $\frac{dv'}{dt}$, $\frac{dw'}{dt}$;

$$\frac{du'}{dx'} + \frac{dv'}{dy'} + \frac{dw'}{dz'} = 0. \qquad (2\text{-}10)$$

According to the argument of 2.11 these are equally well written for this case

$$\frac{du}{dt} = -\frac{dX}{dx} - \frac{1}{\rho}\frac{dp}{dx} + \frac{m}{\rho}\nabla^2 u, \qquad (2\text{-}11)$$

$$\frac{du}{dx} + \frac{dv}{dy} + \frac{dw}{dz} = 0 \qquad (2\text{-}12)$$

In these equations X is the scalar potential of external body forces (e.g. gravity), m is the fluid viscosity, ρ is the fluid density.

To find equations equivalent to (2-11,12) for the spherical coordinate system of 2.12 note that (2-9,10) may be written in vector form

$$\frac{d\underline{u}}{dt} = -\underline{\nabla}\left(\frac{p}{\rho} + X\right) + \frac{m}{\rho}\nabla^2\underline{u}\ , \qquad (2\text{-}13)$$

$$\underline{\nabla}\cdot\underline{u} = 0\ ;$$

the relationship

$$\nabla^2\underline{u} = \underline{\nabla}(\underline{\nabla}\cdot\underline{u}) - \underline{\nabla}\times(\underline{\nabla}\times\underline{u}) = -\underline{\nabla}\times(\underline{\nabla}\times\underline{u})$$

in this case allows (2-13) to be written

$$\frac{d\underline{u}}{dt} = -\underline{\nabla}\left(\frac{p}{\rho} + X\right) - \underline{\nabla}\times(\underline{\nabla}\times\underline{u})\ \frac{m}{\rho}\ . \qquad (2\text{-}14)$$

When this equation is transformed using the usual expressions for orthogonal curvilinear coordinates (e.g. page 407, Rouse (1959)) and remembering the simplifications provided by assumptions (a) to (c) of 2.11 and 2.12, the required equations equivalent to (2-11,12) are found to be

$$\frac{du_r}{dt} = -\frac{d}{dr}\left(\frac{p}{\rho} + X\right) - \frac{n}{r^2\sin\theta}\left[\left(\frac{d^2(ru_\theta)}{dr\,d\theta} - \frac{d^2u_r}{d\theta^2}\right)\sin\theta + \left(\frac{d(ru_\theta)}{dr} - \frac{du_r}{d\theta}\right)\cos\theta\right] \qquad (2\text{-}15a)$$

$$\frac{du_\theta}{dt} = -\frac{1}{r}\frac{d}{d\theta}\left(\frac{p}{\rho} + X\right) + \frac{n}{r}\left[\frac{d^2(ru_\theta)}{dr^2} - \frac{d^2u_r}{d\theta dr}\right] \qquad (2\text{-}15b)$$

$$\frac{du_\phi}{dt} = 0 = \frac{1}{r\sin\theta}\frac{d}{d\phi}\left(\frac{p}{\rho} + X\right) \qquad (2\text{-}15c)$$

$$\frac{d}{dr}(r^2\sin\theta\, u_r) + \frac{d}{d\theta}(r\sin\theta\, u_\theta) = 0, \qquad (2\text{-}16)$$

where $n = \frac{m}{\rho}$ is the kinematic viscosity. (2-15c) is degenerate as $\frac{d}{d\phi}$ has been specified zero in 2.12; it should be noted that this imposes a restriction on X.

(2-16) suggests the use of a Stokes stream function, Ψ, to reduce two unknowns u_r, u_θ, to one, Ψ;

$$\frac{d\Psi}{d\theta} = u_r\, r^2 \sin\theta, \quad \frac{d\Psi}{dr} = -\, u_\theta\, r \sin\theta. \tag{2-17}$$

(2-15,17) now express the relationship between two functions in three variables, $p(r,\theta,t)$ and $\Psi(r,\theta,t)$.

The form which Ψ will be shown to take at $r = a$, where from (2-23) and (2-17)

$$\left(\frac{d\Psi}{d\theta}\right)_{r=a} = v_r'(t)\, a^2 \sin\theta \cos\theta,$$

$$\left(\frac{d\Psi}{dr}\right)_{r=a} = -\, v_r'(t)\, a \sin^2\theta,$$

suggests that Ψ could take the particular form

$$\Psi(r,\theta,t) = f(r,t) \sin^2\theta, \tag{2-18}$$

whence, from (2-17,18)

$$u_r = \frac{2f\cos\theta}{r^2}, \qquad u_\theta = -\,\frac{df}{dr}\frac{\sin\theta}{r}. \tag{2-19}$$

After substitution and rearrangement (2-15) become

$$\frac{d}{dr}\left(\frac{p}{\rho} + X\right) = \frac{2n\cos\theta}{r^2}\left(\frac{d^2f}{dr^2} - \frac{2f}{r^2}\right) - \frac{2\cos\theta}{r^2}\frac{df}{dt}, \tag{2-20a}$$

$$\frac{d}{d\theta}\left(\frac{p}{\rho} + X\right) = -\, n \sin\theta \frac{d}{dr}\left(\frac{d^2f}{dr^2} - \frac{2f}{r^2}\right) + \frac{d^2f}{dr\,dt}\sin\theta \tag{2-20b}$$

Denote the operation on f, $\frac{d^2f}{dr^2} - \frac{2f}{r^2}$, by the

operator H(f) and eliminate p and X by differentiation of (2-20a,b) with respect to θ, r respectively, equating the resulting expressions:

$$m \frac{d^2 H(f)}{dr^2} - \rho \frac{dH(f)}{dt} - \frac{2m}{r^2} H(f) = 0 \qquad (2\text{-}21)$$

which may also be written

$$H(m\, H(f) - \rho \frac{df}{dt}) = 0 \,. \qquad (2\text{-}22)$$

2.3 Boundary Conditions.

(a) Assume no slipping occurs at the sphere surface. Remembering that u_r, u_θ are absolute fluid velocity components referred to the moving frame; Figure 2-3 shows

$$u_r(a,\theta,t) = v_r'(t)\cos\theta, \quad u_\theta(a,\theta,t) = -v_r'(t)\sin\theta \qquad (2\text{-}23)$$

(b) Assume fluid far from the sphere is uninfluenced by the motion of the sphere.

$$\lim_{r\to\infty} u_r(r,\theta,t) = 0, \quad \lim_{r\to\infty} u_\theta(r,\theta,t) = 0 \qquad (2\text{-}24)$$

(c) The initial conditions (t=0) are known:

$$u_r(r,\theta,0) = u_{r_o}(r,\theta), \quad u_\theta(r,\theta,0) = u_{\theta_o}(r,\theta) \qquad (2\text{-}25)$$

(2-23,24,25) imply

$$\lim_{r\to\infty} u_{r_o}(r,\theta) = 0, \quad \lim_{r\to\infty} u_{\theta_o}(r,\theta) = 0 \quad \text{and}$$

$$u_{r_o}(a,\theta) = v_r'(0)\cos\theta, \quad u_{\theta_o}(a,\theta) = -v_r'(0)\sin\theta$$

Should $v_r'(0)$ be zero, the particular case is of initial rest everywhere.

With the aid of (2-19), (2-23,24,25) may be written in terms of the unknown function f:

$$f(a,t) = \frac{a^2 v_r'(t)}{2}, \qquad \left[\frac{\partial f(r,t)}{\partial r}\right]_{r=a} = a\, v_r'(t) \tag{2-26}$$

$$\lim_{r\to\infty} \frac{f(r,t)}{r^2} = 0, \qquad \lim_{r\to\infty} \frac{1}{r}\frac{\partial f(r,t)}{\partial r} = 0 \tag{2-27}$$

$$f(r,0) = \frac{r^2 u_{r_o}}{2\cos\theta} = q_1(r), \text{say},$$

$$\frac{1}{r}\left[\frac{\partial f(r,t)}{\partial r}\right]_{t=0} = -\frac{u_{\theta_o}}{\sin\theta} = q_2(r), \text{ say.} \tag{2-28}$$

(2-26,27,28) imply

$$\lim_{r\to\infty} \frac{q_1(r)}{r^2} = 0, \qquad \lim_{r\to\infty} q_2(r) = 0,$$

$$q_1(a) = \frac{a^2 v_r'(0)}{2}, \qquad q_2(a) = v_r'(0).$$

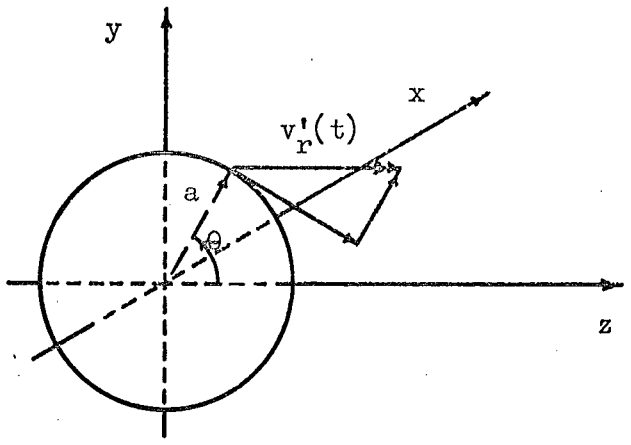

Figure 2-3. The sphere boundary condition.

2.4 An integration of the equation (2-22).

The problem statement beginning 2.2 has now been resolved into the task of solving (2-22) under boundary conditions (2-26,27,28). In (2-22) put

$$F(r,t) = m\,H(f) - \rho\frac{df}{dt} \qquad (2\text{-}29)$$

so that

$$H(F) = \frac{d^2F}{dr^2} - \frac{2F}{r^2} = 0 \qquad (2\text{-}30)$$

The general solution is

$$F(r,t) = -\frac{dA(t)}{dt}\frac{1}{r} - \frac{dB(t)}{dt}\,r^2$$

where A(t) and B(t) are arbitrary functions of t written in this form for later convenience.

From (2-29), the general solution f(r,t) of (2-22) will be a solution of

$$m\,H(f) - \rho\frac{df}{dt} = -\frac{dA(t)}{dt}\frac{1}{r} - \frac{dB(t)}{dt}\,r^2 \qquad (2\text{-}31)$$

For a particular integral note that H(f) = 0 has solutions like those of (2-30), e.g.

$$\frac{1}{\rho}\left[A(t)\frac{1}{r} + B(t)r^2\right] \qquad (2\text{-}32)$$

is a solution which, when differentiated with respect to t, gives

$$\frac{1}{\rho}\left[\frac{dA(t)}{dt}\frac{1}{r} + \frac{dB(t)}{dt}\,r^2\right]$$

Thus (2-32) will satisfy (2-31) and is a particular integral.

To complete the solution of (2-31) the complementary

function is needed from

$$H(f) = \frac{1}{n}\frac{df}{dt} \text{ , i.e. } \frac{d^2f}{dr^2} - \frac{2f}{r^2} = \frac{1}{n}\frac{df}{dt} \qquad (2\text{-}33)$$

This parabolic equation resembles the one-dimensional heat flow equation but the term involving f prevents a simple solution. The operator equalities

$$\left(\frac{d}{dr} + \frac{1}{r}\right)\left(\frac{d}{dr} - \frac{1}{r}\right) = \frac{d^2}{dr^2}$$

$$\left(\frac{d}{dr} - \frac{1}{r}\right)\left(\frac{d}{dr} + \frac{1}{r}\right) = \frac{d^2}{dr^2} - \frac{2}{r^2}$$

$$\frac{d}{dt}\left(\frac{d}{dr} + \frac{1}{r}\right) = \left(\frac{d}{dr} + \frac{1}{r}\right)\frac{d}{dt}$$

show that (2-33) may be written

$$\left(\frac{d}{dr} - \frac{1}{r}\right)\left(\frac{d}{dr} + \frac{1}{r}\right)(f) = \frac{1}{n}\frac{df}{dt} \text{ .} \qquad (2\text{-}34)$$

Putting

$$\left(\frac{d}{dr} + \frac{1}{r}\right)(f(r,t)) = h(r,t) \qquad (2\text{-}35)$$

and operating on (2-34) by $\left(\frac{d}{dr} + \frac{1}{r}\right)$ gives

$$\left(\frac{d}{dr} + \frac{1}{r}\right)\left(\frac{d}{dr} - \frac{1}{r}\right)(h) = \frac{1}{n}\left(\frac{d}{dr} + \frac{1}{r}\right)\frac{df}{dt}$$

or

$$\frac{d^2h}{dr^2} = \frac{1}{n}\frac{dh}{dt} \text{ .} \qquad (2\text{-}36)$$

In this way (2-33) is converted to the problem of solving the homogeneous one-dimensional heat flow equation (2-36) for h(r,t).

From (2-35)

$$\frac{d}{dr}(rf) = rh$$

so that the required complementary function solution of (2-31) is

$$f(r,t) = \frac{1}{r}\left[\int_{a'}^{r} r\,h(r,t)\,dr + C(t)\right] \qquad (2\text{-}37)$$

where a' is an arbitrary constant, C(t) an arbitrary function of t and h(r,t) is a solution of (2-36) to be found.

The general solution of (2-31), from (2-32,37) is

$$f(r,t) = \frac{1}{\rho}\left[A(t)\frac{1}{r} + B(t)r^2\right] + \frac{1}{r}\left[\int_{a'}^{r} r\,h(r,t)\,dr + C(t)\right]$$

which can be rewritten in terms of two new arbitrary functions P(t), Q(t) as

$$f(r,t) = P(t)\frac{1}{r} + Q(t)r^2 + \frac{1}{r}\int_{a'}^{r} r\,h(r,t)\,dr \qquad (2\text{-}38)$$

2.41 Boundary Conditions on h(r,t).

a', P(t), Q(t), h(r,t) must now be made to satisfy the conditions imposed on f(r,t) by (2-26,27,28), section 2.3. These six equations, restated using (2-38), are

$$P(t)\frac{1}{a} + Q(t)a^2 + \frac{1}{a}\int_{a'}^{a} r\,h(r,t)\,dr = \frac{a^2 v_r'(t)}{2} \qquad (2\text{-}39a)$$

$$-\frac{P(t)}{a^2} + 2a\,Q(t) + h(a,t) - \frac{1}{a^2}\int_{a'}^{a} r\,h(r,t)\,dr = a\,v_r'(t) \qquad (2\text{-}39b)$$

$$\lim_{r\to\infty}\left[\frac{P(t)}{r^3} + Q(t) + \frac{1}{r^3}\int_{a'}^{r} r\,h(r,t)\,dr\right] = 0 \qquad (2\text{-}40a)$$

$$(2\text{-}40b)$$

$$\lim_{r\to\infty}\left[-\frac{P(t)}{r^3} + 2\,Q(t) + \frac{1}{r}\,h(r,t) - \frac{1}{r^3}\int_{a'}^{r} r\,h(r,t)\,dr\right] = 0$$

$$\frac{P(0)}{r} + r^2\,Q(0) + \frac{1}{r}\int_{a'}^{r} r\,h(r,0)\,dr = q_1(r) \qquad (2\text{-}41a)$$

$$-\frac{P(0)}{r^3} + 2\,Q(0) + \frac{1}{r}\,h(r,0) - \frac{1}{r^3}\int_{a'}^{r} r\,h(r,0)\,dr =$$

$$= q_2(r). \qquad (2\text{-}41b)$$

$h(r,t)$ will be bounded for large r, whatever t, (see the solution (2-47), below) ensuring that $\frac{1}{r}\,h(r,t)$ and $\frac{1}{r^3}\int_{a'}^{r} r\,h(r,t)\,dr$ tend to zero as r tends to ∞, so that

$$Q(t) = 0, \quad \text{for all } t\,. \qquad (2\text{-}42)$$

(2-39) (effectively two equations in the three unknowns P, a', $h(a,t)$) are insufficient, but by making the convenient choice

$$a' = a \qquad (2\text{-}43)$$

yield

$$P(t) = \frac{a^3 v_r'(t)}{2} \qquad (2\text{-}44)$$

$$h(a,t) = \frac{3a\, v_r'(t)}{2} \qquad (2\text{-}45)$$

(2-41a) differentiated with respect to r is, in view of (2-42,43)

$$-\frac{P(0)}{r^2} + h(r,0) - \frac{1}{r^2}\int_a^r r\, h(r,0)\, dr = \frac{dq_1}{dr} ,$$

or

$$h(r,0) = \frac{dq_1}{dr} + \frac{q_1}{r} = b(r) \text{ , say.} \qquad (2\text{-}46)$$

2.42 A problem in heat flow.

Recall (2-36, 45, 46) repeated here;

$$\frac{\partial^2 h}{\partial r^2} = \frac{1}{n}\frac{\partial h}{\partial t} \qquad a < r < \infty, \quad 0 < t < \infty$$

$$h(a,t) = \frac{3a\, v_r'(t)}{2} \qquad 0 < t < \infty$$

$$h(r,0) = b(r) \qquad a < r < \infty$$

This well-known problem in heat flow could be called "the first boundary value problem on a semi-infinite interval", and is fully treated in most texts on heat flow or partial differential equations (e.g. Tikhonov and Samarskii, (1964)). A minor modification present here is that the r,t plane is bounded by r = a, t = 0 lines rather than the usual r = 0, t = 0, but this is overcome by the substitution

$$x = r - a.$$

The solution is in the form of one integral term expressing the dependence on the initial conditions ($t = 0$) and another integral term expressing the dependence on the boundary conditions ($r = a$).

$$h(r,t) = \frac{1}{2\sqrt{\pi n t}} \int_a^\infty \left[e^{-\frac{(r-r')^2}{4nt}} - e^{-\frac{(r-2a+r')^2}{4nt}} \right] b(r')\, dr'$$

$$+ \frac{3a}{4\sqrt{\pi n}} \left[\int_0^t \frac{r-a}{(t-t')^{1.5}} e^{-\frac{(r-a)^2}{4n(t-t')}} v_r'(t')\, dt' \right]. \qquad (2\text{-}47)$$

(2-38,42,43,44) combine to show

$$f(r,t) = \frac{a^3 v_r'(t)}{2r} + \frac{1}{r} \int_a^r r\, h(r,t)\, dr. \qquad (2\text{-}48)$$

$\left(\frac{d^2 f}{dr^2}\right)_{r=a}$ and $\left(\frac{d^3 f}{dr^3}\right)_{r=a}$ are required in 2.5 and are derived in Appendix A.

2.5 Evaluation of the resistance.

The relationship between the internal stress tensor, $\underline{T}$, and the velocity vector, $\underline{u}$, is now invoked to calculate the resistance, which, by the symmetry of the situation, 2.12 (c), is a force in the Oz direction, Figure 2-2.

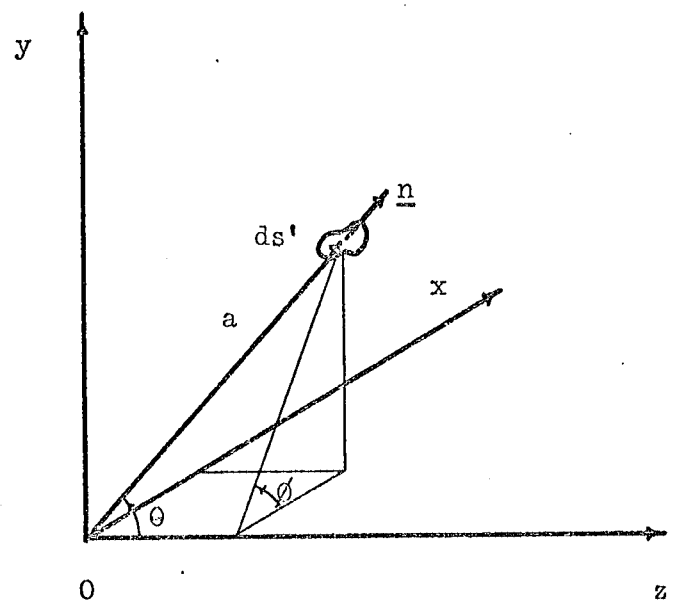

Figure 2-4. A surface element on the sphere.

The notation used is (Figure 2-4): $T_{r\theta}$ is the stress component on a surface perpendicular to r, in the direction of θ. Thus T_{rr}, $T_{\theta\theta}$, $T_{\phi\phi}$ are normal stresses (diagonal elements of $\underline{T}$), $T_{r\theta}$, $T_{r\phi}$, $T_{\theta r}$, $T_{\theta\phi}$, $T_{\phi\theta}$, $T_{\phi r}$ are shear stresses.

ds' is an element of area with normal $\underline{n}$, on the surface of the sphere centre 0, radius a, and the three stress components acting upon this surface are T_{rr}, $T_{r\theta}$, $T_{r\phi}$. These are related to the absolute velocity components referred to the moving axes u_r, u_θ, u_ϕ, by (page 203, Rouse (1959))

$$\left.\begin{aligned} T_{rr} &= -p + 2m\frac{du_r}{dr} \\ T_{r\theta} &= m\left[\frac{1}{r}\frac{du_r}{d\theta} + r\frac{d}{dr}\left(\frac{u_\theta}{r}\right)\right] \\ &= m\left(\frac{1}{r}\frac{du_r}{d\theta} + \frac{du_\theta}{dr} - \frac{u_\theta}{r}\right) \\ T_{r\phi} &= m\left[r\frac{d}{dr}\left(\frac{u_\phi}{r}\right) + \frac{1}{r\sin\theta}\frac{du_r}{d\phi}\right] = 0, \text{ as} \\ \frac{d}{d\phi} &= 0 = u_\phi \text{ , 2.12(c).} \end{aligned}\right\} \quad (2\text{-}49)$$

With the n-direction counted positive the z component of the elementary force exerted on ds' by the liquid is

$$(T_{rr}\cos\theta - T_{r\theta}\sin\theta)\, ds' ,$$

and the resistance, R, is

$$R = \int_{s'} (T_{rr}\cos\theta - T_{r\theta}\sin\theta)\, ds' \qquad (2\text{-}50)$$

From Figure 2-4,

$$ds' = a\, d\theta\, a\sin\theta\, d\phi . \qquad (2\text{-}51)$$

(2-49,50,51) give

$$R = -\int_0^{2\pi}\left[\int_0^{\pi}\left(p\cos\theta - 2m\frac{du_r}{dr}\cos\theta + m\frac{du_\theta}{dr}\sin\theta + \frac{m}{r}\frac{du_r}{d\theta}\sin\theta - \frac{m\,u_\theta}{r}\sin\theta\right) a^2\sin\theta\, d\theta\right] d\phi$$

whence

$$R = -2\pi a^2 \int_0^\pi p \cos\theta \sin\theta \, d\theta - 2\pi a^2 m \int_0^\pi \left[\left(\frac{du_\theta}{dr} + \frac{1}{r}\frac{du_r}{d\theta} - \frac{u_\theta}{r}\right)\sin\theta - 2\frac{du_r}{dr}\cos\theta\right]\sin\theta \, d\theta, \quad (2\text{-}52)$$

wherein the unknown functions p, u_r, u_θ and derivatives are to be taken at (a,θ,t).

From (2-19,26), <u>at r = a</u>

$$\frac{du_\theta}{dr} = -\sin\theta\left(\frac{d^2f}{dr^2}\frac{1}{a} - \frac{df}{dr}\frac{1}{a^2}\right)$$

$$= \frac{\sin\theta}{a}\left(v_r' - \frac{d^2f}{dr^2}\right)$$

$$\frac{1}{a}\left(\frac{du_r}{d\theta} - u_\theta\right) = -\frac{2f\sin\theta}{a^3} + \frac{df}{dr}\frac{\sin\theta}{a^2}$$

$$= \frac{-a^2v_r'\sin\theta + a^2v_r'\sin\theta}{a^3}$$

$$= 0$$

$$\frac{du_r}{dr} = 2\cos\theta\left(\frac{df}{dr}\frac{1}{a^2} - \frac{2f}{a^3}\right)$$

$$= \frac{2\cos\theta(a^2v_r' - a^2v_r')}{a^3}$$

$$= 0.$$

The three preceding equations reduce (2-52) to

$$R = -2\pi a^2 \int_0^\pi p \cos\theta \sin\theta \, d\theta$$

$$- 2\pi a^2 m \int_0^\pi \frac{\sin^3\theta}{a} \left[v_r' - \left(\frac{d^2 f}{dr^2}\right)_{r=a} \right] d\theta$$

$$= -2\pi a^2 \int_0^\pi p \cos\theta \sin\theta \, d\theta - \frac{8\pi a m}{3} \left[v_r' - \left(\frac{d^2 f}{dr^2}\right)_{r=a} \right] \tag{2-53}$$

The term containing p is integrable by parts, as

$$2 \int_0^\pi p \cos\theta \sin\theta \, d\theta = \left[p \sin^2\theta \right]_0^\pi - \int_0^\pi \frac{dp}{d\theta} \sin^2\theta \, d\theta$$

$$= - \int_0^\pi \frac{dp}{d\theta} \sin^2\theta \, d\theta. \tag{2-54}$$

$\left(\frac{dp}{d\theta}\right)_{r=a}$ is obtained from (2-20b);

$$\frac{1}{\rho} \frac{dp}{d\theta} = - \frac{dX}{d\theta} - n \sin\theta \left[\frac{d^3 f}{dr^3} - 2 \frac{d}{dr}\left(\frac{f}{r^2}\right) \right] + \sin\theta \frac{d}{dt}\left(\frac{df}{dr}\right)$$

$$\left(\frac{dp}{d\theta}\right)_{r=a} = - \rho \left(\frac{dX}{d\theta}\right)_{r=a} - \sin\theta \left[m \left(\frac{d^3 f}{dr^3} - 2 \frac{d}{dr}\left(\frac{f}{r^2}\right) \right) \right.$$

$$\left. + \rho \frac{d}{dt}\left(\frac{df}{dr}\right) \right]_{r=a} . \tag{2-55}$$

From (2-26)

$$\left[\frac{d}{dt}\left(\frac{df}{dr}\right) \right]_{r=a} = a \frac{dv_r'}{dt}$$

$$\left[\frac{d}{dr}\left(\frac{f}{r^2}\right) \right]_{r=a} = \frac{1}{a^2} \left(\frac{df}{dr} - \frac{2f}{r}\right)_{r=a} = 0.$$

Thus (2-55) becomes

$$\left(\frac{dp}{d\theta}\right)_{r=a} = -\rho\left(\frac{dX}{d\theta}\right)_{r=a} - m\sin\theta\left(\frac{d^3f}{dr^3}\right)_{r=a} - \rho\sin\theta\, a\,\frac{dv_r'}{dt}$$

and this in turn in (2-54) gives

$$2\int_0^{\pi} p\cos\theta\sin\theta\, d\theta = \rho\int_0^{\pi}\left(\frac{dX}{d\theta}\right)_{r=a}\sin^2\theta\, d\theta + \int_0^{\pi}\left[m\left(\frac{d^3f}{dr^3}\right)_{r=a} - \rho\, a\,\frac{dv_r'}{dt}\right]\sin^3\theta\, d\theta$$

$$= \rho\int_0^{\pi}\left(\frac{dX}{d\theta}\right)_{r=a}\sin^2\theta\, d\theta + \frac{4}{3}\left[m\left(\frac{d^3f}{dr^3}\right)_{r=a} - \rho\, a\,\frac{dv_r'}{dt}\right]. \quad (2\text{-}56)$$

The problem is now completed by substituting (2-56) into (2-53) and using the values for $\left(\frac{d^2f}{dr^2}\right)_{r=a}$ and $\left(\frac{d^3f}{dr^3}\right)_{r=a}$ from Appendix A;

$$R = -\pi a^2\rho\int_0^{\pi}\left(\frac{dX}{d\theta}\right)_{r=a}\sin^2\theta\, d\theta - \frac{4\pi a^2}{3}\left[m\left(\frac{d^3f}{dr^3}\right)_{r=a} - \rho\, a\,\frac{dv_r'}{dt}\right] - \frac{8\pi\, a\, m}{3}\left[v_r' - \left(\frac{d^2f}{dr^2}\right)_{r=a}\right]$$

$$R = -\pi a^2 \rho \int_0^{\pi} \left(\frac{dX}{d\theta}\right)_{r=a} \sin^2\theta \, d\theta - \frac{4\pi a^2}{3}\left[\frac{3m\, v_r'}{2a} + \frac{\rho_a}{2}\frac{dv_r'}{dt} - \frac{m}{a}\left(\frac{dh}{dr}\right)_{r=a}\right] - \frac{8\pi am}{3}\left[\frac{3v_r'}{2} - \left(\frac{dh}{dr}\right)_{r=a}\right]$$

$$= -\pi a^2 \rho \int_0^{\pi} \left(\frac{dX}{d\theta}\right)_{r=a} \sin^2\theta \, d\theta - 6\pi am v_r' - \frac{2}{3}\pi a^3 \rho \frac{dv_r'}{dt} + 4\pi am \left(\frac{dh}{dr}\right)_{r=a} .$$

Finally, from (A-15) of Appendix A

$$R = -\pi a^2 \rho \int_0^{\pi} \left(\frac{dX}{d\theta}\right)_{r=a} \sin^2\theta \, d\theta - 6\pi am v_r' - \frac{2}{3}\pi a^3 \rho \frac{dv_r'}{dt} - 6a^2\sqrt{\pi m \rho} \int_0^t \frac{1}{\sqrt{t-t'}} \frac{dv_r'(t')}{dt'} dt' + \frac{4a\sqrt{\pi m \rho}}{\sqrt{t}} \int_a^{\infty} \frac{db(r')}{dr'} e^{-\frac{(r'-a)^2}{4nt}} dr' . \quad (2\text{-}57)$$

The full equation of motion caused by the scalar potential X and the resistance R is

$$\frac{4}{3}\pi a^3 \rho_s \frac{dv_r'}{dt} = -\frac{4}{3}\pi a^3 \rho_s \left(\frac{dX}{dz}\right)_{xy} + R . \quad (2\text{-}58)$$

Now $\left(\frac{dX}{dz}\right)_{xy} = \frac{dX}{dr}\left(\frac{dr}{dz}\right)_{xy} + \frac{dX}{d\theta}\left(\frac{d\theta}{dz}\right)_{xy}$,

$r^2 = x^2 + y^2 + z^2$ and $\cos\theta = \frac{z}{r}$, Figure 2-2,

so $\left(\frac{dX}{dz}\right)_{xy} = \frac{dX}{dr}\cos\theta - \frac{1}{r}\frac{dX}{d\theta}\sin\theta$.

The complete equation of slow, rectilinear motion of a spherical particle in a viscous, incompressible fluid at rest is

$$\frac{4}{3}\pi a^3 \rho_s \frac{dv'_r}{dt} = -\frac{4}{3}\pi a^3 \rho_s \left(\frac{dX}{dr}\cos\theta - \frac{1}{r}\frac{dX}{d\theta}\sin\theta\right) -$$

$$\pi a^2 \rho \int_0^{\pi} \left(\frac{dX}{d\theta}\right)_{r=a} \sin^2\theta \, d\theta - 6\pi a m v'_r - \frac{2}{3}\pi a^3 \frac{dv'_r}{dt}$$

$$- 6a^2\sqrt{\pi m \rho} \int_0^t \frac{1}{\sqrt{t-t'}} \frac{dv'_r(t')}{dt'} \, dt'$$

$$+ \frac{4a\sqrt{\pi m \rho}}{\sqrt{t}} \int_a^{\infty} \frac{db(r')}{dr'} e^{-\frac{(r'-a)^2}{4nt}} \, dr'. \qquad (2\text{-}59)$$

Temporarily denote the terms of (2-59) by

$$T_1 = - T_2 - T_3 - T_4 - T_5 - T_6 + T_7 .$$

T_1 is the mass-acceleration product of the particle;

T_2 is the particle force derived from the scalar force potential, X, in the direction of motion (z);

T_3 is the surface force on the particle due to the pressure distribution induced in the fluid by X;

T_4 is the Stokes linear resistance (as for steady flow);

T_5 is the added mass term, describing the exchange of energy with the fluid motion;

T_6 is the history or "Basset" term;

T_7 is the term describing the effect of the initial conditions.

2.51 Comments on the complete equation of motion.

Comprehensive as (2-59) may seem, two additions could be mentioned. The first concerns the Basset term, T_6, above In solving the problem of 2.42 it transpires that more general initial conditions can be taken into account; e.g. if

$$h(a,t) = \frac{3av_r'(t)}{2}, \quad t_o < t < \infty,$$

$$h(r,t_o) = b(r) \quad ,$$

then the lower integral limit zero in T_6 may be replaced by t_o. (Further details on the generality of such conditions in e.g. Tikhonov and Samarskii (1964)).

Secondly, the equation (2-59) describes a force balance. Hjelmfelt and Mockros (1967) have included another term (T_8, say) to allow an impulsive force, magnitude k, to act at $t = t_i$

$$T_8 = \pm k\, \delta(t-t_i) \quad ,$$

where $\delta(t-t_i)$ is the Dirac delta function. The authors do not state whether the validity of this step has been carefully considered. (c.f. Pearcey and Hill (1956)).

2.52 A simple case - free fall under gravity.

The complete equation of motion takes a simpler form in the case of free fall where initially the sphere and fluid were at rest at $t \leq 0$. Then, if Oz is taken vertically downwards

$$X = - gz = - gr \cos\theta \tag{2-60}$$

and, from (2-25, 28, 46) ,

$$b(r) = 0 \ . \tag{2-61}$$

From (2-60)

$$\frac{dX}{dz} = \frac{dX}{dr} \cos\theta - \frac{1}{r} \frac{dX}{d\theta} \sin\theta = - g \tag{2-62}$$

$$\left(\frac{dX}{d\theta} \right)_{r=a} = g \, a \sin\theta \ . \tag{2-63}$$

Substituting (2-61, 62, 63) into (2-59)

$$\frac{4}{3}\pi a^3 \rho_s \frac{dv_r'}{dt} = \frac{4}{3}\pi a^3 \rho_s g - \pi a^3 \rho g \int_0^{\pi} \sin^3\theta \, d\theta -$$

$$6\pi a m v_r' - \frac{2}{3}\pi a^3 \rho \frac{dv_r'}{dt} - 6a^2 \sqrt{\pi m \rho} \int_0^t \frac{1}{\sqrt{t-t'}} \frac{dv_r'(t')}{dt'} \, dt'$$

$$= \frac{4}{3}\pi a^3 (\rho_s - \rho) g - 6\pi a m v_r' - \frac{2}{3}\pi a^3 \rho \frac{dv_r'}{dt} -$$

$$6a^2 \sqrt{\pi m \rho} \int_0^t \frac{1}{\sqrt{t-t'}} \frac{dv_r'(t')}{dt'} \, dt' \ . \tag{2-64}$$

This is the equation from which most work in this field begins, and has been called the Basset-Boussinesq-

Oseen equation. It has been verified experimentally at low Reynold's numbers by various workers (e.g. Hjelmfelt and Mockros (1967), Figure 3-1).

2.6 Integration in the gravitational case of 2.52.

Brush, Hau-Wong Ho and Ben-Chie Yen (1964) showed that (2-64) can be integrated using Laplace transforms. The transformed equation is, where $L\{v_r'(t)\} = f(s)$ etc., and writing $d = 2a$,

$$s\,f(s) + \frac{18n}{\left[\frac{\rho_s}{\rho} + \frac{1}{2}\right] d^2} f(s) + \frac{9\sqrt{ns}}{\left[\frac{\rho_s}{\rho} + \frac{1}{2}\right] d} f(s) - \frac{\left[\frac{\rho_s}{\rho} - 1\right] g}{\left[\frac{\rho_s}{\rho} + \frac{1}{2}\right] s} = 0$$

whence

$$f(s) = \frac{\left[\frac{\rho_s}{\rho} - 1\right] g}{\left[\frac{\rho_s}{\rho} + \frac{1}{2}\right]} \cdot \frac{1}{s\left[s + \frac{9\sqrt{n}}{\left[\frac{\rho_s}{\rho} + \frac{1}{2}\right] d}\sqrt{s} + \frac{18n}{\left[\frac{\rho_s}{\rho} + \frac{1}{2}\right] d^2}\right]}. \qquad (2\text{-}65)$$

This can be expressed in terms of its partial fractions

$$f(s) = \frac{\left[\frac{\rho_s}{\rho} - 1\right] g}{\left[\frac{\rho_s}{\rho} + \frac{1}{2}\right]} \left[\frac{\frac{1}{bc}}{s} + \frac{\frac{1}{b(b-c)}}{\sqrt{s}(\sqrt{s}+b)} - \frac{\frac{1}{c(b-c)}}{\sqrt{s}(\sqrt{s}+c)}\right],$$

where $b,c = \frac{9\sqrt{n}}{2d\left[\frac{\rho_s}{\rho} + \frac{1}{2}\right]} \pm \frac{3\sqrt{n}}{2d\left[\frac{\rho_s}{\rho} + \frac{1}{2}\right]} \left[5 - 8\frac{\rho_s}{\rho}\right]^{\frac{1}{2}}$, (2-65a)

and the solution follows from known inverse transforms (e.g. Abramowitz and Stegun (1965));

$$v_r'(t) = \frac{\left[\frac{\rho_s}{\rho} - 1\right] g}{\left[\frac{\rho_s}{\rho} + \frac{1}{2}\right]} \left[\frac{1}{bc} + \frac{1}{b(b-c)} e^{b^2 t} \operatorname{erfc}(b\sqrt{t}) \right.$$

$$\left. - \frac{1}{c(b-c)} e^{c^2 t} \operatorname{erfc}(c\sqrt{t}) \right] . \quad (2\text{-}66)$$

It is clear from (2-65a) that b,c become complex if $\frac{\rho_s}{\rho} > \frac{5}{8}$ and more suitable forms for these cases are given by Brush, Hau-Wong Ho and Ben-Chie Yen (1964) and Hjelmfelt and Mockros (1967).

2.7 Extension to a moving fluid.

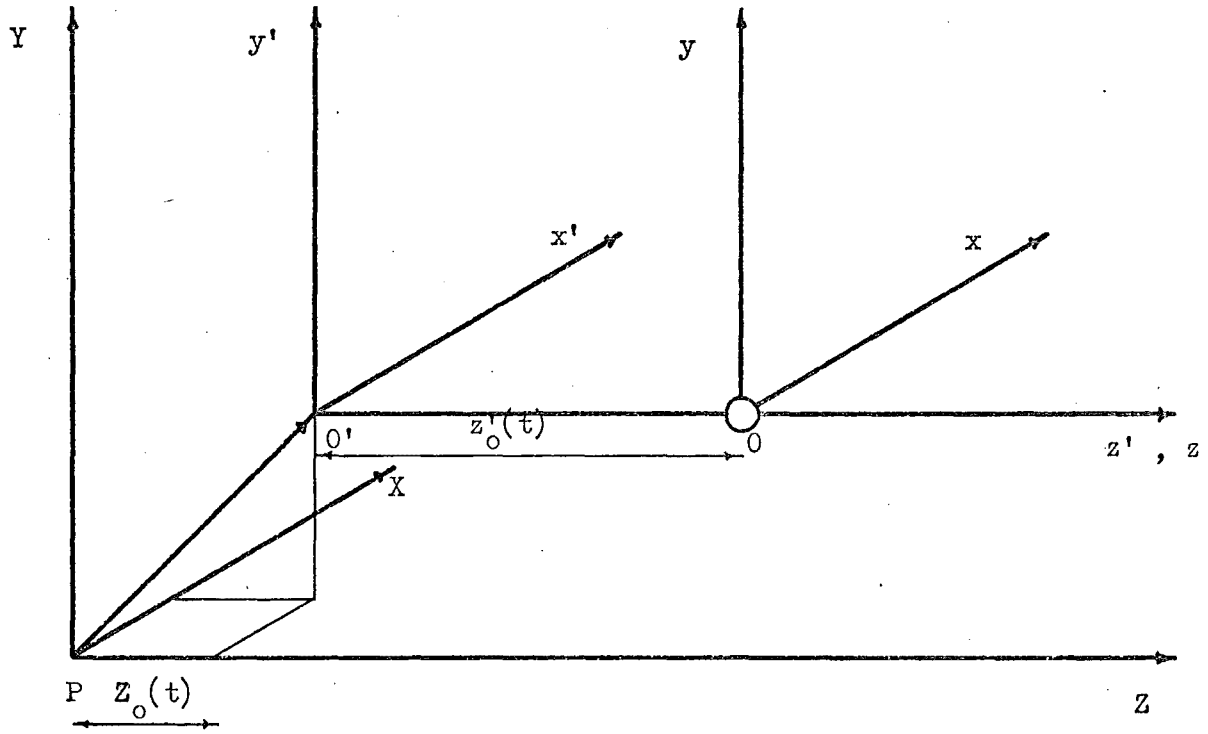

Figure 2-5. Rectangular coordinate systems.

The complete equation of motion (2-59) required the ambient fluid to be at rest at large distances from the sphere. It is an equation in $v_r'(t)$ referred to O' x' y' z', describing the forces measured by an observer in that frame when both the observer and the frame are at rest, or moving with constant velocity, with respect to an inertial frame.

O' x' y' z' is now considered to move parallel to O' z' and PZ at a speed $v''(t)$, where PXYZ is an inertial frame to which $v''(t)$ is referred, Figure 2-5.

$$v''(t) = \frac{dZ_o(t)}{dt} \quad .$$

The Principle of Independence of Forces allows the new situation to be described by the sum of the forces measured when O' x' y' z' was not accelerating and the force associated with the acceleration $\frac{dv''}{dt}$ (a 'fictitious' force to an observer in O' x' y' z'). Two points connected with the summation should be made:

(a) The velocity of the sphere relative to PXYZ is

$$v_p''(t) = \frac{dZ_o}{dt} + \frac{dz_o}{dt}$$

$$= v''(t) + v_r'(t)$$

$$\text{i.e. } v_p''(t) - v''(t) = v_r'(t) \quad . \qquad (2\text{-}67)$$

(b) An overall pressure gradient is set up in the fluid fixed to O' x' y' z' by the acceleration $\frac{dv''}{dt}$

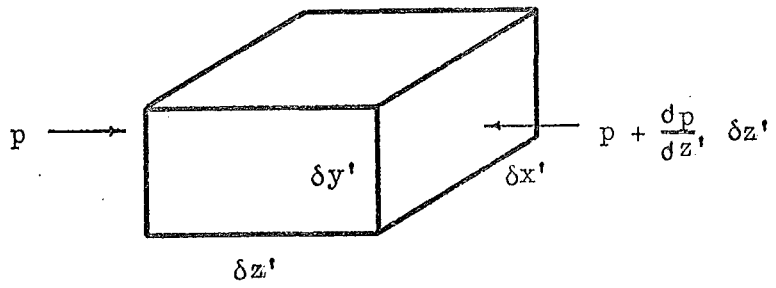

$$- \frac{dp}{dz'} \delta z' \, \delta x' \, \delta y' = \rho \, \delta x' \, \delta y' \, \delta z' \, \frac{dv''}{dt} .$$

When integrated over the surface of the sphere the force in the z direction appears (c.f. buoyant force)

$$\frac{4}{3}\pi a^3 \rho \, \frac{dv''}{dt} . \qquad (2\text{-}68)$$

(Note that by fixing the fluid as a whole to frame O'x'y'z', speed v"(t), a homogeneous field is implied, $\frac{dv''}{dy'} = \frac{dv''}{dz'} = 0$, and there is no viscous force on the element. When the field is not homogeneous and $\underline{v}'' = \underline{v}''(t,\underline{x})$ Corrsin and Lumley (1956), Hinze (1959) and Soo (1967) have used the Navier-Stokes equation (2-13) for the pressure gradient although Tchen (1947) merely replaces $\frac{dv''}{dt}$ by $\frac{dv''}{dt} + v'' \frac{dv''}{dx'}$).

Invoking the principle and assembling (2-59,67,68), the complete equation of slow relative, rectilinear motion of a sphere, speed $v_p''(t)$, in a viscous fluid, speed v"(t), is

$$\frac{4}{3}\pi a^3 \rho_s \frac{dv''_p}{dt} = \frac{4}{3}\pi a^3 \rho \frac{dv''}{dt} - \frac{4}{3}\pi a^3 \rho_s \frac{dX}{dZ}$$

$$- \pi a^2 \rho \int_0^{\pi} \left(\frac{dX}{d\theta}\right)_{r=a} \sin^2\theta \, d\theta - 6\pi a m (v''_p - v'')$$

$$- \frac{2}{3}\pi a^3 \rho \left(\frac{dv''_p}{dt} - \frac{dv''}{dt}\right) - 6a^2 \sqrt{\pi m \rho} \int_0^t \frac{1}{\sqrt{t-t'}}$$

$$\left[\frac{dv''_p}{dt'} - \frac{dv''}{dt'}\right] dt'$$

$$+ \frac{4a\sqrt{\pi m \rho}}{\sqrt{t}} \int_a^{\infty} \frac{db(r')}{dr'} e^{-\frac{(r'-a)^2}{4nt}} dr'. \quad (2\text{-}69)$$

The usefulness of this equation is limited by the complex dependence of r, θ on t, but this objection will not arise in certain simple cases.

2.71 Moving fluid and gravity.

The complete equation can be simplified as it was in 2.52.

$$X = - g Z . \quad (2\text{-}70)$$

The initial condition

$$b(r) = 0 \quad (2\text{-}71)$$

now implies that, at t = 0, the sphere had no motion relative to the fluid (c.f. (2-61)). (2-69) now becomes

$$\frac{4}{3}\pi a^3 \rho_s \frac{dv''_p}{dt} = \frac{4}{3}\pi a^3 \rho \frac{dv''}{dt} + \frac{4}{3}\pi a^3 (\rho_s - \rho) g - 6\pi a m (v''_p - v'')$$

(over page)

(equation continued from previous page)

$$- \frac{2}{3}\pi a^3 \rho \left[\frac{dv''_p}{dt} - \frac{dv''}{dt}\right] - 6a^2 \sqrt{\pi m \rho} \int_0^t \frac{1}{\sqrt{t-t'}} \left[\frac{dv''_p}{dt'} - \frac{dv''}{dt'}\right] dt'. \tag{2-72}$$

This equation was first suggested by Tchen (1947), as an extension of (2-64).

2.72 Moving fluid and an inertial field.

This is the case described by the derivation in 2.7 before the effect of gravity is added. Dropping terms derived from the scalar force potential, X, (2-69) becomes, for an inertial field set up by the motion $\frac{dv''}{dt}$, with zero initial conditions

$$\frac{4}{3}\pi a^3 \rho_s \frac{dv''_p}{dt} = \frac{4}{3}\pi a^3 \rho \frac{dv''}{dt} - 6\pi a m (v''_p - v'') - \frac{2}{3}\pi a^3 \rho \left[\frac{dv''_p}{dt} - \frac{dv''}{dt}\right] - 6a^2 \sqrt{\pi m \rho} \int_0^t \frac{1}{\sqrt{t-t'}} \left[\frac{dv''_p}{dt'} - \frac{dv''}{dt'}\right] dt'. \tag{2-73}$$

(2-73) can be put in a form of interest to an observer moving with the fluid by subtracting $\frac{4}{3}\pi a^3 \rho_s \frac{dv''}{dt}$ from both sides;

$$\frac{4}{3}\pi a^3 \rho_s \left[\frac{dv''_p}{dt} - \frac{dv''}{dt}\right] = \frac{4}{3}\pi a^3 (\rho_s - \rho)\left(-\frac{dv''}{dt}\right) - 6\pi a m (v''_p - v'') - \frac{2}{3}\pi a^3 \rho \left[\frac{dv''_p}{dt} - \frac{dv''}{dt}\right] - 6a^2 \sqrt{\pi m \rho} \int_0^t \frac{1}{\sqrt{t-t'}} \left[\frac{dv''_p}{dt'} - \frac{dv''}{dt'}\right] dt'. \tag{2-74}$$

Put $v'_r(t) = v''_p(t) - v''(t)$ is the speed which the fluid-borne observer notes as the sphere's absolute speed. (2-74) then becomes identical to the equation describing gravitational free fall in a still fluid, (2-64), except that $-\frac{dv''}{dt}$ has replaced the gravitational acceleration g. In particular, should $-\frac{dv''}{dt} = g$, the observer would detect no difference in the behaviour of the sphere whether its motion were caused by gravity, or by retardation $\frac{dv''}{dt}$ relative to an inertial frame. This merely expresses one aspect of the Principle of Equivalence of gravitational and inertial fields, and reference will be made to it in later parts of the thesis. In particular, the similarity between drag on a particle dropped in a still fluid and that on a particle with slip velocity in a decelerating fluid should be noted.

Care is needed when the fluid velocity is a function of both time and position, $\underline{v}'' = \underline{v}''(t,\underline{x})$. It was noted in the previous section that Navier-Stokes equation should then be used for the pressure gradient, and in this term

$$\frac{dv''_i}{dt} = \frac{dv''_i}{dt} + v''_j \frac{dv''_i}{dx'_j} \quad .$$

However, in evaluating the resistance experienced by the particle, one must note that $\frac{dx_i}{dt} = v''_{p_i}$ and in other terms of (2-73), the time derivative,

$$\frac{d}{dt} = \frac{\partial}{\partial t} + v''_{p_i} \frac{\partial}{\partial x'_i}$$

(see page 356, Hinze (1959)).

2.73 Integration in the moving fluid cases; gravitational and inertial.

The gravitational case.

The non-homogeneous equation in $v''_p(t)$, (2-72), was solved by Tchen (1947). His method, a complex process of differentiation and substitution, changed the first-order, integro-differential equation to a second order equation which did not involve the unknown, v''_p, in an integral term. His eventual solution is

$$v''_p(t) = \frac{1}{w} \int_{-\infty}^{t} e^{-k(t-t')} \sin w(t-t') \, F(t') \, dt', \quad (2\text{-}75)$$

in which

$$k = bc \left(1-\frac{3c}{2}\right),$$

$$w^2 = b^2c^2 - k^2 = 3b^2c^3 \left(1-\frac{3c}{4}\right),$$

$$c = \frac{3\rho}{2\rho_s + \rho},$$

$$b = \frac{3nc}{a^2},$$

$$v_s = \frac{2ga^2}{9n} \frac{\rho_s - \rho}{\rho} \quad \text{(settling speed in still fluid)},$$

and $$F(t) = b^2c^2 (v''-v_s) + bc (1-2c) \frac{dv''}{dt} + c \frac{d^2v''}{dt^2}$$

$$- \sqrt{\frac{nc}{\pi}} \frac{3c(c-1)}{a} \int_0^{\infty} \frac{1}{\sqrt{t'}} \frac{d^2v''(t-t')}{dt'} \, dt'.$$

The solution below, (2-80), is of similar form to that in 2.6 for the gravitational, still fluid case. It is an alternative to (2-75) which could be more suitable for motion which is not periodic and comprises terms showing the effects of gravity and the fluid motion separately.

Subtract $\frac{4}{3}\pi a^3 \rho_s \frac{dv''}{dt}$ from each side of (2-72), put $v_r(t) = v_p''(t) - v''(t)$ and divide by $\frac{4}{3}\pi a^3 \rho$;

$$\left[\frac{\rho_s}{\rho} + \frac{1}{2}\right] \frac{dv_r}{dt} + \frac{9nv_r}{2a^2} + \frac{9}{2a}\sqrt{\frac{n}{\pi}} \int_0^t \frac{1}{\sqrt{t-t'}} \frac{dv_r}{dt'}\, dt'$$

$$= \left[\frac{\rho_s}{\rho} - 1\right] \left(g - \frac{dv''}{dt}\right).$$

Taking Laplace transforms with $L\{v_r(t)\} = f(s)$, $L\{v''(t)\} = h(s)$, and allowing that $v_r(0) = 0$, i.e. equal particle and fluid velocities at $t = 0$;

$$\left[\frac{\rho_s}{\rho} + \frac{1}{2}\right] s\, f(s) + \frac{9n}{2a^2} f(s) + \frac{9}{2a}\sqrt{\frac{n}{\pi}} \left[s\, f(s) \sqrt{\frac{\pi}{s}}\right]$$

$$= \left[\frac{\rho_s}{\rho} - 1\right] \left[\frac{g}{s} - s\, h(s) + v''(0)\right],$$

$$f(s) = \frac{\left[\frac{\rho_s}{\rho} - 1\right]}{\left[\frac{\rho_s}{\rho} + \frac{1}{2}\right]} \left\{ \frac{g}{s\left[s + \frac{9\sqrt{n}}{2a\left[\frac{\rho_s}{\rho} + \frac{1}{2}\right]} \sqrt{s} + \frac{9n}{2a^2\left[\frac{\rho_s}{\rho} + \frac{1}{2}\right]}\right]} \right.$$

$$\left. - \frac{s\, h(s) - v''(0)}{\left[s + \frac{9\sqrt{n}}{2a\left[\frac{\rho_s}{\rho} + \frac{1}{2}\right]} \sqrt{s} + \frac{9n}{2a^2\left[\frac{\rho_s}{\rho} + \frac{1}{2}\right]}\right]} \right\}. \qquad (2\text{-}76)$$

The first term on the right side is identical to that in (2-65) and its inverse transform has been given - the right side of (2-66). The second term gives a convolution integral, the numerator being the transform of $\frac{dv''}{dt}$ and the denominator having partial fractions

$$\frac{\frac{1}{b-c}}{\sqrt{s}+c} - \frac{\frac{1}{b-c}}{\sqrt{s}+b} = \frac{1}{(\sqrt{s}+b)(\sqrt{s}+c)}, \qquad (2\text{-}77)$$

where b, c are defined by (2-65a).

The two fractions have known inverse transforms (29.3.88, Abramowitz and Stegun (1965)) and their difference gives the inverse transform

$$\frac{1}{b-c}\left[b\, e^{b^2t}\, \mathrm{erfc}\,(b\sqrt{t}) - c\, e^{c^2t}\, \mathrm{erfc}(c\sqrt{t})\right]. \qquad (2\text{-}78)$$

From (2-66,76,78) f(s) has inverse transform

$$\begin{aligned} v_r(t) = {} & \frac{\left[\frac{\rho_s}{\rho}-1\right]}{\left[\frac{\rho_s}{\rho}+\frac{1}{2}\right]} g\left[\frac{1}{bc} + \frac{1}{b(b-c)} e^{b^2t}\, \mathrm{erfc}(b\sqrt{t})\right. \\ & \left. - \frac{1}{c(b-c)}\, e^{c^2t}\, \mathrm{erfc}\,(c\sqrt{t})\right] \\ & - \frac{\left[\frac{\rho_s}{\rho}-1\right]}{\left[\frac{\rho_s}{\rho}+\frac{1}{2}\right]} \int_0^t \frac{1}{b-c}\left[b\, e^{b^2t'}\, \mathrm{erfc}\,(b\sqrt{t'})\right. \\ & \left. - c\, e^{c^2t'}\, \mathrm{erfc}\,(c\sqrt{t'})\right] \frac{dv''(t-t')}{dt'}\, dt', \\ = {} & E_1(t) - E_2(t), \text{ say,} \end{aligned} \qquad (2\text{-}79)$$

or finally,

$$v_p''(t) = v''(t) + E_1(t) - E_2(t). \qquad (2\text{-}80)$$

The particle speed is seen to comprise the fluid speed summed with the "peculiar motion" caused by gravity and the motion caused by the inertial effect of fluid accelerations.

While (2-80) has the same defect as (2-66), that b,c become complex for $\frac{\rho_s}{\rho} > \frac{5}{8}$, the remedies are also the same; either replace b, c by $B \pm iC$ and use the forms given by Brush, Hau-wong Ho and Ben-chie Yen (1964), or to use tables of erfc for complex arguments (Table 7.9, Abramowitz and Stegun (1965)) as outlined by Hjelmfelt and Mockros (1967).

The inertial case.

(2-73) differs from (2-72) only by the absence of a gravitational term and the solution is clearly

$$v_p''(t) = v''(t) - E_2(t). \qquad (2\text{-}81)$$

Obviously, if a body of fluid containing a particle at rest is released to allow the fluid and particle to fall freely under the influence of gravity, $\frac{dv''}{dt}$ in the expanded form of (2-79) is g and $E_1(t) = E_2(t)$ (which may be verified by differentiating $E_1(t)$ with respect to t), showing that $v_p''(t) = v''(t)$ as common sense predicts.

CHAPTER THREE.

3. THEORY OF PARTICLE MOTION; HIGHER REYNOLDS NUMBERS.

3.1 Introduction.

The slow, rectilinear motion of a rigid sphere acted upon by a scalar force potential in an infinite region of viscous, incompressible fluid at rest has been shown to be described by the integro-differential equation (2-59) provided:

(a) the motion is sufficiently slow for local to greatly exceed convective accelerations,

(b) there is no slipping at the sphere-fluid interface, and

(c) fluid far from the sphere is uninfluenced by its motion.

In particular, for free fall from rest under gravity, this equation may be easily integrated to (2-66). That the theory agrees with observation has been demonstrated by Brush, Ben-Chie Yen and Hau-Wong Ho (1964) and Hjelmfelt and Mockros (1967). Figure 3-1 is redrawn from Hjelmfelt and Mockros, who compared results of spheres falling in glycerine with the theoretical displacement-time curve obtained by integrating (2-66).

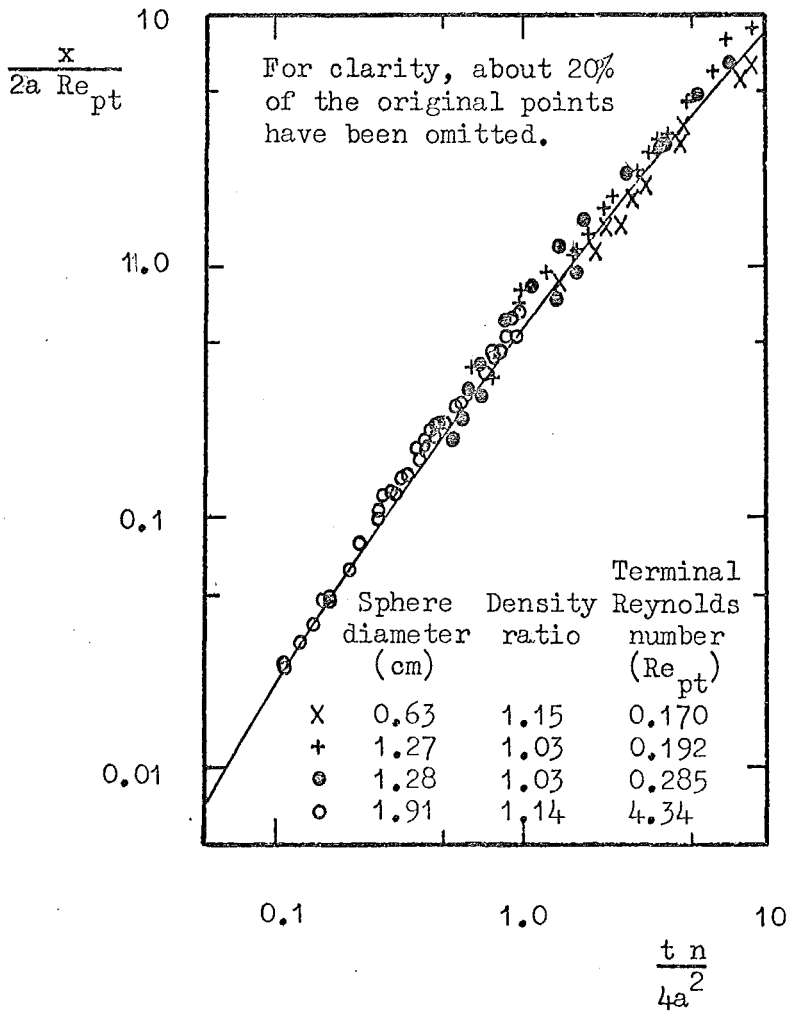

Figure 3-1. Comparison of the displacement-time relation from (2-66) with experiment, Hjelmfelt and Mockros (1967).

There is no theoretical difficulty in extending the analysis to an ambient fluid moving in the direction of the rectilinear motion of the sphere with a speed which is a function of time (2.7). Thus (2-75) or (2-80) adequately describe the motion of a sphere moving vertically while surrounded by fluid whose (laminar) speed is not steady. However, the parenthetical qualification that the fluid motion should be laminar, together with (a) above, raises queries which must be answered before treating cases more commonly found in real flows. Outstanding questions are these:

How does the expression for resistance to particle motion (2-57) change;

1. when the ambient fluid flow remains laminar distant from the sphere but the relative particle Reynolds number, Re_p, increases to such values that, for steady flow, the resistance would no longer be linear in (v_p-v)?

2. when the ambient fluid flow is turbulent but Re_p (based upon mean particle and fluid speeds) is small enough to correspond to the region (a), above?

3. when both; the ambient fluid flow is turbulent and Re_p increases as in 1?

In so far as answers to these questions are separable they will be answered separately in the following sections. The subject is mathematically intractable and dimensional

analysis aided by physical argument is used.

3.2 Non-linear resistance; laminar ambient flow.

Dimensional analysis of steady-state drag using the five variables ρ, v_p, a, m, D, with the first three as repeating variables yields dimensionless groups $\frac{\rho v_p a}{m}$, $\frac{D}{\rho v_p^2 a^2}$, or the familiar form

$$D = C_D(Re_p) \frac{\rho v_p |v_p|}{2} \pi a^2 , \qquad (3\text{-}1)$$

or, if $C_D(Re_p) = \frac{4C_D'(Re_p)}{Re_p}$

$$D = C_D'(Re_p)\, \pi a m v_p . \qquad (3\text{-}2)$$

D, drag

C_D, C_D' steady-state drag coefficients

Re_p, particle Reynolds number $\frac{2\rho |v_p| a}{m}$

v_p, particle speed (constant, and in still fluid $v = 0$)

m, fluid dynamic viscosity

a, particle (sphere) radius

ρ, the fluid density.

It has been established by experiment that C_D is approximately constant for very high Re_p and that C_D' is approximately constant for low Re_p; this latter evidence has been shown to agree with the theory of Stokes; $C_D' = 6$ for Re_p small compared to unity. The full solution to Oseen's approximation, Goldstein (1929), gives

$$C_D' = 6(1 + \frac{3Re_p}{16} - \frac{19(Re_p)^2}{1280} + \ldots).$$

What variables, including perhaps operations on v_p, should be used for non-steady speed are not obvious. The known analytical expression for non-steady drag at low Re_p, (2-57), shows that values of the pertinent variables at time t do not completely specify the value of the resistance at time t - the history term demands that notice be taken of values at all previous times, t', from initiation of motion until time t.

The variables known to be adequate for a description of steady drag at high particle Reynolds numbers, (3-1), are all included in the analytical expression for low Reynolds number steady drag, (3-2), explicitly in the full solution to Oseen's approximation, but ρ disappears from Stokes' expression [illegible]. To describe higher Reynolds number non-steady drag one might then choose the variables appearing in the analytical expression for low Reynolds numbers, (2-57). Instead of $C_D' \pi amv_p$ for steady viscous drag, the terms from (2-57) to consider are

$$6\pi amv_p + \frac{2}{3}\pi a^3\rho \frac{dv_p}{dt} + 6a^2\sqrt{\pi m\rho} \int_0^t \frac{1}{\sqrt{t-t'}} \frac{dv_p}{dt'} dt' .$$

Apart from the variables already considered in steady drag two operations on v_p are now present, the first time derivative and the integral of its "history" at previous

instants t'. Two ways of continuing the analysis are suggested:

(a) A simple approach is to accept the two operations on v_p as two extra variables, assuming that their form may be retained as Re_p increases. The variables are then

$$\rho,\ v_p,\ a,\ m,\ D,\ \dot{v}_p(t) = \frac{dv_p}{dt}\ ,\ \int_0^t \frac{\dot{v}_p(t')}{\sqrt{t-t'}}\,dt'\ .$$

The same repeating variables ρ, v_p, a with m, D and the two extra variables in t give $\frac{\rho v_p a}{m}$, $\frac{D}{\rho v_p^2 a^2}$ as in the steady state case and two more dimensionless groups:

$\frac{a\dot{v}_p}{v_p^2}$, the acceleration number, Ac (c.f. Froude number),

$\frac{\sqrt{a}}{\sqrt{v_p^3}} \int_0^t \frac{\dot{v}_p(t')}{\sqrt{t-t'}}\,dt'$, which will herein be denoted by Hi.

The non-steady drag is

$$D = \rho |v_p| v_p a^2 F_1(Re_p,\ Ac,\ Hi) \qquad (3\text{-}4)$$

and by choosing F_1 of the form

$$\frac{12\pi}{Re_p} + \frac{2\pi}{3} Ac + 6\sqrt{\frac{2\pi}{Re_p}}\ Hi$$

the known expression for low particle Reynolds numbers (2-57) is obtained (not taking any scalar force potential or other than rest initial conditions into account).

(b) Approach (a) can be generalised by not limiting time derivatives of v_p to the first and by not prescribing the form of the history term. Instead, include all non-zero derivatives and time t as variables, recognising that a history term involving previous instants t' might be necessary in unknown functions of the resulting dimensionless groups. The chosen variables are

$$\rho,\ v_p,\ a,\ m,\ D,\ {}_n\dot{v}_p(t),\ t$$

where ${}_n\dot{v}_p(t)$ is the 'n'th derivative of the particle speed, $\frac{d^n v_p(t)}{dt^n}$. The two extra dimensionless groups are now

$$\frac{a^n\ {}_n\dot{v}_p}{v_p^{n+1}}, \quad \text{and}$$

$$\frac{v_p t}{a}, \text{ say } Ac_n \text{ and } Ti \text{ respectively } (Ac_1 = Ac).$$

The alternative form to (3-4) is

$$D = \rho |v_p|\, v_p a^2\, F_2\,(Re_p,\ Ac_n, Ti). \qquad (3\text{-}5)$$

To obtain (2-57) for low particle Reynolds numbers F_2 must be chosen of the form

$$\frac{12\pi}{Re_p} + \frac{2\pi}{3} Ac + 6\sqrt{\frac{2\pi}{Re_p}} Ac \sqrt{Ti} \quad \frac{1}{\sqrt{t}\ \dot{v}_p} \int_0^t \frac{\dot{v}_p(t')}{\sqrt{t-t'}}\, dt'$$

(Again there is no scalar force potential gradient, and the fluid is initially at rest.)

Either (3-4) or (3-5) could be thought of as a solution

for non-steady, non-linear resistance in the same way as (3-1) is the solution for steady, non-linear resistance, where $C_D(Re_p)$ must be found by careful experiments (the so-called standard curve of C_D, Re_p).

Trials to determine this relationship have continued since the turn of the century, C_D actually depending upon Re_p, relative surface roughness, ambient fluid turbulence; the empirical determination of the dependence of F_1 upon the three parameters Re_p, Ac, Hi (or worse, upon (n+2) parameters Re_p, Ac_n, Ti) would be a formidable task.

Some experimental evidence is available on the form of F_1 or F_2, but different workers have used differing approaches and reached conclusions which are sometimes directly contradictory, more often inconclusive. A comprehensive review by Torobin and Gauvin (1959a, 1959b, 1959c, 1960a, 1960b, 1961a) and a later paper by Clamen and Gauvin (1969) clearly illustrate this and related problems. It seems clear from the review, and Torobin and Gauvin's own experiments in particular (1960b, 1961b, 1961c) that much of the confusion about the answer to the first question posed in 3.1, on non-linear resistance in laminar ambient fluid, has been caused by the intrusion of flow disturbances (turbulence) - the matter referred to in the second and third questions. Some of the results are shown in Figure 3-2, drawn using results collected mostly from Torobin and Gauvin's review.

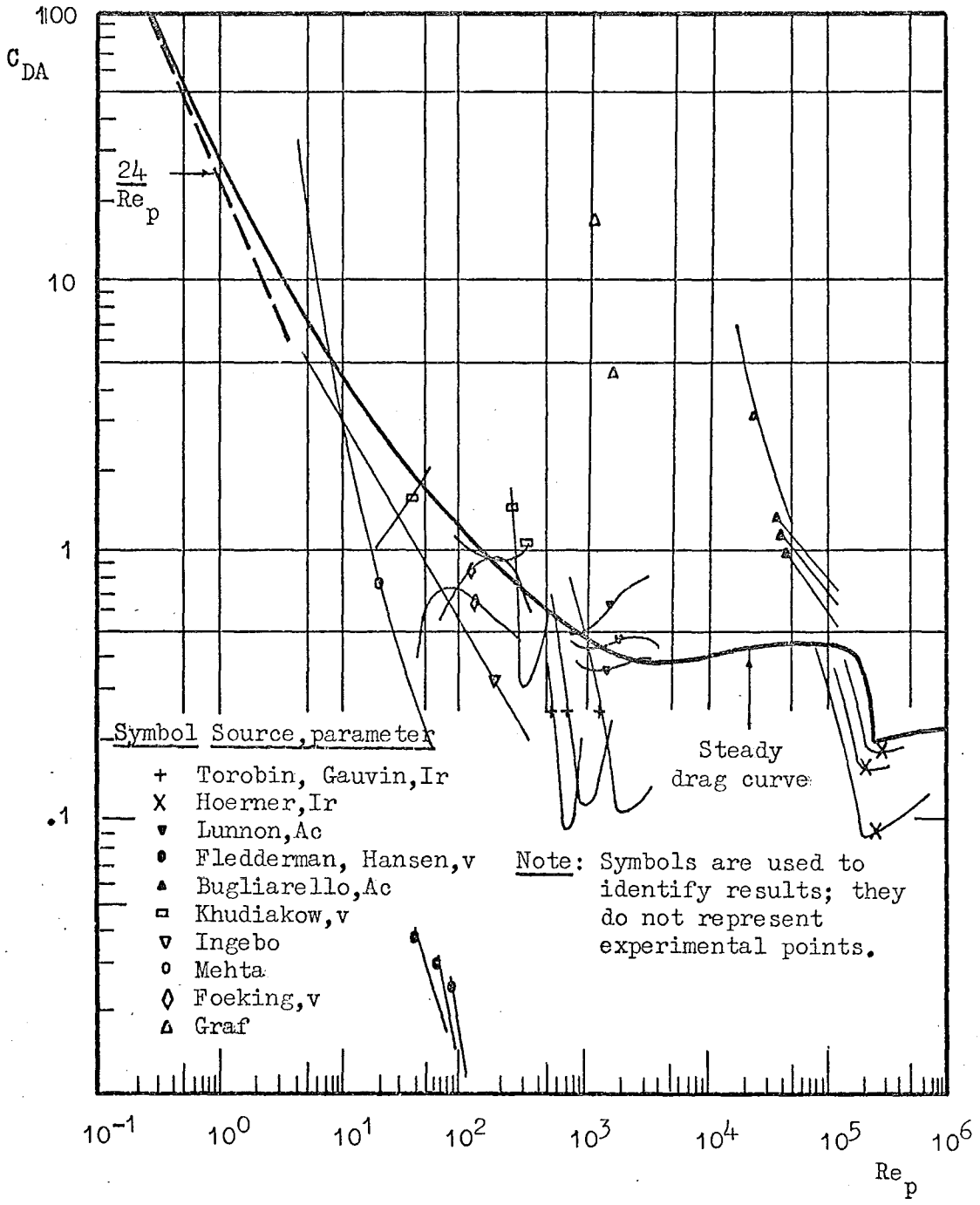

Figure 3-2. Non-steady drag coefficients.

3.21 Particular forms for F_1 in (3-4) or F_2 in (3-5).

The nature of F_1 or F_2 will be considered in this sub-section presuming that turbulence is not present in the ambient flow, and turbulence considered in 3.3, 3.31.

Forms of the equation for drag have been suggested which are effectively choices of particular F_1 or F_2. Commonly (Lunnon (1924), Graf (1967), Tchen (1947))

$$F\ (Re_p, Ac) = \frac{\pi}{2}\frac{|v_p|}{v_p} C_D(Re_p) + \frac{4\pi}{3} Ac\ C_A(Ac)\ , \qquad (3\text{-}6)$$

i.e. any history effect is neglected or included in the acceleration coefficient, C_A. Substitution of (3-6) in (3-4 or 5) yields

$$D = C_D(Re_p)\ \frac{\rho |v_p| v_p}{2}\ \pi a^2 + C_A(Ac)\ \frac{4\pi}{3}\ a^3 \rho\ \dot{v}_p \qquad (3\text{-}7)$$

which expresses the drag as a sum of the empirically known steady-state drag and an added mass term whose coefficient, a function of the acceleration, is to be determined. number

Lunnon (1924) and Graf(1967) have felt that (3-7) fits their experimental results but Torobin and Gauvin and others thought it better to take an overall drag coefficient, C_{DA}. The approach is favoured by those who consider the added mass concept "loses theoretical significance and practical utility"(Torobin and Gauvin (1959c)) when the flow passes beyond the very beginning of rectilinear motion. In this approach

$$F(Re_p, Ac) = \frac{\pi}{2} \frac{|v_p|}{v_p} C_{DA}(Re_p, Ac)$$

so that, from (3-4 or 5)

$$D = C_{DA}(Re_p, Ac) \frac{\rho v_p |v_p|}{2} \pi a^2 .$$

The evidence on the dependence of C_{DA} upon its parameters conflicts. Torobin and Gauvin (1960b) detected no acceleration effect but dependence upon the relative turbulence intensity of the ambient flow as well as upon Re_p. Lunnon(1926) and Bugliarello (quoted in Torobin and Gauvin (1959c)) found C_{DA} to depend upon both Ac and Re_p. Keim (1956), working with cylinders accelerated from rest also found dependence upon Ac and Re_p but Iverson and Balent (1951), with discs, correlated their results using Ac alone. Some of these results are included in Figure 3-2.

To the writer's knowledge, the only other form for F_1 or F_2 reported was suggested by Odar and Hamilton (1964), who studied a sphere oscillating with simple harmonic motion in a fluid. Their drag expression is obtained by putting

$$F(Re_p, Ac, Hi) = \frac{\pi}{2} \frac{|v_p|}{v_p} C_D(Re_p) + \frac{4\pi}{3} Ac \, C_A(Ac) + C_H(+) \sqrt{\frac{\pi}{Re_p}} Hi$$

so that

$$D = C_D(Re_p) \frac{\rho v_p |v_p|}{2} \pi a^2 + C_A(Ac) \frac{4\pi}{3} a^3 \rho \dot{v}_p +$$

(over page)

(equation continued from previous page)

$$C_H(+)\ a^2 \sqrt{\pi m \rho} \int_0^t \frac{1}{\sqrt{t-t'}}\, \dot{v}_p(t')\, dt' \ .$$

$C_H(+)$ was said to be a function of dimensionless combinations of v_p, t, a, and was later found experimentally to be a function of Ac alone, for Re_p up to 62.

3.3 Turbulent ambient flow.

Returning now to the second and third questions posed in 3.1; namely, how does the resistance to particle motion change when the ambient fluid flow is turbulent? The starting point to derive the analytical expression for the resistance at low particle Reynolds numbers in laminar ambient flow (2-57) involves

(a) Navier-Stokes equation (2-13),

(b) continuity equation (2-10),

(c) boundary conditions (2-23,24,25).

For turbulent ambient flow the following must be considered:

(d) Reynolds equation (3-10),

(e) continuity equation (as for (2-10), but mean velocity components),

(f) boundary conditions as before (for the mean flow).

In the remainder of this chapter v_p, v denote mean speeds, and would be written $\overline{v}_p$, $\overline{v}$ in the usual notation, $v_p = \overline{v}_p + v'$.

3.31 Dimensional analysis considering turbulence parameters.

Extending the dimensional analysis of 3.2 requires a choice of variables to allow for the dependence of drag upon turbulence. Such choice is not straight-forward; Townsend (1956) states (page 12) "... the statistical description of a turbulent field requires a knowledge of the complete joint probability distribution function for the velocity components at all points in space." Clearly, this cannot be realised in practice but to specify a 3-dimensional turbulent field, which may be anistropic, these parameters seem important : three typical periods, P_i (or frequencies); three typical length scales, L_i; and three intensive measures of energy, say, $\sqrt{\overline{u_i'^2}}$.

Using ρ, v_p, a for repeating variables as in 3.2 the dimensional analysis yields the groups involved in (3-4) or (3-5) as before and nine more:

$\frac{v_p P_i}{a}$, Strouhal numbers,

$\frac{L_i}{a}$, and

$\frac{\sqrt{\overline{u_i'^2}}}{v_p}$, turbulent intensities,

i = 1,2,3 in the three expressions. When there is rectilinear mean motion of fluid, speed v, and spherical particle, speed v_p, the first and last expressions are

more meaningful written in terms of slip speed, $v_p - v$, and such intensities will be referred to thus:

$$\frac{\sqrt{\overline{u_i'^2}}}{v_p - v} = Ir_i, \text{ relative turbulent intensities.}$$

(note that not all workers in the field use this terminology, many calling $\sqrt{\overline{u_i'^2}}$ intensities, and relative intensities when divided by v).

(3-4) now becomes

$$D = \rho |v_p| v_p a^2 F_3(Re_p, Ac, Hi, \frac{v_p P_i}{a}, \frac{L_i}{a}, Ir_i) \quad (3\text{-}8)$$

(3-5) becomes

$$D = \rho |v_p| v_p a^2 F_4(Re_p, Ac_n, Ti, \frac{v_p P_i}{a}, \frac{L_i}{a}, Ir_i). \quad (3\text{-}9)$$

Effective forms for F_3 or F_4 have rarely been suggested. Torobin and Gauvin (1960b) refer to wind tunnel tests, by Dryden and co-workers (referenced as Dryden (1929,1931,1935,1937); see also article 219, Goldstein (1938)), which seem best correlated by a plot of Re_c against

$$\frac{\sqrt{\overline{v'^2}}}{v} \left(\frac{2a}{L_e}\right)^{\frac{1}{5}}, \text{ where}$$

Re_c is "critical" particle Reynolds number corresponding to $\frac{2D}{\rho v |v| \pi a^2} = 0.3$,

L_e is an Eulerian integral (transverse) scale, and the sphere was fixed, $v_p = 0$, in a stream mean speed

v, longitudinal fluctuations v'.

This relationship had been advanced by Taylor (1936) from a consideration of the effect of pressure fluctuations in the free stream upon transition from laminar to turbulent flow in the boundary layer (which was assumed characterized by the Karman-Pohlhausen theory, see Schlichting (1960)). Taylor used grid mesh length rather than L_e but his original statement was in terms of micro-scale, λ. Retracing his argument but retaining λ, the appropriate relation is

$$Re_c = F\left[\frac{\sqrt{\overline{(v')^2}}}{\nu}\sqrt{\frac{2a}{\lambda}}\right] .$$

The one-fifth power in the previous expression arises from the relation Taylor uses to relate grid mesh length, M, to λ

$$\frac{\lambda}{M} = A\sqrt{\frac{m}{\rho M\overline{(v')^2}}} .$$

Torobin and Gauvin (1960b) use this equation to relate L_e to λ, stating that it is true for isotropic turbulence. They continue a largely qualitative discussion of other results, including their own with a suggested relationship (3-12) which will now be examined in a new light.

The approximation involved in neglecting the quadratic term in Navier-Stokes equation (2-13), as done in 2.11, is expressed in this way by Milne-Thompson (article 19.62, 1955). The dimensions of the retained viscosity terms,

$\frac{m\, d^2u_i}{\rho\, dx_j dx_j}$, are those of $\frac{m\, v_p}{\rho\, a^2}$ and the dimensions of the neglected terms, $u_j \frac{du_i}{dx_j}$, are those of $\frac{v_p^2}{a}$. Neglect of the quadratic term therefore requires the ratio

$$\frac{\frac{v_p^2}{a}}{\frac{m\, v_p}{\rho\, a^2}} = \frac{\rho\, a\, v_p}{m}$$

to be small, i.e. small Reynolds number, as is generally accepted.

Now extend the reasoning to further neglect the final term in Reynolds equation (1.187, Hughes and Gaylord (1964)),

$$\frac{d\bar{u}_i}{dt} + \bar{u}_j \frac{d\bar{u}_i}{dx_j} = -\left[\frac{1}{\rho}\frac{d\bar{p}}{dx_i} + \frac{dX}{dx_i}\right] + n\frac{d^2\bar{u}_i}{dx_j dx_j} - \frac{d}{dx_j}\overline{u_i' u_j'}, \qquad (3\text{-}10)$$

whose dimensions are those of $\frac{\overline{v'^2}}{a}$; their neglect requires the ratio

$$\frac{\frac{\overline{v'^2}}{a}}{\frac{m\, v_p}{\rho\, a^2}} = \frac{\rho\, a\, \overline{v'^2}}{m\, v_p} = \frac{\rho\, a\, v_p}{m}\left[\frac{\sqrt{\overline{v'^2}}}{v_p}\right]^2 \qquad (3\text{-}11)$$

to be small. $\frac{2\rho\, a\, v_p}{m}$, the particle Reynolds number, is already required to be small for the neglect of the quadratic terms; when it is not small drag is a function of it. Now it appears that to further neglect Reynolds

stresses, $\frac{\sqrt{\overline{v'^2}}}{v_p}$ must not be large; it seems reasonable that when Reynolds stresses are not small drag will depend upon (3-11). This dimensionless product of particle Reynolds number and the square of turbulence intensity does not seem to have been advanced from such reasoning in discussions on drag but a closely similar product was proposed by van der Hegge Zijnen (1958) (quoted in Torobin and Gauvin (1960b)) in connection with heat transfer from cylinders to a turbulent air flow. At low Reynolds number (60 to 580), heat transfer rate was experimentally found to be unaffected by turbulence intensities up to 13%; at higher Reynolds numbers (600 to 25,800) the rate was affected and the increase a function of

$$\frac{a\,v}{n}\,,\quad \frac{\sqrt{\overline{v'^2}}}{v}\quad \text{and}\quad \frac{L_e}{a}\quad (L_e \text{ is Eulerian scale}).$$

Van der Hegge Zijnen proposed that the first two be combined into their product,

$$a\frac{\sqrt{\overline{v'^2}}}{n}\,,\ \text{which is (3-11) multiplied by}\ \frac{v_p}{\sqrt{\overline{v'^2}}}\,.$$

Torobin and Gauvin (1960b) suspect such combination "... since it presupposes that the functional form of both parameters will be identical ..." If, for instance, the true functional form of the first two parameters is $\frac{a\,v}{n}$,

$\left[\frac{\sqrt{\overline{v'^2}}}{v}\right]^2$, their product yields (3-11) (except that (3-11) refers to a sphere in motion with fluid speed v=0 whereas van der Hegge Zijnen has a fluid stream in motion with v_p=0). (This argument does not, of couse, prove that the functional form is as instanced; it merely shows that the results of van der Hegge Zijnen's work are not incompatible with (3-11)).

In their own experiments on drag coefficients of spheres in both steady and accelerated motion, Torobin and Gauvin found F_3 or F_4 in (3-8,9) to be a function of Re_p, Ir, with no effect caused by acceleration, and no dependence on the time since beginning the motion (i.e. no dependence on Ac in (3-8), Ac_n or Ti in (3-9)). By considering a ratio of turbulent energy incident on "quasi-laminar" flow near a sphere to energy associated with viscous damping of fluctuations they suggest that a criterion for transition to a turbulent boundary layer is

$$Re_c \, Ir^2 = \text{constant.} \qquad (3\text{-}12)$$

Their argument is very similar to that which gave (3-11); they suggest a critical value of the energy ratio which will allow sufficient penetration of free-stream fluctuations for production of turbulence in the boundary layer flow. Then, at transition, the ratio, which equals

(3-12), should be constant for whatever individual values of Re_c, Ir (actually these authors say for "high turbulent levels"). Compared with their experimental results they consider the fit of the theory "surprisingly good"; Figure 10, Torobin and Gauvin (1960b). They qualify their results by predicting that the steeply-sloped transition curves will not exist at Reynolds numbers much below 100 and at very small Reynolds numbers, as skin friction would predominate, "relative turbulence effects would probably always cause a drag increase..."

The difficulties in determining F_1 or F_2 cited in 3.2 can be added to for F_3 or F_4.

1. As is clear from the abundant literature on turbulence, adequate description of a three-dimensional field is extremely difficult. $\overline{u_i'^2}$ conveys nothing about the distributions of $u_i'^2$ spatially, temporally or with frequency except mean values; should L_i be chosen as Eulerian space scales (for instance), these too are effectively point values and, if P_i are important the description of a spectrum of periods or frequencies by one value is also inadequate.

2. Simplifying cases of isotropy (when, among other simplifications, $\overline{u'^2} = \overline{v'^2} = \overline{w'^2}$) or homogeneity (when, among other simplifications, $\overline{u_i'^2}$ are independent of position) do not remove all the problems of 1.

3. Should F_3 or F_4 actually depend respectively on all twelve or (n+11) parameters in their arguments a comprehensive series of tests would be impracticable and the results difficult to present and use.

4. The influence of turbulence on e.g. Ac or Hi in particular, is not known.

5. A moderate turbulence intensity in the ambient fluid can be very great compared, as in Ir, to the sphere-fluid relative speed.

Little more can be said about F_3 or F_4 from available experimental evidence than what Torobin and Gauvin (1960b) have said in conclusions to Part V of their review:

"The extent to which the free-stream turbulence exerts an influence on the particulate momentum transfer depends upon the magnitude of the relative turbulence parameters and the Reynolds number. The intensity value would seem to be the predominating turbulence parameter with the scale lengths occupying a secondary position. Increasing intensities cause a systematic regression of the transition region of the drag coefficient curve towards lower Reynolds numbers, together with a moderate increase of the drag coefficients for both the subcritical and supercritical Reynolds numbers. The free-stream turbulence also diminishes the drag coefficient dependency on the acceleration which had been previously noted in laminar systems and this

probably results from a decreased orderliness in the wake structure as a result of the turbulence."

It seems that F_3 or F_4, even if correct, cannot be simplified until more information is available, although one may speculate that certain of the parameters will have negligible effect in certain circumstances, as is known to be the case for very low particle Reynolds numbers and very low turbulence levels when $F_3 = F_1$ or $F_4 = F_2$ (see 3-4,5,8,9)

3.4 Importance of the parameters in the drag term.

In previous sections of this chapter the problem of non-steady drag has been examined by dimensional analysis. Some experimental results from previous workers and their suggested forms for drag expressions have been fitted into the resulting pattern. Except for very low particle Reynolds numbers and very low relative turbulence intensities the explicit form of drag expressions is unknown, and even what parameters should be included in such expressions is uncertain. To provide a better understanding of the physical situation a simple model is proposed, from which the relative importance of the parameters in F_3 or F_4 is determined. (For an excellent use of such a model and clarification of some of the vorticity dynamics employed see article 5.4 of Batchelor (1967)). It must be acknowledged that the method has severe limitations and

is justified only by the lack of a reasonable alternative. Using energy and vorticity considerations and the observed flow patterns, essentially the same argument is repeatedly applied to steady and non-steady drag at low Re_p (3.41), steady and non-steady drag at higher Re_p (3.42), and finally steady and non-steady drag when the ambient fluid is in turbulent motion (3.43). The relative motion of a smooth sphere is considered.

3.41 Importance of parameters at very low particle Reynolds numbers.

The drag, D_c, on a sphere moving at constant speed in a viscous fluid is known to be

$$D_c = 6\pi a m v_p. \qquad (3\text{-}13)$$

This arises from the velocity distribution near the sphere boundary and comprises skin friction ($4\pi a m v_p$) and form drag ($2\pi a m v_p$). The no-slip condition at the sphere boundary creates vorticity there which spreads outwards by molecular diffusion and is convected by the relative motion, and the sphere is moving through fluid in which this vorticity is present.

The drag force is now doing work in steady motion (unlike the inviscid case, where there is drag only when the particle is accelerating), adding kinetic energy to the fluid motion at a constant rate.

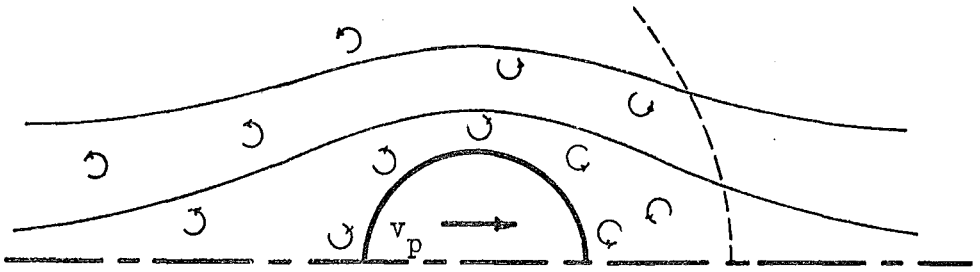

It will be convenient in the following to consider as separate the fluid kinetic energy associated with the mean flow pattern, Em, and that associated with the addition of vorticity, Ew, which is superimposed upon this. Em is not changing in steady motion, the kinetic energy added increasing Ew at a rate

$$D_c \, v_p = \frac{dEw}{dt} \, . \qquad (3\text{-}14)$$

Now consider the sphere accelerating through the viscous fluid yet still at very low Re_p.

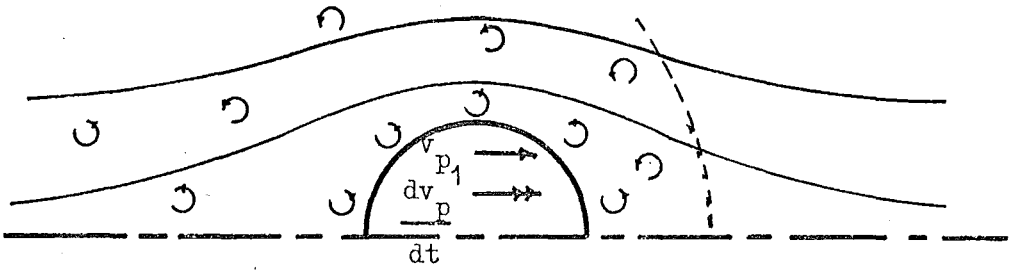

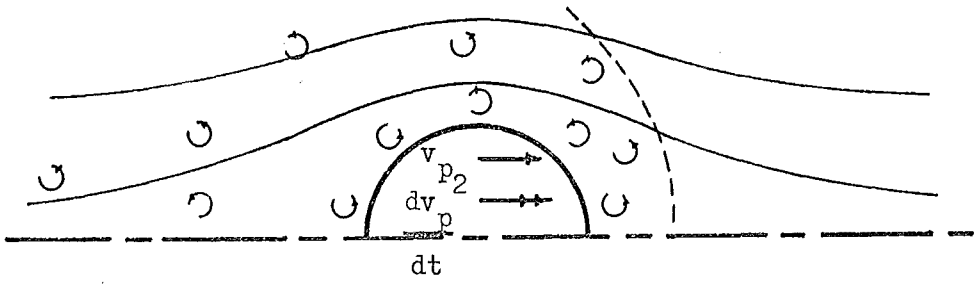

The situation differs from the steady-state in at least two ways:

(i) At $t+\delta t$, the sphere finds itself in vorticity different from that which would have been present had the motion been steady (at v_{p_2}) - instead of overtaking decaying vorticity generated at previous instants by the sphere speed v_{p_2}, the decaying vorticity encountered is that generated at previous instants by a sphere moving with a range of lower speeds characteristic of the accelerating motion. This aspect of the velocity distribution gives a "history" force not present in steady motion which is (T_6 in (2-59))

$$6a^2\sqrt{\pi m \rho}\int_{t_o}^{t}\frac{1}{\sqrt{t-t'}}\,\dot{v}_p(t')\,dt'$$

(ii) The fluid kinetic energy associated with the

mean motion has clearly increased between t and t+δt, quite apart from the fact that addition of energy to vorticity is now at an increased rate. If an external force, P, is acting to accelerate the sphere, mass m_p, and thereby doing work,

$$P\, v_p = \frac{d}{dt}\left(\frac{1}{2} m_p v_p^2 + Em + Ew\right)$$

so that

$$P - \frac{1}{v_p}\frac{d}{dt}(Em + Ew) = m_p \frac{dv_p}{dt} . \qquad (3\text{-}15)$$

The accelerating force is seen to comprise the external force less an added mass force, $\frac{1}{v_p}\frac{dEm}{dt}$, and less a viscous drag force, $\frac{1}{v_p}\frac{dEw}{dt}$. In fact, the mathematical treatment of this low Reynolds number case (Chapter Two) shows that the added mass term has the same form as in inviscid flow and the viscous drag has the same form as the steady speed drag, (3-13).

In inviscid flow there is no addition of vorticity via Ew as the no-slip condition does not have to be met and (3-15) becomes

$$P - \frac{1}{v_p}\frac{dEm}{dt} = m_p \frac{dv_p}{dt}$$

and as the energy of the fluid motion is $\frac{\pi a^3}{3}\rho\, v_p^2$ in this case (article 15.32, Milne-Thompson (1955)),

$$P - \frac{2\pi a^3}{3}\rho\frac{dv_p}{dt} = m_p \frac{dv_p}{dt} ,$$

i.e. the added mass force is that already noted in Chapter Two (T_5 in (2-59)),

$$\frac{2\pi a^3}{3} \rho \frac{dv_p}{dt} .$$

3.42 Importance of parameters at higher particle Reynolds numbers.

Consider, now, the sphere to be moving at constant velocity in laminar ambient fluid, but at much higher particle Reynolds numbers than above (say greater than 100 in contrast to less than unity). With convection of vorticity now much more effective than diffusion the familiar wake structure (and its equally familiar mathematical difficulties) appears. The linear dependence of drag on v_p when skin friction predominated is now nearer to the dependence of drag on v_p^2 suggested by the Bernoulli equation. The constant, 6, in (3-13) can be replaced by $C_D'(Re_p)$ to give (3-2) or, as is more usual, the equation is rewritten in terms of the square of velocity as (3-1),

$$D_c = C_D(Re_p) \frac{\rho v_p |v_p|}{2} \pi a^2 . \qquad (3\text{-}16)$$

The drag is now largely form drag (pressure on upstream face approximates stagnation pressure while wake pressure approximates the free-stream value), and induced drag (due to the energy in the trailing vortices). Skin friction is of the same order as for a stream-lined body of similar surface area in similar flow and is probably smaller than

either form or induced drag. The vorticity is effectively confined to the wake region and a mean flow exists outside it. (3-14) applies with the new value of D_c.

The argument given for low Re_p is retraced, acknowledging that the corresponding mathematical description for the present case is unknown.

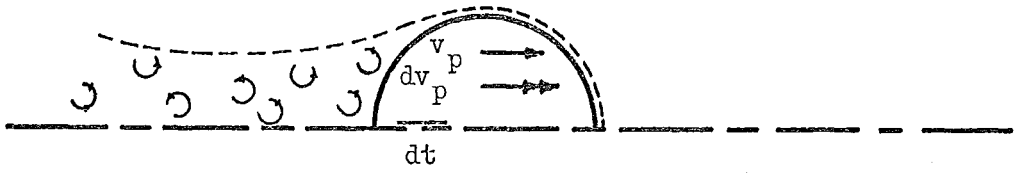

(i) Vorticity produced at the surface of the sphere is now being convected downstream in the thin boundary layer as it is produced. Vorticity diffuses outwards at a speed whose order is $\frac{m}{\rho l}$ (c.f. 5.4, Batchelor (1967)), where l is the distance from the sphere and if $\frac{\rho v_p a}{m}$ is much greater than unity, as here, the convection

(represented by v_p) is at a much higher rate than diffusion (represented by $\frac{m}{\rho a}$ for diffusion distances of the order of the sphere dimension). Comparing this situation with (i) of 3.41, it seems that the opportunity for the sphere to detect differences in vorticity at its surface which depend upon the vorticity generation at previous speeds is now almost entirely lost. The predominance of convection over diffusion confines the vorticity to the thin boundary layer and, although the boundary layer shape and overall flow pattern might change, a history effect because the sphere is "overtaking" differing vorticity distributions does not now seem likely. Skin friction may well be different but this is small as has been mentioned.

(ii) The argument of 3.41 (ii) concerning the increase in kinetic energy of the mean flow between t and $t+\delta t$ could still be expected to apply. However, there is now difficulty in deciding what is meant by Em and what by Ew. An important uncertainty is in what way the flow pattern around a sphere, speed v_p, which has been and is accelerating at $\frac{dv_p}{dt}$, differs from that around a sphere which has been and is moving at a steady speed, also v_p. Keim (1956) suggests that a lag is exhibited, accelerating flow patterns resembling steady flow patterns of lower Re_p, and consideration of the changes which have to be made (e.g. to boundary layer separation position) reinforces this view.

(3-15) may be said to still hold but $\frac{1}{v_p}\frac{dEw}{dt}$ is not necessarily the same value, D_c, as was used in (3-16), although for low Re_p this is known to be true (see 3.41(ii)). And, for some reasonable interpretation of Em (defined in 3.41 as "the kinetic energy associated with the mean flow pattern") it seems that an added mass force will exist and continue to depend upon Re_p and Ac, though not in the explicit manner of 3.41(ii). The essential point of this contention is simply that for kinetic energy of the mean fluid motion to be increased, energy must be transferred (transformation from some other form is not an issue) from a convenient source or a force must do work. Work from a force-distance effect on the sphere seems much more likely than energy transfer from another source, e.g. vorticity from the no-slip condition.

It is known that a decrease in drag occurs (at Re_p in the order of 10^5 for a sphere fixed (v_p=0) in ambient flow) when the separated boundary layer becomes turbulent, reducing the low pressure area on the downstream surface of the sphere, and that there is a slight drag increase as Re_p increases above this transition, likely to be the result of increased skin friction as the laminar-turbulent transition moves along the sphere surface towards the forward stagnation point. This does not contradict the argument concerning acceleration effects, but complicates

it for the transition region.

It is suggested, then, that for particle Reynolds numbers well above the Stokes region, and in the absence of ambient fluid turbulence, the total drag D of (3-4) is likely to have the functional form

$$D = \rho v_p^2 a^2 F_1(Re_p, Ac).$$

If it is accepted that higher derivatives of the particle speed than the first will be important, i.e. if one expects different drag according to the type of acceleration, the argument suggests that (3-5) would have the functional form

$$D = \rho v_p^2 a^2 F_2(Re_p, Ac_n).$$

3.43 Importance of parameters - turbulent ambient flow.

For the second repetition of the argument of 3.41 it is stipulated that the ambient fluid has turbulent motion; the relative motion of a sphere is of interest, the point of view of an observer moving with the mean speed of the fluid remote from the sphere. Two characteristics of turbulent flow concern us:

(a) The marked increase in diffusion rate of transportable quantities (which vorticity is in effect, article 5.2 Batchelor (1967)).

(b) The random motion of fluid "eddies".

The operation of (a) and (b) would probably change both

tangential and normal stress on the sphere from their values in laminar ambient flow. It has been suggested, and has been experimentally observed (section 3.3) that the magnitude of certain parameters describing the turbulence (intensity, scale) would affect the amount of change made to these stresses and their area of application so that the drag will depend upon the magnitude of such turbulence parameters. It is also suggested, and observed, that the ratio of inertial to viscous effects in the mean flow is still an effective variable so that particle Reynolds number, Re_p (now based on the mean relative flow), must be included in the required formulation of the drag. Although low Re_p flows might be expected to have distinctive qualities, as they do when turbulence is absent, as the form of expression for neither low nor high Re_p is known it is as well to consider them together.

Modifying (3-16) in view of the above

$$D_c = C_D\ (Re_p,\ \text{turbulence parameters})\ \frac{\rho\, v_p |v_p|}{2}\ \pi a^2\ ,$$

and reconsidering 3.41 (i & ii):

(i) Vorticity transfer is now effected by convection, and both molecular and turbulent diffusion. The physical nature of turbulent diffusion is not well understood (Chapter 6, Tchen and Schubauer (1959) or (1961)) but one may speculate that, for appreciable turbulent intensities and low particle Reynolds numbers, any systematic propagation

by molecular diffusion (c.f. 3.41(i)) would be lost in the random wandering due to turbulent diffusion. At higher particle Reynolds numbers, it has already been shown (3.42(i)) how any history effect could be of much diminished importance as convection predominates over diffusion of vorticity, and turbulence of the ambient fluid would not restore its importance. For all particle Reynolds numbers, therefore, no history effect would be expected.

(ii) Again the argument of 3.41(ii) (and 3.42(ii)) should apply. There is now another possible source of kinetic energy, that of the turbulent fluctuations, but the kinetic energy of the mean fluid motion is most unlikely to be increased at the expense of this supply; the reverse is known to be true. Much more likely is the force-distance effect of the sphere's motion, so that drag will still depend upon the acceleration. A sphere moving at relative speed v_{p_2} in a turbulent fluid, and one moving at v_{p_1} ($< v_{p_2}$) in an otherwise identical field of turbulence would be unlikely to have the same fluid kinetic energy associated with their motions, no matter how that energy is shared between the mean "streamline" motion, the turbulent fluctuations and the wake (ignoring conversion, e.g. to heat). Thus in changing from one speed to the other a force must be in effect which depends upon the rate of change, i.e. upon the acceleration.

3.44 Effect of density ratio and relative scale of turbulence.

At low particle Reynolds numbers, in the absence of turbulence, particle density has no effect on drag (see the equations following (3-4,5)); particle density is, of course, a factor determining the motion as shown in the full equation of motion (2-58). In turbulent flow the equation of motion applied to the detailed flow determines to what extent the particle will follow the fluid turbulent fluctuations. (For simple fluctuations, Hjelmfelt and Mockros (1966) have shown particle-fluid phase and amplitude relations for different density ratios). The extent to which turbulent fluctuations are followed influences $|v_p - v|$, upon which drag depends, so that in turbulent motion density ratio will affect drag. Apart from the explicit influence of particle density on the motion as shown by the mass-acceleration product of an equation of motion in the mean speeds v_p, v, density ratio influences the drag by way of the detailed flow and should be considered as a parameter in the drag term, although other workers in the field have not included it.

The other factor determining to what extent turbulent fluctuations influence particle motion is the ratio of particle diameter to turbulence scale. The motion of a particle considerably larger than the largest eddies present would be little affected by counteracting influences

of all the eddies over its surface; the motion of a particle small compared to the smallest eddies present would be much more influenced. Indeed, small particles of near-neutral buoyancy have been used to make Lagrangian measurements (i.e. following the particles) of turbulent water characteristics by Vanoni and Brooks (1955) on the assumption that they follow turbulent fluctuations exactly. Which scale is to be used as a parameter in F_3 or F_4 has not been specified, although an Eulerian spatial integral scale was used in Dryden's work (see 3.31). The relationship of this scale to microscale is known for isotropic turbulence and it may be that either microscale or integral scale are suitable parameters, even when the turbulence is anisotropic.

3.45 Importance of parameters in the drag term- a possible answer.

From the dimensional analysis of 3.31 and the subsequent argument of 3.4 to 3.44 the following possible description emerges to answer the questions posed in 3.1:

Table 3-1.

Form of the drag expressions.

A. Very low Ir_i

a. Very low Re_p $\quad D = \rho\, v_p^2\, a^2\, F(Re_p, Ac, Hi)$

b. Higher Re_p $\quad D = \rho\, v_p^2\, a^2\, F(Re_p, Ac)$

B. Higher Ir_i

a. Very low Re_p $\quad D = \rho\, v_p^2\, a^2\, F(Re_p, Ac, Ir_i, \frac{L_i}{a}, \frac{\rho_s}{\rho})$

b. Higher Re_p $\quad D = \rho\, v_p^2\, a^2\, F(Re_p, Ac, Ir_i, \frac{L_i}{a}, \frac{\rho_s}{\rho})$

Aa is well established (3.1), Ab is supported by much experimental evidence (3.21) while column B remains to be tested although Torobin and Gauvin have reviewed what little is known (3.31).

The particular forms of these functions are even less decided except that for Aa, which is given for F_1 or F_2 following (3-4,5) respectively. This theoretically derived result has been verified by experiment and the only qualification to its endorsement is that its derivation employs the same simplification as does the derivation of the steady Stokes drag, $6\pi a m v_p$, i.e. the sphere is treated as a stationary source of vorticity. The Oseen-Lamb improvement for steady flow (e.g. Rouse (1959)) treats the sphere as a moving source - it partially takes inertial terms into account, giving a more accurate picture of flow away from the sphere and the expression for drag given in

3.2. The particular form for Aa referred to could then be in error by not fully taking flow not near the sphere into account.

For Ab, most success has been achieved with (3.2)

$$F(Re_p, Ac) = \frac{\pi}{2} \frac{|v_p|}{v_p} C_{DA}(Re_p, Ac).$$

Experimental verification has been confused by the effects of turbulence in the ambient flow and more results are needed. Also, different types of acceleration give different results (Torobin and Gauvin (1959c)) and it might be that Ac_n (i.e. higher time derivatives of the velocity) are required.

Dryden, Kuethe, Schubauer, Mock and Skramstad (Dryden (1929, 1931, 1935, 1937) or see article 219, Goldstein (1938)) and Torobin and Gauvin have conducted experiments to determine the form of functions in column B. As has been mentioned in 3.31, they correlate their results best by

$$Re_c = f\left(Ir\left[\frac{2a}{L_e}\right]^{\frac{1}{5}}\right), \quad \text{(Dryden et al.)},$$

$$Re_c\, Ir^2 = \text{constant}, \quad \text{(Torobin and Gauvin)}.$$

To venture further than this in predicting the form of the expression for drag, or even to more adequately discuss the suggested forms reviewed in 3.21, is not justified by the present theoretical or experimental knowledge of the subject.

CHAPTER FOUR.

4. THEORETICAL ASPECTS OF THE EXPERIMENTS.

4.1 Introduction.

In 3.45 a possible form for the drag coefficient, C_{DA}, of a smooth sphere in non-steady, turbulent flow was proposed. Choosing the streamwise components of turbulence scale, L, and particle relative turbulence intensity, Ir, (they are the most meaningful for downstream progress of a particle) the form is,

$$C_{DA}\ (Re_p,\ Ac,\ Ir,\ \frac{L}{a},\ \frac{\rho s}{\rho}\ ). \qquad (4\text{-}1)$$

Several methods of measuring such drag coefficients have been used. Forces on spheres held in moving fluids by wires, threads or a sting have been measured but the resulting drag coefficients (e.g. Hoerner's results, Figure 3-2) are different from those measured when spheres are moving freely, in a still or moving fluid. Of the many measurements of drag coefficient made using spheres falling freely under gravity in a still fluid, most have been for steady speed only; also, it is obviously difficult to account for turbulence parameters in a still fluid. The results obtained by measuring the average slip speed of a suspension of spheres moving in a length of pipe and relating it to the pressure drop caused by the flow of the

suspension (e.g. Foeking's results, Figure 3-2) do not involve non-steady effects and rely on unsatisfactory averaging processes (see Torobin and Gauvin (1960b)). Torobin and Gauvin (1961b,c) and Gauvin and Clamen (1969) used a method which allows all the parameters in (4-1) to be measured. They projected particles at speeds both higher and lower than that of a surrounding steady, turbulent air stream, comparing average particle speed over a short distance with the average air speed measured by a total head probe. This last method is the most satisfactory so far reported.

The method used in this study is both akin to gravitational C_{DA} measurements and a useful and interesting complement to the method used by Torobin, Gauvin and Clamen. Slip of a particle in homogeneous, non-steady flow of a volume of fluid is similar to the gravitational acceleration of a particle in still fluid (see 2.71) but would be very difficult to provide experimentally. Instead, the convective deceleration of water passing through a diffuser was used to set up an inertial field. Particles whose density differed from that of water then had slip speed induced by the field and average particle speed over a short distance was compared with the local average water speed measured by a total head probe. The following favourable aspects of the method should be noted:

1. A local, mean velocity difference is obtained.

2. The deceleration and the turbulence parameters of the fluid can be altered merely by a change in flow rate.

3. The equipment necessary is simple and inexpensive.

4. The situation approximates commonly encountered flows; e.g. the flow in a centrifugal pump (or compressor) impeller.

5. The effects on C_{DA} values of this different method of determining them, and of using water instead of air, can be usefully compared with other results, those of Torobin and Gauvin in particular.

The fluid flow in a diffuser operating without stall, as in the experiments to be described, is locally steady but non-uniform with respect to coordinates fixed in the flow boundaries. The motion of the particles with respect to coordinates fixed in the fluid is non-steady. The method requires measurement of the non-steady (Lagrangian) velocity differences and the parameters in (4-1).

4.2 Calculation of non-steady drag coefficients.

It is explained in 2.7 that the pressure gradient which is included in the equation of motion (2-73) for a particle, velocity $\underline{vp}$, in a moving fluid whose velocity is $\underline{v}\ (\underline{x},t)$, must be determined from the Navier-Stokes equation (2-13). With fluid in rectilinear acceleration, $\frac{dv}{dt}$,

causing an inertial field, and v_p, v rectilinear speeds in the direction of $\frac{dv}{dt}$, the equation of motion (2-73) may be rewritten as

$$\frac{4}{3}\pi a^3 \rho_s \frac{dv_p}{dt} = \frac{4}{3}\pi a^3 \rho\left[\frac{dv}{dt} - n\left(\frac{d^2v}{dx^2} + \frac{d^2v}{dy^2} + \frac{d^2v}{dz^2}\right)\right] - D, \qquad (4\text{-}2)$$

where drag, D, replaces the last three terms of (2-73). Scalar force potential, X in (2-13), has been neglected as there was no external force in the flow direction for the experiments in this study. For higher Reynolds numbers and turbulent flow the expression for non-steady drag proposed in this thesis is given in Table 1 of 3.45, modified as in (4-1). By putting F in this table equal to $\frac{\pi}{2} C_{DA}$, where C_{DA} is the non-steady drag coefficient, and adapting the expression to a slip speed $(v_p - v)$, (4-2) becomes

$$\frac{4}{3}\pi a^3 \rho_s \frac{dv_p}{dt} = \frac{4}{3}\pi a^3 \rho\left[\frac{dv}{dt} - n\left(\frac{d^2v}{dx^2} + \frac{d^2v}{dy^2} + \frac{d^2v}{dz^2}\right)\right]$$

$$- C_{DA}\left(Re_p, Ac, Ir, \frac{L}{a}, \frac{\rho_s}{\rho}\right) \frac{\rho|v_p - v|\ (v_p - v)}{2} \pi a^2. \qquad (4\text{-}3)$$

The C_{DA} measurements were made in the plane-walled diffuser, 5.22. For a given particle which at time t is at downstream position x in the diffuser (coordinates attached to the flow boundaries), $x = x(t)$, $\frac{dx}{dt} = v_p$ and

$$\frac{dv_p}{dt} = v_p \frac{dv_p}{dx}. \qquad (4\text{-}4)$$

This requires the assumption that particle velocity components in the y,z directions are small compared to the component in the x direction, v_p. (Also, $\frac{dv_p}{dy}$, $\frac{dv_p}{dz}$ should be small compared to $\frac{dv_p}{dx}$). This is very likely for particles near the diffuser central axis, but if a particle is travelling parallel to a diverging wall of this particular diffuser the y component of particle velocity is 100 tan(5 degrees) = 8.75% of the x component; all measurements considered came from the central 60% of the diffuser in both y and z directions, some from the central 20% only. The diffuser flow was steady ($\frac{dv}{dt} = 0$) and non-uniform so that

$$\frac{dv}{dt} = v \frac{dv}{dx} \text{ , approximately,} \qquad (4\text{-}5)$$

where an assumption about water velocity components similar to that required for (4-4) has been made.

A simplification can now be introduced by considering the orders of magnitude of $\frac{dv}{dt}$ and $n v^2 v$ in (4-3). The curvatures of the six measured $\frac{v}{v_m}$, $\frac{y}{y_m}$ and $\frac{v}{v_m}$, $\frac{z}{z_m}$ profiles within the diffuser, Figure 6-2, are approximately constant over their central 50% regions. v_m is the central axis (maximum) water speed at a given downstream position; y, z are the horizontal and vertical directions respectively, measured from the central axis; y_m, z_m are the half-width and half-height respectively, of the diffuser. Figure 4-1 shows the slopes obtained by graphical differentiation of

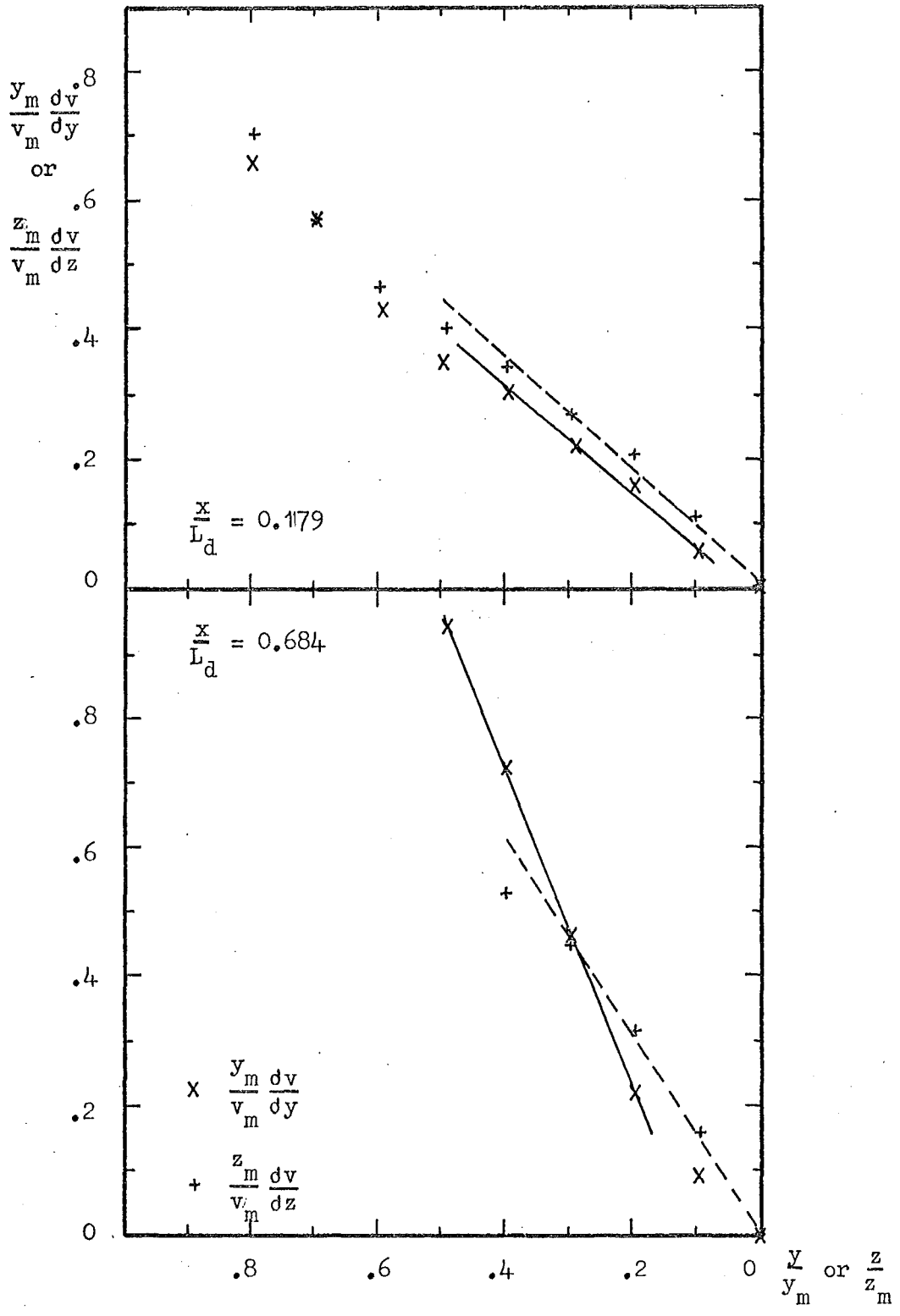

Figure 4-1. Velocity profile curvatures.

the vertical and horizontal profiles at 0.25 and 0.75 of the diffuser length. The slopes of these curves are $\frac{y_m^2}{v_m}\frac{d^2v}{dy^2}$ and $\frac{z_m^2}{v_m}\frac{d^2v}{dz^2}$. The slopes of the straight lines shown on the figure give approximate values of these quantities which were used to estimate the value of $n\,\nabla^2 v$, as $\frac{d^2v}{dx^2}$ was approximately zero within the diffuser (see Figure 6-1).

Table 4-1.

Central 50% velocity profile curvatures.(1)

$\frac{x}{L_d}$ (2)	Profile direction	$\frac{y_m^2}{v_m}\frac{d^2v}{dy^2}$	$\frac{z_m^2}{v_m}\frac{d^2v}{dz^2}$	$\frac{d^2v}{dy^2}$	$\frac{d^2v}{dz^2}$	$-n\,\nabla^2 v$ (3) (ft.sec^{-2})
.179	vertical		- .90		-2770	.049
.179	horizontal	- .83		-1290		
.684	vertical		-1.54		-2740	.055
.684	horizontal	-2.57		-1890		

(1) Lengths in feet, speeds in ft.sec^{-1}.

(2) L_d is the diffuser length, 11.33 inches.

(3) Taking kinematic viscosity, n, as 1.2×10^{-5} ft.^{2}sec^{-1}.

Compared with $v\frac{dv}{dx}$ (in the order of 60 ft.sec^{-2} at $\frac{x}{L_d} = 0.179$, 45 ft.sec^{-2} at $\frac{x}{L_d} = 0.684$, see 6.2) the influence of the Laplacian term is negligible and was dropped from the expression used to calculate drag coefficients. Equations (4-3,4,5) then lead to

$$C_{DA}\left(Re_p, Ac, Ir, \frac{L}{a}, \frac{\rho_s}{\rho}\right) = \frac{8a}{3|v_p-v|(v_p-v)}\left(v\frac{dv}{dx} - \frac{\rho_s}{\rho}v_p\frac{dv_p}{dx}\right). \quad (4\text{-}6)$$

4.3 Calculation of the parameters influencing C_{DA}.

For measured v_p-v, calculation of Re_p is straightforward. The streamwise components of I and L are measured (see 4.6, 5.4) and Ir at a given position is $\frac{I\,v}{v_p-v}$. The ratio $\frac{\rho_s}{\rho}$ and a are measured and only Ac requires further comment. It is defined in 3.2 and for slip speed, v_p-v, is

$$Ac = \frac{a\,\frac{d}{dt}(v_p-v)}{(v_p-v)^2} .$$

The slip speed is a function of t, the time at which the particle, speed v_p, is at x in the diffuser. In this case

$$\frac{d}{dt} = \frac{\partial}{\partial t} + \frac{dx}{dt}\frac{\partial}{\partial x}$$

$$= v_p\frac{\partial}{\partial x} \quad \text{when } \frac{\partial}{\partial t} = 0.$$

Hence Ac is calculated from the measured mean speeds and their gradient in the diffuser as

$$Ac = \frac{a\,v_p\left[\frac{dv_p}{dx} - \frac{dv}{dx}\right]}{(v_p-v)^2} .$$

4.4 Spatial, temporal and ensemble averages.

v_p and v in Chapter 3 were temporal means of turbulent speeds (3.3). As v was experimentally measured by a total head probe (5.3) the measurement at each position was a

temporal mean of the turbulent water speed (although it might well have been in error due to the non-vanishing squares of fluctuating components, see Hinze (1959)). v_p for each particle was measured photographically (5.5) at certain positions in its trajectory by a method which gave an average over a short distance, corresponding to a short time interval - it could be considered as either a temporal or spatial average. At a fixed position in the diffuser v_p so measured can vary considerably between physically identical particles, or between a number of trajectories of the same particle recirculating; it could be compared with a measurement of v from a total head probe over such a very short period that an insufficient sample of the normal population of instantaneous speeds is obtained. To be able to compare particle and water mean speeds an ensemble average was taken of measured particle speeds over all (identical) particles at fixed positions in the diffuser. As the fixed positions were actually finite volumes about a fixed point the sample is obtained, not from a single population of particle instantaneous speeds, but from the set of similar populations occurring in the volume. Thus spatial, ensemble and temporal averaging are all implied by the method of obtaining particle mean speeds.

The methods of averaging to obtain v_p and v affect the values of these means so obtained, and thus affect the C_{DA}

values calculated from (4-6). This dependence upon methods of averaging should be borne in mind when comparing drag coefficients for non-steady, turbulent flow measured by different methods.

4.5 Water velocity contours from measured profiles.

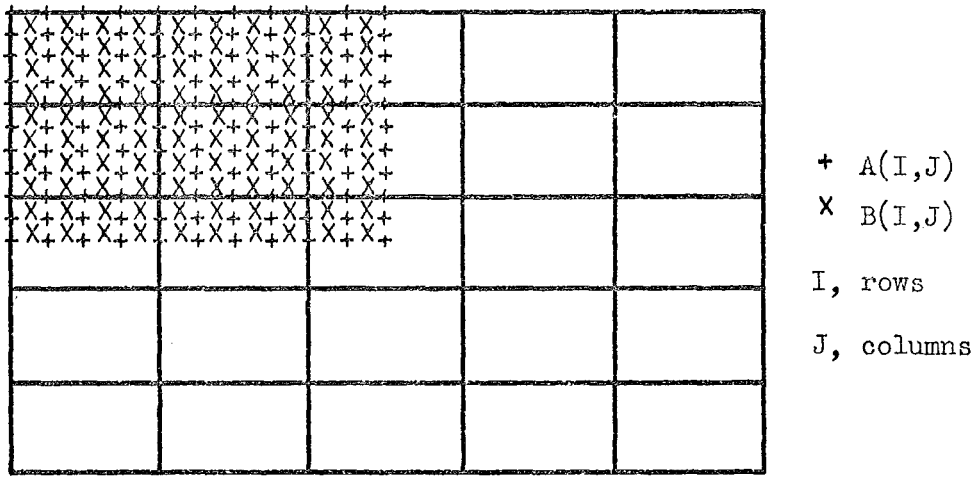

Figure 4-2. Flow cross-section showing the square arrays A(I,J), B(I,J) on rectangular grids.

A(1,J), J = 1 to 11 and A(I,1), I = 1 to 11 are specified to be zero (solid boundary);

A(11,J), J = 1 to 11 and A(I,11), I = 1 to 11 are known from measured velocity profiles.

Two water velocity profiles were measured at each of the five flow sections; one before, three within and one after the diffuser (see 6.2). The profiles gave values on the horizontal and vertical planes containing the diffuser central axis. To compare water and particle speeds at other parts of the flow cross-section the water speeds were estimated by the procedure described below.

The velocity contours at a flow section were assumed to be symmetrical with respect to the measured profiles and points A(I,J) were set out in a square, 11 x 11 array over one quarter of the flow section, Figure 4-2. As the flow section is in general rectangular, separation of grid points differs in the Y,Z directions.

The most satisfactory method to calculate the internal array values A(I,J), was to reduce the measured value at the same horizontal (Z) position, A(I,11), in the same proportion as the measured value A(11,J) was reduced from the central axis value, A(11,11);

$$A(I,J) = A(I,11)\,\frac{A(11,J)}{A(11,11)} \quad . \qquad (4\text{-}8)$$

The method is justified by the resulting speed contours, of which Figure 4-3 is an example. They were realistic and showed a variation in shape similar to Nikuradse's results for rectangular pipes, illustrated in Figure 105, Goldstein (1938). Also, numerical integration gave calculated flow rates, at the five flow sections where total head traverses

were taken, of 0.204, 0.198, 0.201, 0.198 and 0.177 $ft.^3 sec.^{-1}$. The flow rate measured by stopwatch and calibrated pit was 0.214 $ft.^3 sec.^{-1}$. All but the last calibrated flow rate, which is downstream of the diffuser and therefore less important, were considered satisfactory; calculated speeds at the downstream flow section were increased by the factor $\frac{0.20}{0.18}$.

For the numerical integrations, and to calculate a mean for each Y,Z grid position (c.f. Figures 4-2 and 5-16), an internal 10 x 10 array was calculated from

$$B(I,J) = \frac{1}{4}\left[A(I,J) + A(I,J+1) + A(I+1,J) + A(I+1,J+1)\right].$$

The arrays and flow rates were calculated using a Fortran IV program for an IBM 360/44; the results are presented in Table 6-1.

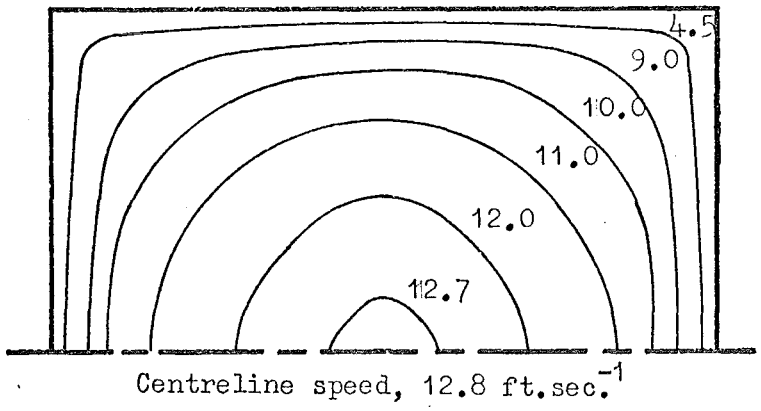

Figure 4-3. Calculated velocity contours in square conduit.

4.6 Turbulence parameters.

The hot-film probe and constant temperature anemometer used to make turbulence measurements are described in 5.4; this section presents certain definitions and equations for later use.

The calibration curve of a hot-film probe fits a form of King's law (Raichlen (1967)),

$$\frac{i^2 R_t}{R_t - R_f} = A + B\, v^c \text{ , where} \qquad (4\text{-}9)$$

i is instantaneous probe current,

R_t is probe operating resistance, assumed constant for an applied overheat ratio, $\frac{R_t - R_f}{R_f}$,

R_f is probe resistance at the fluid temperature,

A,B are constants, measured as intercept and slope respectively of an $\bar{i}^2 - \bar{v}^c$ calibration curve (see 4-11),

c the exponent, is 0.5 in King's original law (see Hinze (1959)) and approximately 0.5 for hot film probes. In two experiments, Raichlen (1967) obtained c = 0.66,0.55.

For mean and fluctuating components $i = \bar{i} + i'$, $v = \bar{v} + v'$, $e = \bar{e} + e'$ (where e is instantaneous bridge voltage), c less than unity and fluctuations small compared to the means,

$$\bar{i}^2 R_t + 2\bar{i}\, i' R_t = A(R_t - R_f) + B(\bar{v}^c + c\, v' \bar{v}^{c-1})(R_t - R_f), \qquad (4\text{-}10)$$

wherein $i'^2 R_t$ and terms $\frac{c(c-1)}{2!} v'^2 \bar{v}^{c-2}$ or smaller have been neglected.

To the next order of approximation

$$\bar{i}^2 R_t = A(R_t-R_f) + B \bar{v}^c(R_t-R_f), \qquad (4\text{-}11)$$

and as $\bar{e} = \bar{i} R_t$

$$\bar{e}_o^2 = A(R_t-R_f) R_t \quad , \quad \text{and}$$

$$\bar{e}^2 - \bar{e}_o^2 = B \bar{v}^c(R_t-R_f) R_t, \qquad (4\text{-}12)$$

where $\bar{e}_o$ is the bridge D.C. voltage corresponding to still fluid, $\bar{v} = 0$. Subtracting (4-11) from (4-10) gives

$$2\bar{i}\, i' R_t = B\, c\, v' \bar{v}^{c-1}(R_t-R_f).$$

As the fluctuating bridge voltage, e', $= i' R_t$, its root-mean-square value is

$$e'_{rms} = \frac{B\, c}{2\bar{i}} v'_{rms} \bar{v}^{c-1}(R_t-R_f). \qquad (4\text{-}13)$$

Using the value of B from this equation and noting that $\bar{e} = \bar{i} R_t$ (4-12) becomes

$$\bar{e}^2 - \bar{e}_o^2 = \frac{2\bar{e}\, e'_{rms}\, \bar{v}}{c\, v'_{rms}} \quad ,$$

i.e. turbulence intensity,

$$I = \frac{v'_{rms}}{\bar{v}} = \frac{2\bar{e}\, e'_{rms}}{c(\bar{e}^2-\bar{e}_o^2)} \quad . \qquad (4\text{-}14)$$

This requires readings of $\bar{e}$, e'_{rms} at the given fluid speed, temperature and probe overheat ratio, and $\bar{e}_o$ at the same fluid temperature and overheat ratio but with the fluid motion stopped. The values of I were found using (4-14), a low overheat ratio (to prevent bubbling), assuming

$c = 0.5$ and accepting a possible systematic error of $(2c_a-1)I$ in I, where c_a is the actual value of c. This accuracy was acceptable to indicate the nature of the dependence of C_{DA} upon I, and using (4-14) made an $\bar{e}$, $\bar{v}$ calibration unnecessary, an advantage because of prevailing conditions in the flow circuit (internal rust, possible air entrainment at the tank free surface, ordinary laboratory water supply; see 5.2).

Energy spectrum.

Taylor's (1938) one-dimensional energy spectrum function, E(n), is defined by

$$\int_0^\infty E(n)\, dn = \overline{v'^2};$$

$\overline{v'^2}$ is the total fluctuation energy per unit mass from all frequencies, n. For finite bandwidth $\Delta n(n)$ about central frequency, n,

$$E(n) \simeq \frac{\overline{v'^2}(n)}{\Delta n(n)} \quad . \tag{4-15}$$

Longitudinal correlation.

The longitudinal, spatial correlation coefficient, f(x'), is

$$f(x') = \frac{\overline{v'(x)\, v'(x+x')}}{\overline{v'^2}(x)\ \overline{v'^2}(x+x')} \quad ,$$

where x is downstream position, x' is downstream separation. Taylor (1938) showed that f(x') is related to E(n) by a Fourier transform provided the v' fluctuations are small

compared to $\bar{v}$;

$$f(x') = \frac{1}{v'^2} \int_0^\infty E(n) \cos \frac{2\pi n x'}{\bar{v}} \, dn. \qquad (4\text{-}16)$$

Integral scale.

The Eulerian integral scale in the mean flow direction L_e, is Taylor ((1935)),

$$L_e = \int_0^\infty f(x') \, dx'. \qquad (4\text{-}17)$$

Not only are there known inaccuracies in the way f(x') was calculated (see 5.4), but it is often difficult to determine where f(x') becomes "sensibly zero" in measuring the area under the curve. Two other formulas were used to estimate L_e; both are derived assuming isotropic turbulence. The first, due to Von Karman, applies to large enough Reynolds numbers for an inertial subrange to exist (where the three-dimensional spectrum function depends upon $n^{-\frac{5}{3}}$) and for viscosity effects to be negligible. (The criterion is given by Hinze on page 187; it is satisfied for these experimental results). The formula is given on page 200, Hinze (1959);

$$L_e \simeq \frac{0.375 \, \bar{v}}{\pi n_e} \quad , \qquad (4\text{-}18)$$

n_e is the frequency at which the three-dimensional spectrum function reaches a peak, indicating the range of the energy-containing eddies.

The second formula is an equation for the one-dimensional spectrum function obtained if the spatial

correlation curve is approximated by an exponential function. It is given on pages 60 and 202, Hinze (1959);

$$E(n) = \frac{\overline{4v'^2}}{\bar{v}} \frac{L_e}{1+\frac{4\pi^2 n^2}{\bar{v}^2} L_e^2} ,$$

whence $$\frac{4\pi^2 n^2}{\bar{v}^2} E(n) L_e^2 - \frac{\overline{4v'^2}}{\bar{v}} L_e + E(n) = 0 \qquad (4\text{-}19)$$

and this quadratic can be solved for L_e using measured values of $\overline{v'^2}$ and $E(n)$. n near n_e should give best results (page 203, Hinze).

Microscale.

Microscale in the mean flow direction, Λ, is defined (Taylor (1935)) to be the intercept on the abscissa of the parabola drawn to touch the correlation curve at its vertex ($x'=0$),

$$\frac{1}{\Lambda^2} = \lim_{x' \to 0} \frac{1-f(x')}{x'^2} .$$

Thus

$$\Lambda^2 \simeq \frac{x'^2}{1-f(x')} , \text{ for small } x'. \qquad (4\text{-}20)$$

Because of the relationship between $f(x')$ and $E(n)$, Λ can also be calculated from (page 59, Hinze (1959));

$$\frac{1}{\Lambda^2} = \frac{2\pi^2}{\bar{v}^2 \overline{v'^2}} \int_0^\infty n^2 E(n)\, dn , \qquad (4\text{-}21)$$

where the integral is estimated by measuring the area under a curve of $n^2 E(n)$, n.

A third formula for Λ, which is independent of the measured spectra, is due to Liepmann, Laufer and Liepmann,

quoted by Hinze (1959) on page 110;

$$\frac{1}{\Lambda} = \frac{\pi N_o}{\overline{v}\sqrt{2}} \quad ; \qquad (4\text{-}22)$$

N_o is the average number of zeroes of v' per unit time.

CHAPTER FIVE.

5. EXPERIMENTAL METHODS AND APPARATUS.

5.1 Introduction.

The design and performance of the apparatus required to measure the non-steady drag coefficients of particles entrained in turbulent flow by the method outlined in 4.1, and the procedures involved in its use, are described in this chapter. The plane-walled diffuser in which drag coefficient measurements were made (5.22) diverged in the horizontal direction perpendicular to the horizontal flow of water, and was of uniform height in the vertical direction. Gravity thus acted perpendicularly to the flow direction and the streamwise motion could be considered to be free of external forces. The fall speeds in still fluid of the particles used (5.6) were less than 0.5% of the centreline, horizontal flow speed upstream of the diffuser, less than 0.7% of the same downstream speed.

5.2 The flow circuit.

The partially recirculating circuit shown in Figures (5-1,3) was designed to supply the plane-walled diffuser with a controlled flow of clean water of known physical properties, containing solid particles in suspension. The particles, which are not damaged during transport to or from the diffuser, could be retrieved or left to recirculate.

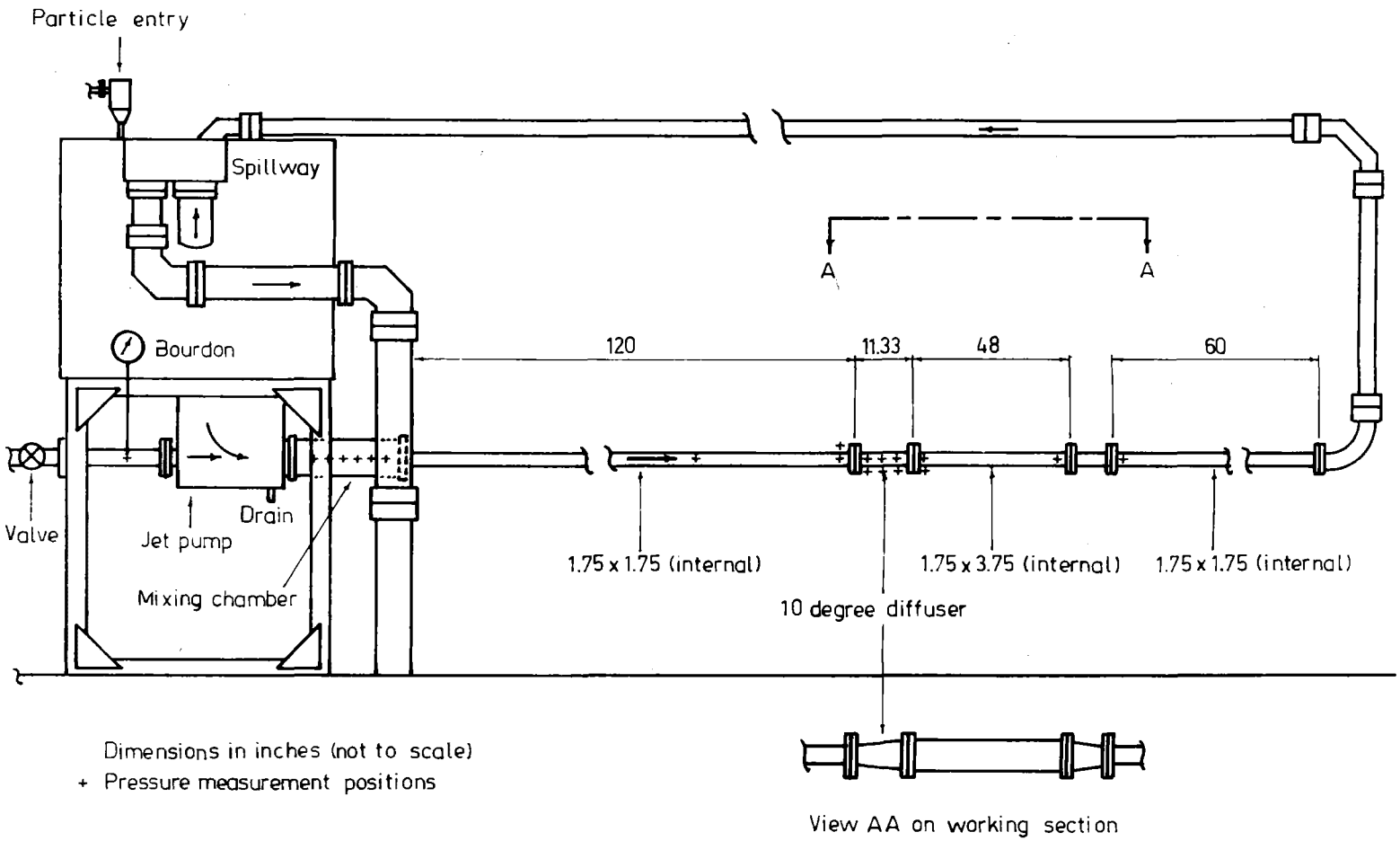

Figure 5-1. The flow circuit.

The main features of the circuit were (Figure 5-1):

1. A water-water jet pump (5.21) whose driving flow was supplied by an 80 H.P. centrifugal pump in the laboratory pump room. The jet pump caused a mixture of driving and driven flow (from the tank) to enter the working section.

2. The circuit flow rate was controlled by a gate valve and monitored by a Bourdon-type pressure gauge.

3. The working section was preceded and followed by straight lengths of 1.75 inches square (internal) steel conduit with 0.125 inches wall thickness (and a small radius at the corners). It was not treated internally and at the times of most experiments had a fine powder coating of rust.

4. The working section was made from transparent Perspex (polymethyl methacrylate), 0.5 inches wall thickness and 1.0 inch flanges. The 10 degree, included horizontal angle diffuser (5.22) was followed by a uniform flow section leading to a 20 degree, included horizontal angle, plane-walled nozzle flanged to the steel conduit. The internal, vertical dimension was 1.75 inches from the jet pump mixing chamber entrance to the downstream end of the square steel conduit.

5. The overhead return was 3 inches diameter aluminium pipe ending 1 foot below the free surface of water in the tank.

6. The 400 gallon, approximately 4x4x4 feet, rivetted steel tank had been internally tarred and was fitted with a curved transition section providing flow to the jet pump.

7. The overflow (equal, for constant tank level, to the jet pump driving flow) left two feet below the tank free surface by a constant head spillway. This kept the tank free surface 1 to 2 inches from the tank top for all driving flows used.

8. A half-inch copper pipe led from a 6 inch diameter constant-head (ball valve) tank above the main tank free surface to the low pressure region in the jet pump mixing chamber; this was used to introduce particles for once-through circuits. (They were caught in a nylon mesh net over the return pipe entry to the tank). Particles recirculating for visualisation studies could be introduced at the small constant-head tank or at the free surface.

9. Circuit water temperature could be measured at the tank free surface or any of the pressure entry stations not otherwise in use. It was usually monitored approximately from the switch-panel display of centrifugal pump water temperature which, under steady conditions, was a few degrees higher than circuit water temperature.

5.21 The jet pump and circuit performance.

The jet pump provided a low-pressure, high velocity region in its mixing chamber where, for the configuration

used in this study, pressure was near or below atmospheric and particles could conveniently be added without damage to themselves or the pump. It was designed using information from Mueller (1964), Bonnington (1956,1964), Silvester (1961) and Stepanoff (1955). Important in the design were the ratios:

driving nozzle area to mixing chamber area, R_A,

driving nozzle diameter to driving nozzle -mixing chamber standoff distance, R_L,

mixing chamber length to mixing chamber diameter, R_M. Performance was also affected by internal surface finish, shapes of the mixing chamber entrance and suction chamber, and diffuser design (when one was fitted).

The jet pump, Figure 5-2, had the curved bellmouth and two walls of the square mixing chamber rubber lined. Mueller suggests $R_A \simeq 0.44$ to 0.50 for maximum efficiency. Two nozzles were tested; for the larger nozzle $R_A = 0.36$ based on total mixing chamber area, $R_a = 0.46$ based on the inscribed circle, which is probably more reasonable. R_A also influences the fraction of discharge flow which is drawn from the tank and the smaller nozzle was fitted to increase this fraction; it gave $R_A = 0.184$ based on the inscribed circle (see the result, Figure 5-5). No sharp optimum for R_L was found by Mueller, but efficiency seemed best at $R_L = 0.7$ to 1.2. For both nozzles used R_L was

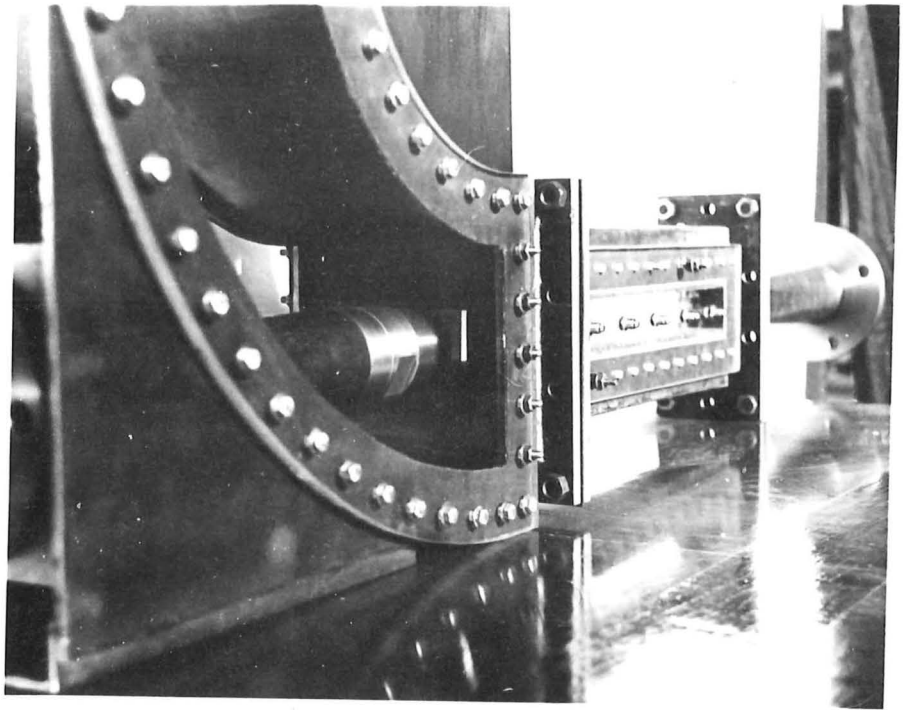

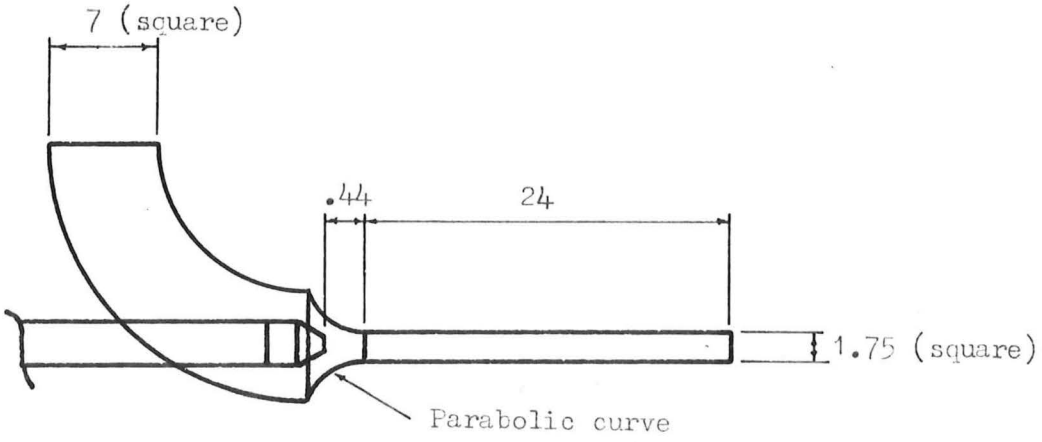

All dimensions in inches (not to scale).

Nozzle diameters 0.75 or 1.188

Figure 5-2. The jet pump.

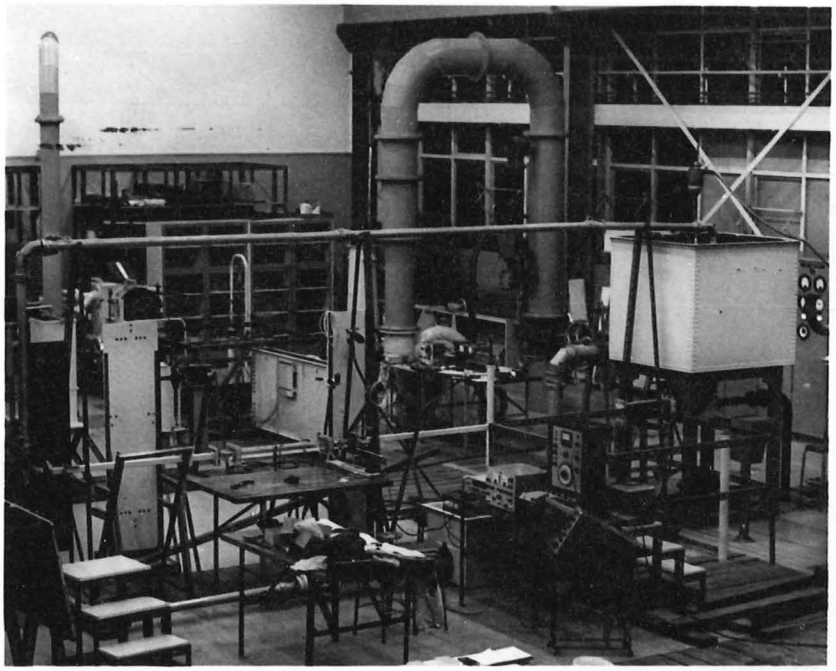

Figure 5-3. The flow circuit.

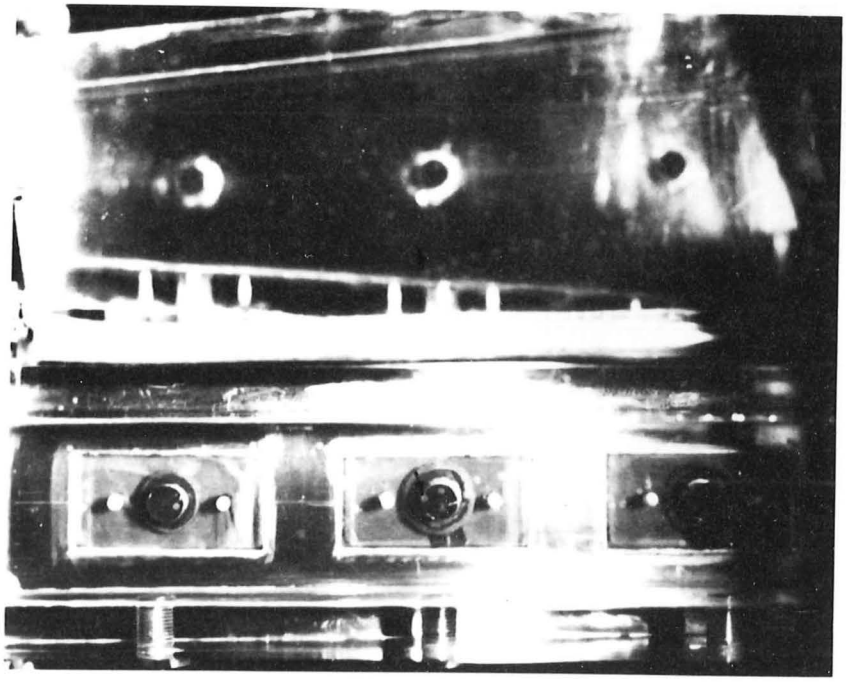

Figure 5-4. A "stall" trajectory in the diffuser.

about 0.6. Optimum R_M depends upon the angle of a diffuser if fitted; R_M should be 5 to 7 from the papers cited. This jet pump had $R_M = 13.5$ (sacrificing some efficiency for the incidental interest of separating momentum exchange and friction loss regions).

To measure jet pump performance, a venturi meter replaced the working section, Figure 5-1, and the overflow was measured by stopwatch and calibrated pit. The efficiency, e, is equal to MN, where M is the ratio of suction flow to driving flow and N is the ratio of $\frac{\text{discharge-suction}}{\text{driving-discharge}}$ dynamic pressures (static plus mean velocity pressure terms). M,N were near 0.5 for the larger nozzle at best efficiency, which was about 27%; use of the smaller nozzle increased the fraction of discharge flow which was suction flow to 60% (M = 1.5), and increased e to approximately 29%. Even in pumps designed for maximum efficiency values of e above 30-35% seldom occur, Figure 5-5.

The pressure distribution in the jet pump mixing chamber was measured for this modified circuit with the venturi meter in place. The low pressure region allowing convenient particle entry is demonstrated by the curves of Figure 5-6.

An approximate relationship between driving flow static head, H_m, and flow rate in the recirculating circuit, Figure 5-1, was determined by diverting the return flow from

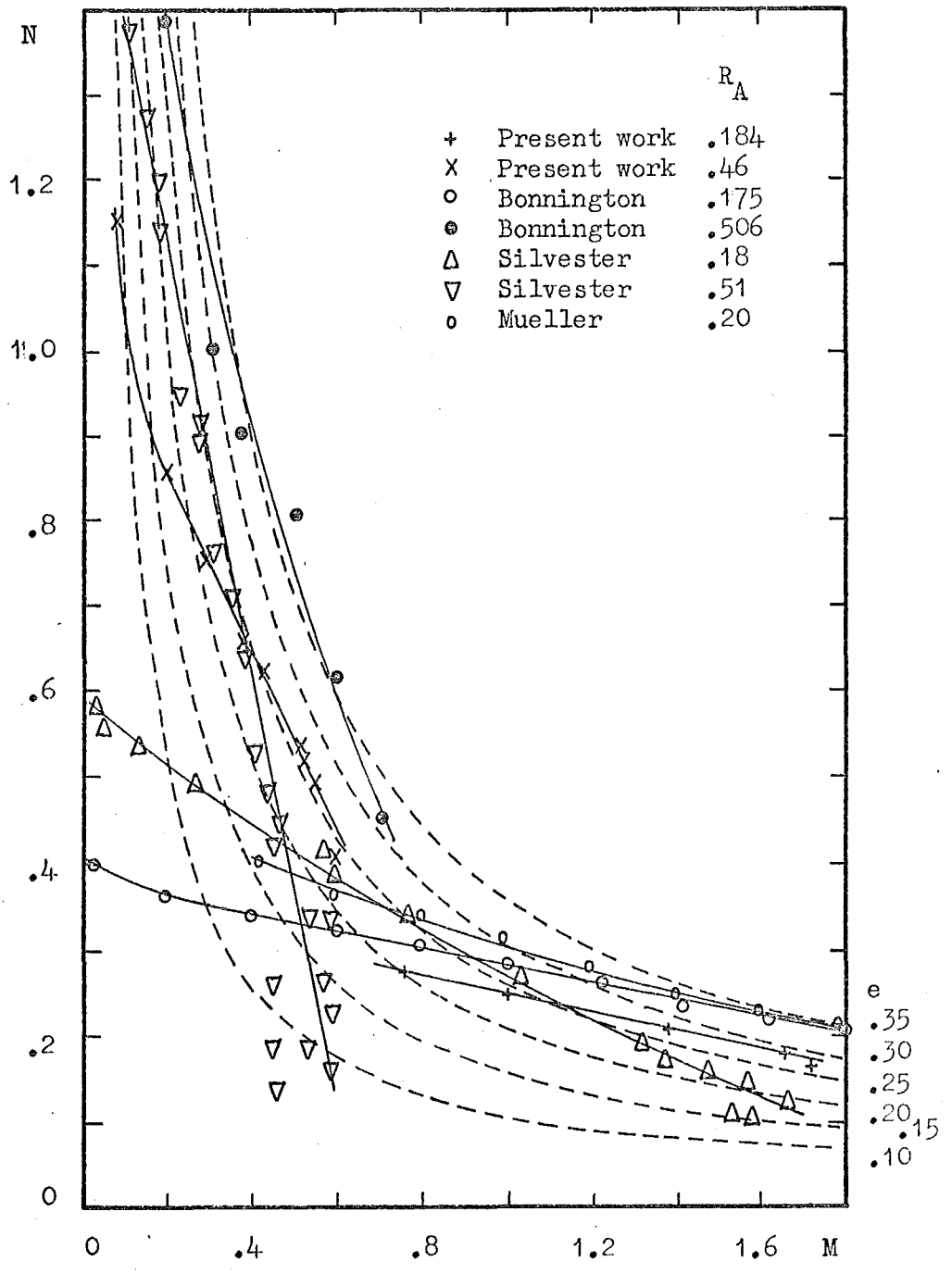

Figure 5-5. Jet pump performance.

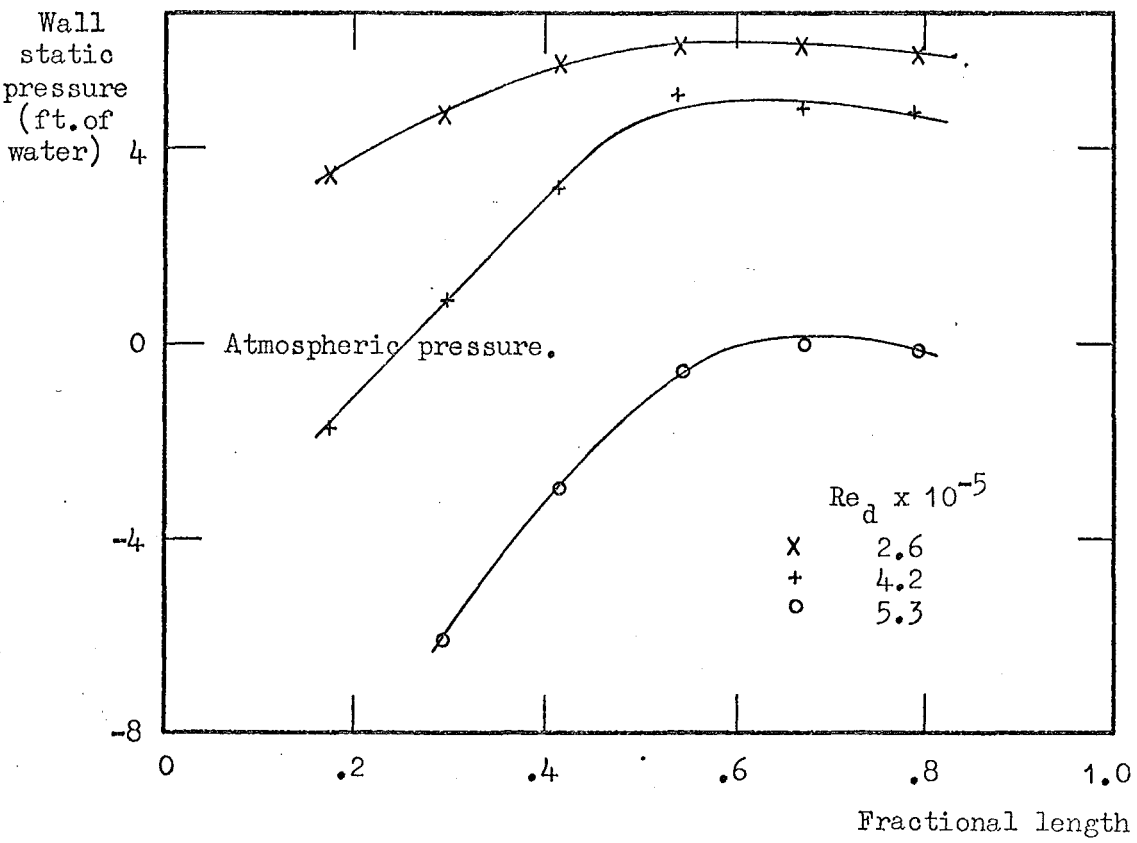

Figure 5-6. Mixing chamber pressure distribution.

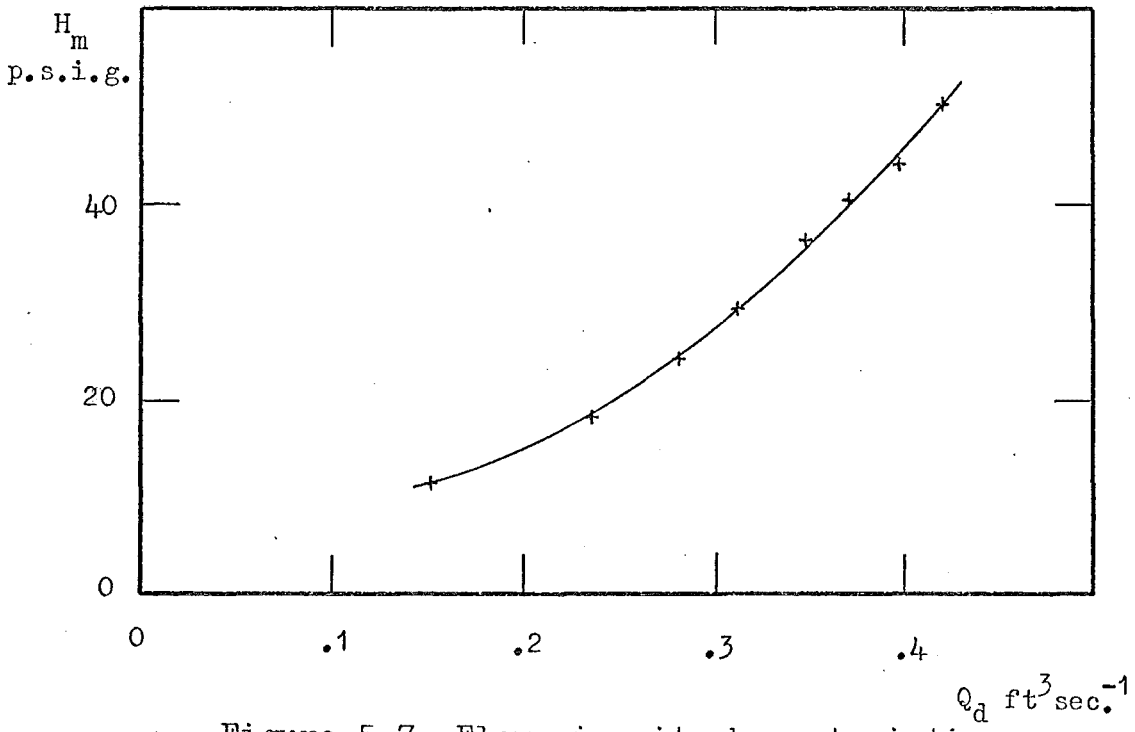

Figure 5-7. Flow circuit characteristic.

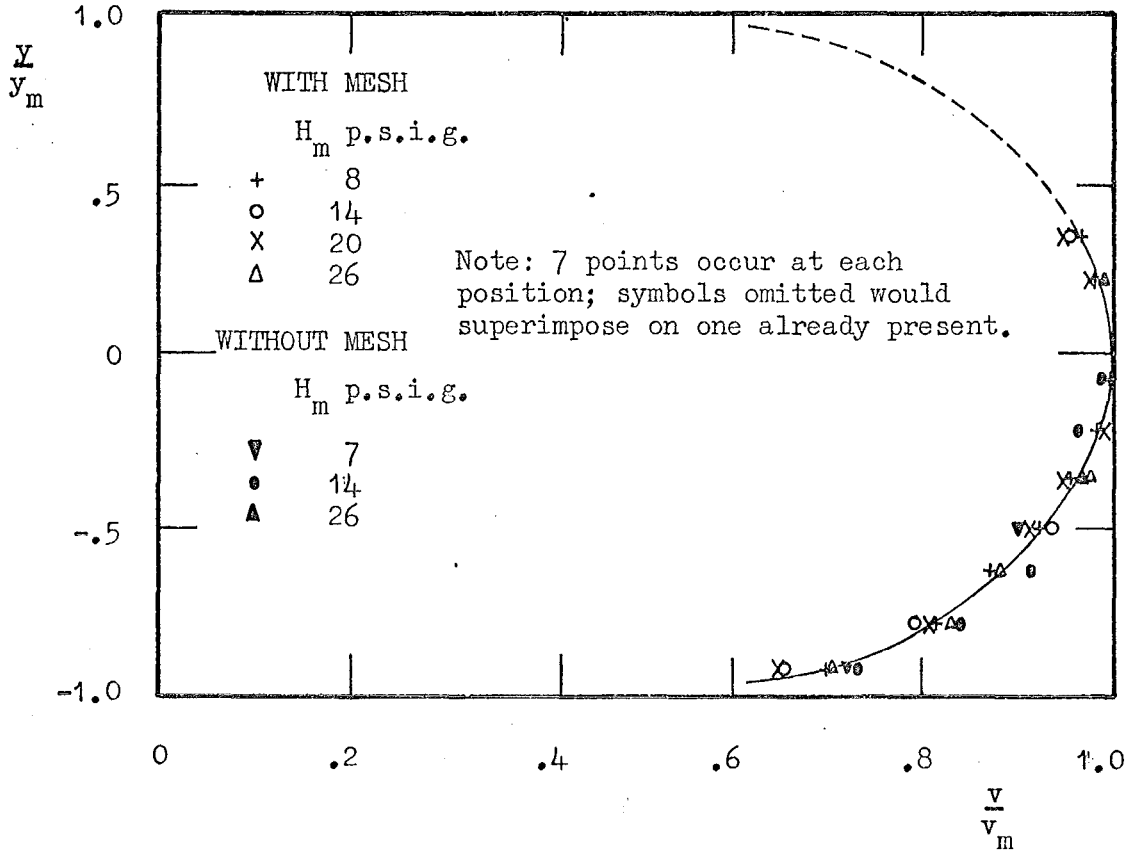

Figure 5-8. Velocity profiles upstream of the diffuser.

the tank to a calibrated pit, supplying make-up water to the tank from another source. Near H_m = 20 p.s.i.g., the set value for the main drag coefficient experiments, Figure 5-7 shows that a 1% error in setting H_m gives about 0.5% error in discharge flow rate, Q_d. The precision of setting H_m (displayed on a Bourdon gauge, 5.3) would be $\pm$ 1% giving an error $\pm$ 0.5% in Q_d from this cause.

At exit from the 10 feet of square steel conduit, Figure 5-1, the velocity profiles were very full and rounded. To show that the flow was fully developed and showed no persistent effect of the jet pump nozzle these profiles were checked over a range of flow rates with those obtained when a 6 wires per inch stainless steel mesh was fitted immediately downstream of the jet pump mixing chamber. The horizontal profiles at 3 flow rates without the mesh and 4 flow rates with the mesh are shown in Figure 5-8. Discharge Reynold's number, $Re_d = \frac{Q_d}{2y_i n}$ (where y_i is the diffuser inlet half-width, which equals the half-height), varied from 7×10^4 at the lowest flow rate with the mesh in place to 2×10^5 at the highest without the mesh; vertical profiles checked for two flow rates showed the same result. Clearly the profiles obtained are characteristic of the conduit and are not affected by the jet pump nozzle.

5.22 The diffuser.

For non-steady drag measurements diffuser performance

is most satisfactory when there is no separation, fluid deceleration is of the required magnitude and horizontal and vertical velocity profiles are symmetrical about the flow direction axis. The 10 degree, included horizontal angle diffuser was designed, from information given by Kline (1959) and Kline, Abbott and Fox (1959), to have unstalled flow. Given the order of the diffuser Reynolds number and some indication of upstream conditions the important quantities are slant length to inlet width ratio, and the included angle. A given inlet area to exit area specifies a relationship between angle and length to inlet width ratio. The restraints on choice are that this relationship must be satisfied and the chosen values must define a point below the "no appreciable stall" line of Kline's graph (included angle against length to inlet width ratio).

Since the diffuser inlet to exit area ratio is 2.143 the geometrical relationship is

$$1 + \frac{L_s}{y_i} \sin \theta = 2.143;$$

L_s, slant length; y_i, inlet half-width; 2θ, included angle. For $2\theta = 10$ degrees, $\frac{L_s}{2y_i} = 6.555$ and these define a point in the "no appreciable stall" area of Kline's graph. Inlet width 1.75 inches then requires slant length 11.48 inches (direct length 11.42 inches). The diffuser used had

2θ = 10 degrees and direct length 11.33 inches.

The water deceleration was to be in the order of, but higher than, gravitational acceleration, and this was achieved (6.2).

The measured velocity profiles (Figure 6-2) show that the dimensionless, boundary layer displacement thickness, $\frac{\delta^+}{y_m}$, of the side-wall boundary layer at mid-height, grows from about 0.1 at entry to 0.5 at exit. δ^+ is measured by the integral

$$\delta^+ = \int_0^{y_m} \frac{v_m - v}{v} \, dy$$

which is conveniently found from such dimensionless plots as those in Figure 6-2; y is the horizontal transverse coordinate measured from the diffuser central axis, y_m its maximum value (the half-width) at a given downstream position, v_m the central axis (maximum) value of water velocity downstream component, v. In a paper following those mentioned above Reneau, Kline and Johnson (1967) call $\frac{\delta^+}{y_i}$ an "inlet blockage parameter" and note that for "very thick" values, say 0.05 (c.f. 0.1 for this) the "no appreciable stall" line of the previous papers should be 1-2 degrees lower. The 10 degree diffuser still satisfies this requirement. High speed 16 m.m cinephotography (5.5) showed possible transient stall confined to small regions in the flow section corners at the diffuser exit. Of the

several thousand 35 m.m. exposures of particle tracks examined during particle speed measurement (5.51), only two or three strongly suggested transient stall further upstream, Figure 5-4. As all particle speed measurements near a wall were discarded the diffuser performance is considered to have been satisfactory.

5.3 Pressure measurement.

17 pressure tappings were located as follows:

(a) A single tapping 2 feet upstream of the jet pump driving nozzle;

(b) 6 along a side wall of the jet pump mixing chamber, used to establish the static pressure distribution;

(c) One each on top and at the mid-height of one side of the steel conduit, 1.125 inches upstream of the diffuser entrance;

(d) 3 on the base and 3 on one side of the diffuser at positions approximately 0.25, 0.50, 0.75 of its length;

(e) 1 each on the base and one side of the 1.75 x 3.75 inch section, 1.75 inches downstream from the diffuser exit.

At (a,b), only static pressure measurements were necessary; at (c,d,e) both static and total head measurements were required. The importance of hole size, alignment, flushness and freedom from projections into the flow (e.g. drilling burrs) has often been pointed out (Shaw (1959)). These factors were carefully attended to for (c,d,e).

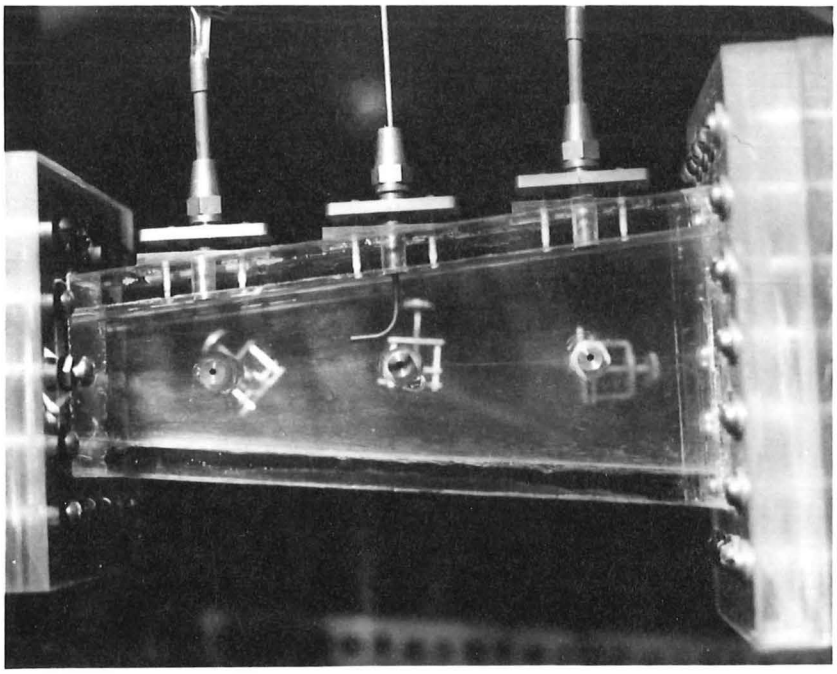

Figure 5-9. Pressure tappings at (d).

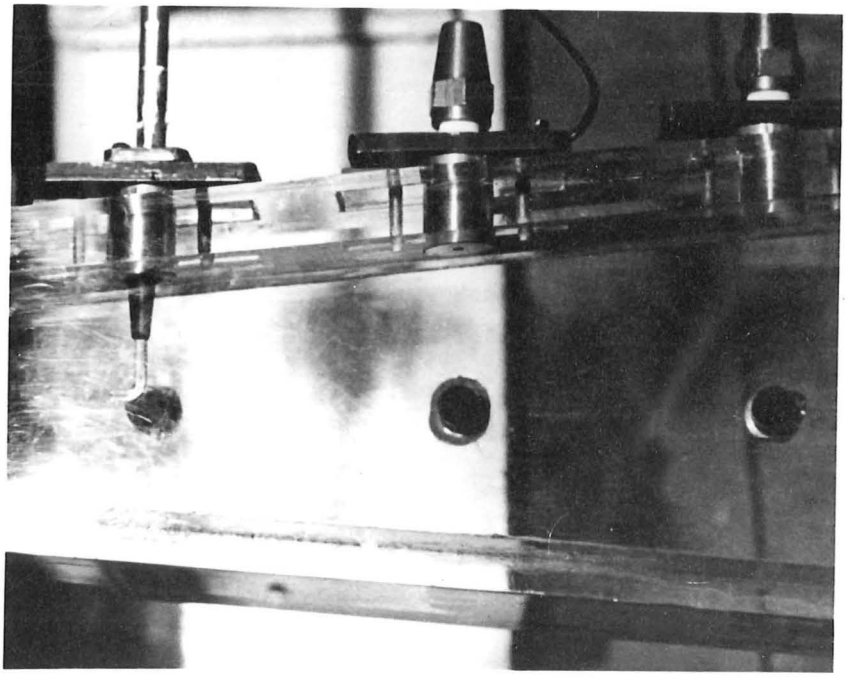

Figure 5-10. The hot-film probe and modified tappings.

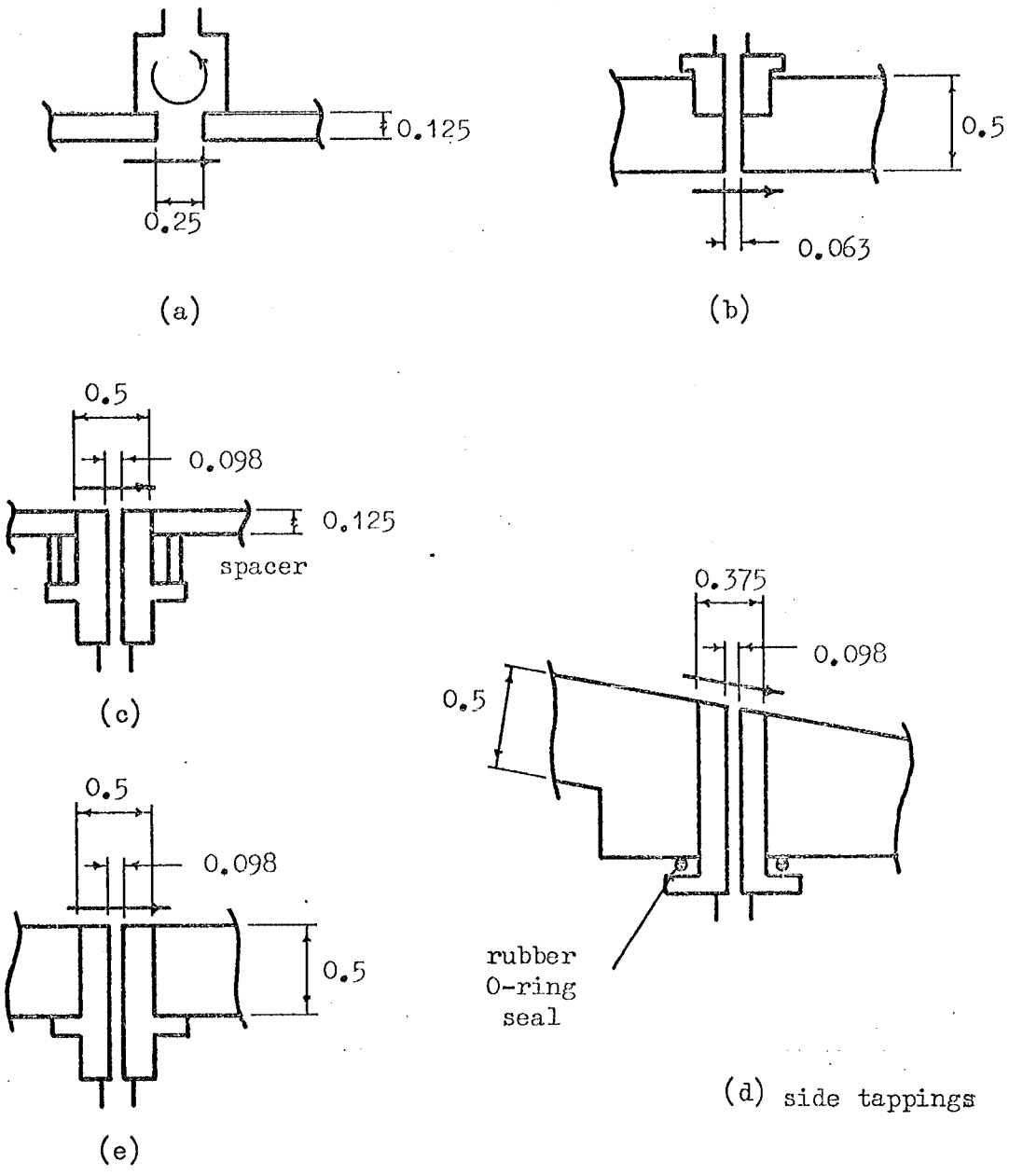

Figure 5-11. The pressure tappings (diagrammatic).

Figure 5-9 shows the (d) tappings, and Figure 5-11 shows all types diagrammatically; the following paragraph refers to Figure 5-11.

Water in the socket of a tapping like (a) tends to circulate, giving a false reading (Shaw (1959)). In this study it was important for (a) to give a reproducibly precise reading, which could be inaccurate; i.e. it was important to be able to establish the same flow rate for drag measurement experiments at different times, but not so important to obtain accurate pressure measurements as these were used only to establish jet pump and circuit performance. Divisions on the Bourdon gauge connected to (a) were 2 p.s.i.g., about 0.13 inches on the gauge face. Each of the (c,d,e) tappings was marked for its correct place and the position when its internal surface was flush. They were identical except for side tappings in the diffuser. Flushness of the 6 tappings in the diffuser was checked by traversing a dial gauge on a lathe saddle along the floor and appropriate wall. Upstream edges of the tappings were within 0.0015 inches of flushness, downstream edges within 0.003 inches. Tappings were then tested in pairs for three circuit flow rates; tappings on adjacent faces at the same downstream position gave the same reading to within 0.15% of static pressure in all cases. It was simplest to have side tappings aligned with their axes perpendicular to the

main flow direction so that a total head traverse measured this component. The effect on static pressure readings of holes at 85 instead of 90 degrees to the wall proved to be negligible. The side tappings were a push fit into the perspex wall, flushness being adjusted using the range of movement provided by the rubber O-ring seal. The sizes of all tappings on the diffuser were a compromise between sufficient outside diameter to allow entry of the curved total head probes and minimum area to interfere with photography.

The total head probes were formed from brass tube of 0.0980 inches O.D., 0.0595 inches I.D. The probe shown in Figure 5-9 had a 0.375 inches radius curve placing the impact face 0.75 inches upstream from the tapping centre. The other probe had a curved portion of 0.0590 inches O.D., 0.0420 inches I.D., also 0.75 inches stem to face but shaped to be able to touch the wall from which it was traversing, and approach to 0.3 inches from the far wall. (The larger probe touched the far wall and came to within 0.5 inches at its stem of the near wall). Results from the two probes were indistinguishable. Maximum probe blockage is 6%, based on a 0.0980 inches diameter cylinder extending horizontally across the entire flow section.

All total and static pressure measurements other than at (a) were made on U-tube manometers with 5 feet scales.

In general, heads above 5 feet of water were read from a mercury-water manometer, those below 5 feet of water were read from a water-air manometer. 0.01 feet divisions on manometer scales allowed estimation to 0.002 feet with a steady, mercury-water meniscus, or 0.005 feet with a steady, water-air meniscus. High pressure water or 28 inches of mercury vacuum was used to back- and forward-flush manometers before use.

For velocity heads a manometer was connected between a total head probe and the static pressure tapping at the same downstream position but on an adjacent face of the flow section (see Figure 5-9, where the base tapping beneath the probe is providing the static pressure reading). The reading had to be compensated for the 0.75 inches horizontal separation of the static pressure tapping and total head probe impact face using the measured static pressure variation through the diffuser, Figure 6-1. Manometer readings were recorded directly onto a desk calculator tape and, if the appropriate compensation was known, differenced, compensated and converted to flow speed. A typical procedure to obtain a velocity profile was:

1. The circuit was cleaned, prepared and filled.

2. The manometers and connecting plastic tubes were flushed and manometer zeroes were checked.

3. Any air trapped in the line to the jet pump driving head Bourdon pressure gauge was bled and the gate valve controlling the circuit flow rate was set.

4. A datum was recorded by placing the total head probe against the boundary with which it made contact.

5. Time, jet pump driving head, water temperature, probe position, left and right manometer column heights and an estimate of the error due to meniscus or liquid column fluctuations were recorded. The readings were repeated as often as necessary to obtain a steady, mean pressure difference.

6. The total head probe was moved to a new position in the traverse (usually 0.125 inches separation), checking alignment visually.

7. 5 and 6 were repeated to the end of the traverse, and then the traverse was repeated in the reverse direction.

Steps 4, 5, 6, and 7 would typically take an hour.

5.4 Turbulence measurement.

A DISA (Denmark) 55 A 01 constant temperature anemometer was used with a DISA 55 A 85 quartz-covered, platinum-film probe as the sensitive element responding to turbulent water velocity (Figures 5-10,12). The film area was 1 x 0.2 m.m on an 80 degree wedge and the resistance was approximately 20 ohms at 20 degrees centigrade. (Full details on this equipment are given in the manuals, DISA

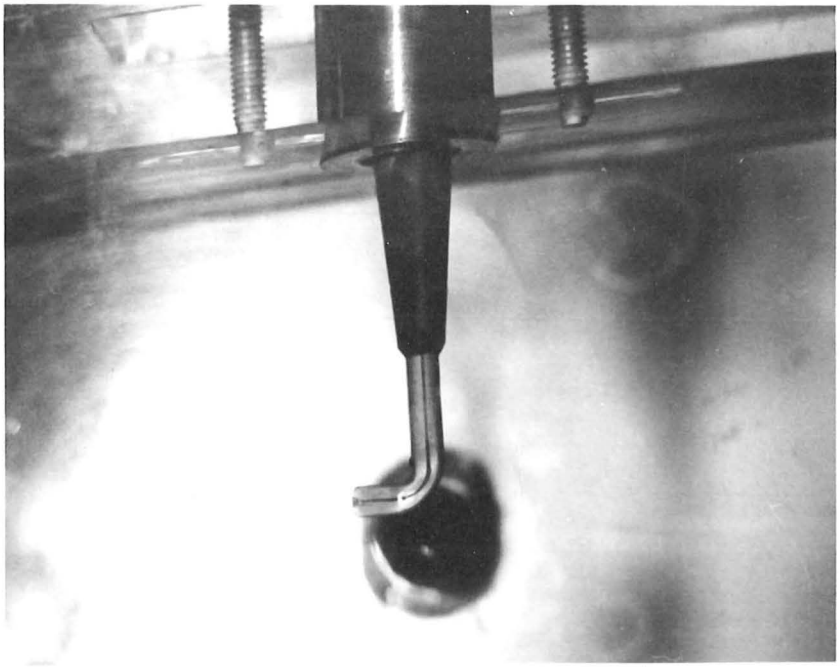

Figure 5-12. The hot-film probe in operation.

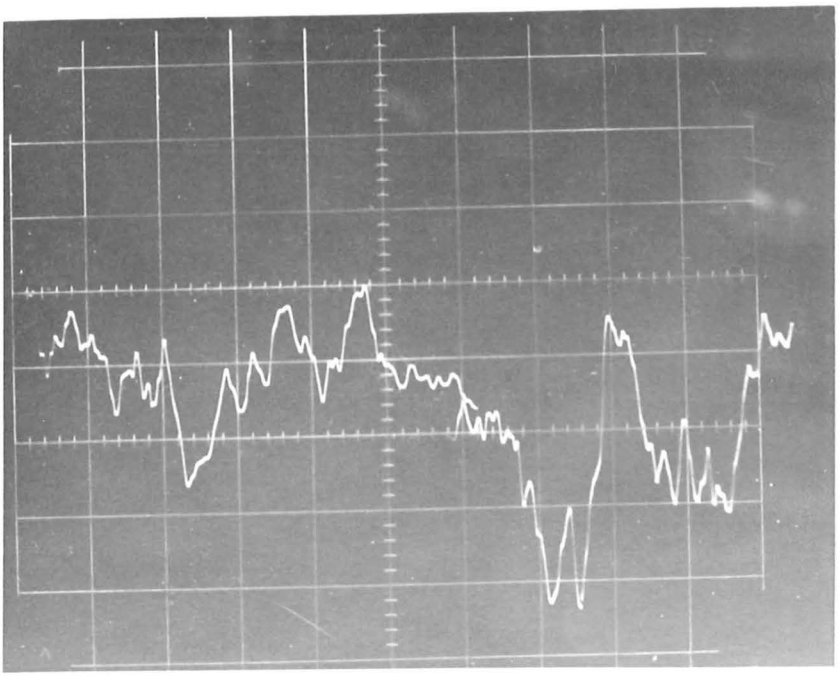

Figure 5-13. The turbulent velocity fluctuations (e').

(1966)). The 7 m.m. diameter probe caused nearly 16% blockage (based on a 7 m.m. cylinder extending right across the flow section), i.e. 19% increase in mean (discharge) speed if the flow rate remained constant. The probe is primarily sensitive to fluctuations in the flow direction and to vertical fluctuations (see Figure 5-12, a plan view with flow from left to right) but not to fluctuations in the horizontal direction perpendicular to the flow (along the wedge edge). $\overline{v'^2}$ for these results is the mean of squares of that combination of the three components recorded by the probe, but it is assumed that this approximates the longitudinal, or flow direction, component. The error involved in this assumption is probably in the order of 1% for the turbulence intensities (2-15%) in these experiments, see Raichlen (1967).

The diffuser side-tappings were enlarged and modified to accept the hot-film probe. It was traversed by a vernier sliding table on a fine screw thread.

The fluctuating voltage signal from the anemometer, e', indicating velocity fluctuations was plotted by a Brüel and Kjaer (Denmark) 3313 spectrum recorder as a function of its root-mean-square value, $f'(e'_{rms})$ against frequency, n, where

$$f'(e'_{rms}) = 20 \log_{10} \frac{e'_{rms}}{10} - z;$$

z is the decibel reading introduced by scale selection.

From this equation and (4-14) with c = 0.5

$$\overline{v'^2}(n) = \left[10 \text{ antilog}_{10} \frac{f'+z}{20}\right]^2 \left[\frac{4\bar{e}\,\bar{v}}{\bar{e}^2-\bar{e}_o^2}\right]^2 , \qquad (5\text{-}1)$$

n being the central frequency of a filter band-width $\Delta n(n)$. The band-pass filters had Δn directly proportional to n, ranging from about 6 Hz bandwidth at 25 Hz to 9200 Hz bandwidth at 40,000 Hz. For pen-recorder stability it was necessary to cut off frequencies below 20 Hz.

The measured values from (5-1) allow energy spectra to be calculated using (4-15). They also provide an approximation to the longitudinal correlation curve, as follows: from (4-16)

$$f(x') \simeq \frac{1}{\overline{v'^2}} \sum_{n_1}^{n_2} E(n)\, \Delta n(n)\, \frac{\cos 2\pi n x'}{\bar{v}} ,$$

and using (4-15),

$$f(x') \simeq \frac{1}{\overline{v'^2}} \sum_{n_1}^{n_2} \overline{v'^2}(n) \cos \frac{2\pi n x'}{\bar{v}} . \qquad (5\text{-}2)$$

n_1 and n_2 are the lowest and highest frequencies respectively, at which a non-zero reading of f' in (5-1) is obtained on a spectrograph. (20 Hz and about 5000 Hz in these experiments). Note that $\overline{v'^2}$ should be the total fluctuation energy per unit mass contributed by the longitudinal fluctuations of all frequencies, 0 to ∞; as measured it was the sum of contributions over frequencies

n_1 to n_2 by some combination of all three components of the fluctuating velocity, but primarily that component in the flow direction, as already mentioned.

The signal, e', from the anemometer was also used to trigger a Philips (Holland) PW4231 digital counter designed to count $\pm$ 5 millivolt pulses. Self-noise from the anemometer and probe was a few millivolts (r.m.s.) so that a low count could be obtained without amplification at zero fluid speed. The unamplified e' signal was expected to give an estimate of the true number of zeroes for use with (4-22). Counts were taken both with and without an amplifier.

Oscillographs and vibrations.

In addition to its use for magnitude testing and fault tracing a Tektronix (U.S.A.) 502 A oscilloscope was used to provide a photographic record of the fluctuating voltage signal, Figure 5-13, and, in conjunction with a Philips (Holland) inductance-type vibration pick-up, to check magnitude and frequency of vibrations at and near the working section.

Procedure.

The turbulence measurements were made at night to obtain a more even ambient temperature, less power interference and to avoid the effects of other demands on laboratory water supply. 16 series of measurements (see

4, below) were made; 3 series at each ... of 4 stations with 4 of the 12 series repeated to check results. A brief outline of procedure follows; many checks and changes (e.g. in probe operating resistance) are left unstated.

1. After cleaning, the circuit was run for 1 to 4 hours to achieve a steady water temperature; meanwhile the electronic apparatus was prepared and calibrated.

2. The circuit was drained to insert the probe, filled, and run for 15 to 30 minutes to regain a steady water temperature.

3. Probe cold resistance was measured and the operating resistance set.

4. A series of measurements was taken: $\bar{e}$, e'_{rms}, 2 or more spectrographs, counts of $N_o t$ over several minutes, photographs of the oscilloscope (e') display, checks on fluid temperature and flow rate.

5. With the flow stopped, $\bar{e}_o$ was noted.

6. The probe was moved to a new position at the same station and 4,5 repeated twice (on the centreline and halfway to the wall on each side).

7. With the measurements at a station completed, the circuit drained and the probe moved to a new station the procedure was repeated from 1 or 2.

5.5 Photographic measurements.

Cine-photography.

Two 16 m.m. films for visual study of the particle flow were exposed in a Beckman and Whitley (U.S.A.) Magnifax Model 999 camera using a modified D.C. drive system. One film was taken using back-lighting by 1000 watt quartz-iodine floodlights, black rape seed and a camera framing rate of approximately 200 frames per second. The other film was taken using front-lighting with the floodlights, white polystyrene particles and a rate of approximately 400 frames per second. Projected at 16 frames per second, particles of actual speed 6-12 feet per second thus appeared to be moving 0.25-1 feet per second, allowing qualitative study of individual particle motions.

Stroboscopic photography.

The stroboscope which became the principal means of lighting was the most powerful available to the writer, but still barely sufficient. It was a Dawe (U.K.) Strobotorch 1202 D, a transistorised unit with a Xenon lamp whose flash duration was of the order of 10 microseconds.

Using stroboscopic photography to give multiple exposures of the particle on one area of film had several advantages over streak photography, with which it was extensively compared.(Figures 5-14,15):

1. The shutter mechanism open time does not enter into computations (as it does in streak photography); it need only be long enough to include several exposures of particle

position, and short enough to limit exposure of the background to film density appreciably below that caused by reflected light from the particle.

2. Particle edge determination was not affected by the shutter mechanism, as in streak photography, but by the flash duration. Particle movement during a 10 microsecond flash was in the order of 10^{-4} feet, virtually indetectable.

3. Flash rate was adjustable to give an average velocity over various distances between consecutive exposures. A short distance (high flash rate) gave better approximation to a point value but increased the relative error in distance measurement.

4. Individual particle shapes and sizes and the overall particle trajectory were shown.

1 inch flanges at each end of the diffuser reduced the observable length of flow to 9.33 inches. A mirror at 45 degrees above the diffuser allowed simultaneous elevation and plan (mirror) views to be recorded by a camera placed at the height of the diffuser, several feet away in a direction perpendicular to the flow.

An Asahi (Japan) Pentax Spotmatic SLR 35 m.m. camera with f 1.8, 55 m.m. lens was used for the stroboscopic photography. (Note that a focal plane shutter is not suitable for streak photography; a Robot (Germany) spring-motor 35 m.m. camera with compound shutter was used for

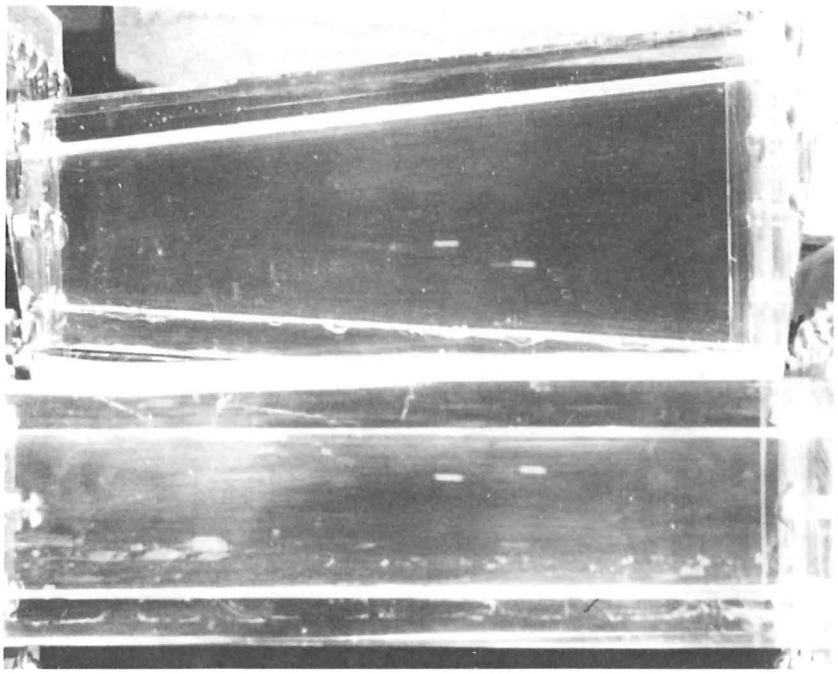

Figure 5-14. Stroboscopic particle photography.

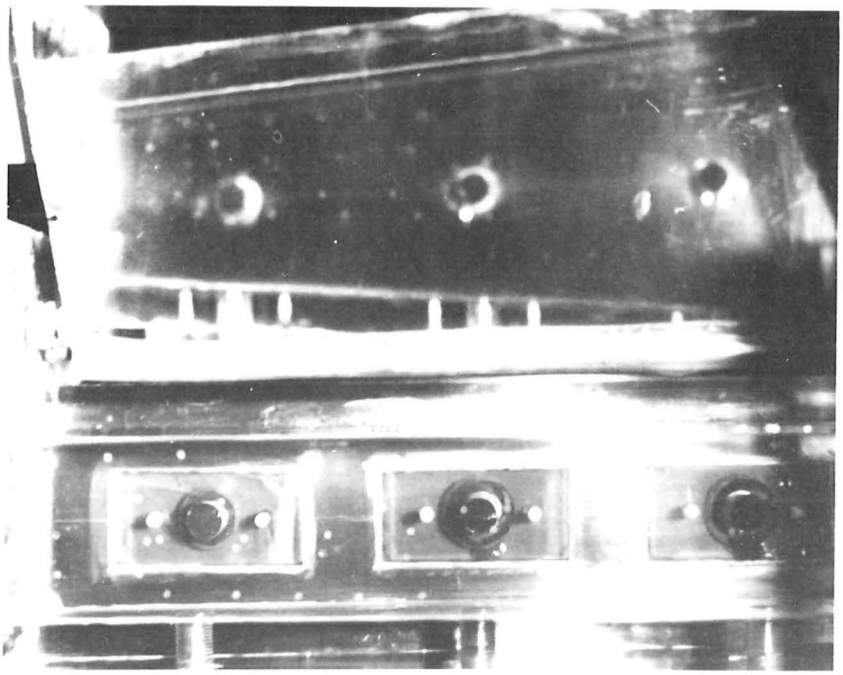

Figure 5-15. Streak particle photography.

this work). The camera was always placed with the film plane 2.250 feet from the centre of the diffuser; by using a template with cutaways for camera lens and diffuser flanges this could be accomplished to within 0.005 feet. The magnifications at positions in both views was then calculated from exposures of a 12 inch steel rule inside the water-filled diffuser, measuring the film distance corresponding to 0.125 inch graduations on the rule.

With the 1000 watt quartz-iodine floodlights used for cine-photography and streak lighting trials, either back-lighting or front-lighting was possible. Because of its much lower illumination the stroboscope was limited to front-lighting. Highly reflective particles (5.6) were used, being photographed against a general background of black cloth. In the particular areas against which measurements were to be made mirrors reflected incident light to distant parts of the laboratory roof. (All photography was performed at night).

Procedure.

The results chosen for detailed analysis (6.5) were taken from about 650 camera exposures on 35 m.m. film. The procedure used to obtain photographs was:

1. The equipment was positioned and the circuit flow rate set.

2. The stroboscope was calibrated against the mains

supply frequency (50 Hz) and the flash rate was set.

3. Background brightness readings were taken with an S.E.I. spot photometer and the stroboscope was positioned to give a minimum, reasonably uniform amount of unwanted reflection.

4. The particles were prepared and wetted, circuit flow rate and stroboscope flash rates were checked, and the camera set.

5. The particles were introduced and the film exposed.

The camera shutter would typically be open for 1/15 second, giving a possible 10 particle exposures using 150 flashes per second. By introducing a steady stream of particles it was possible to ensure a few particles on most camera exposures without causing inter-particle interference or difficulty in interpretation.

A good compromise between film emulsion speed and attainable contrast was obtained using Ilford FP3 (nominally 125 ASA) film and developing for maximum contrast in a caustic hydroquinone developer.

5.51 Measurements from the negatives.

Measurements of the steel rule suggested that variable expansion of the film backing material was not a problem as 3 films processed in different ways gave essentially the same magnifications.

The following information was taken from the negative

film record, see Figure 5-16.

1. The downstream(X), across-stream (Y), and vertical (Z) position assigned to a speed measurement; assigned by noting the grid volume into which a point half-way between successive images of a particle fell.

2. The separation on the film, d_f, of successive images was measured as the difference of two micrometer readings from an arbitrary datum, between a point on the edge of one circular image of a particle to a corresponding point on the next,(usually the furthest downstream point was most clearly defined as the lamp was slightly downstream of the camera).

3. Whether or not a particle stayed in one stream tube (fixed Y,Z) during the observed part of its passage through the diffuser.

Each 35 m.m. exposure was displayed 10 times film image size (approximately full size) on the ground glass screen of a Nikon (Japan) Shadowgraph. The film could be traversed in its own plane by two perpendicular micrometer screws. Transparent Perspex grids the same size as the projected images could be superimposed on the plan and elevation views and X,Y,Z grid positions noted for each pair of particle images used to provide a speed measurement. The separations were then measured by the X micrometer using the elevation (direct, not mirror) view only.

This measurement gives the component of particle velocity in the direction of the main flow; for a particle travelling parallel to the diverging wall the error is less than 0.5%. The information, some 4000 main measurements of (1,2,3), was called (directly or via a tape-recorder) and entered on card punching forms.

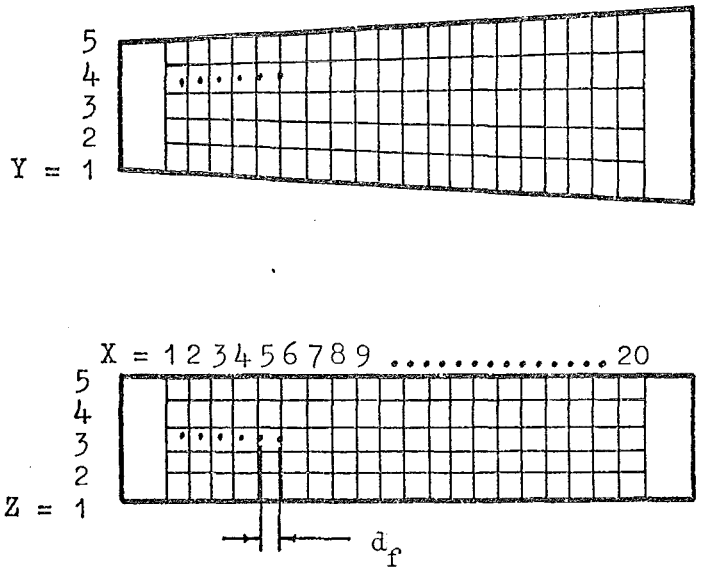

Figure 5-16. A d_f measurement at X,Y,Z = 5,4,3.

5.6 Spherical particles.

Several properties were required of particles to make them suitable for this study:

1. Particle diameters in a range large enough for easy determination and good photographic recording yet small compared to the dimensions of the flow section.

2. The particles were required to be as nearly spherical as possible, to coincide with the theoretical treatments in Chapters 2 and 3.

3. Surface smoothness does not influence drag at very low particle Reynolds numbers (Chapter 2) but it does at higher particle Reynolds numbers (Chapter 3). Very small relative roughness may be expected to give drag comparable to a smooth surface (relative roughness = 0).

4. A relative density sufficiently different from unity to give measurable slip speeds but not so different that particle trajectories were confined to near the top or base of the diffuser by their high rise or fall speeds.

5. High surface reflectivity for photographic recording.

6. Rigidity and mechanical strength sufficient to avoid changes in shape during transit through the circuit.

7. Physical properties (e.g. size, relative density) which were constant over the period of time from measurement to use. This implies, among other things, that water absorption should be negligible.

Polystyrene, rape seed, ballotini, poly-vinyl chloride and silica gel spheres were tested, polystyrene being found to be the most suitable. It was available as a raw material for making expanded plastic foam. Approximately 50% was finer than 0.05 inches diameter, d, and it ranged from 0.02 to 0.10 inches. After sieving, the fraction passed by a 0.081 inches aperture B.S. mesh but retained by a 0.066 inches aperture B.S. mesh was used for the main experiments (6.5). The diameter used for calculations was 0.073 inches. The particles had a smooth, highly reflective, white surface and most were nearly spherical. A minor disadvantage was a tendency for the particles to agglomerate and adsorb air so that sometimes a group of particles all more dense than water would rise to the surface of water in a container and float.

The 0.073 inches diameter fraction was split into relative density ($s = \frac{\rho_s}{\rho}$) ranges by immersion in turn in 4%, 3%, 2% and 1% sodium chloride solutions whose relative densities were accurately determined by the relative density bottle method. The polystyrene remained in that solution in which it first sank (when free of surface tension and adsorbed air). Approximately : 84% of the fraction had s greater than 1.0, 50% greater than 1.020 and 30% greater than 1.028. The two ranges used in the main experiments (6.5), with the values chosen to represent

them in calculations, were:

$1.007 < s < 1.015$, 1.011;

$1.022 < s < 1.029$, 1.025.

When all particles were considered as being in one range in the drag coefficient results, s = 1.015 was used, as approximately twice as many of the 1.011 group appeared in the results. The largest error incurred is for a 1.029 particle considered as 1.015, less than 1.5%.

The steady drag coefficient of a particle depends upon shape as well as particle Reynolds number and the relative roughness of its surface. The steady fall speeds of the polystyrene particles were checked by timing their fall through 24 inches of water (after 6 inches to attain steady speed) in a vertical tube 2 inches in diameter (about 28 particle diameters). The fall speeds were rechecked after soaking the particles for several days; there was no detectable difference.

Equating the net downward force from gravity and buoyancy to the steady drag, (3-1), yields, where v_s is the settling, or fall speed under gravity:

$$C_D = \frac{4gd(s-1)}{3v_s^2} \quad . \qquad (5-3)$$

The effects of adsorbed air on the particle surfaces and disturbances in the water (e.g. due to insufficient pauses between dropping particles) could be avoided by careful technique. Secondary motions such as lateral

oscillations were apparent for the more dense particles but not for the polystyrene, and surface roughness, although not measured, was considered to have been negligible. Thus the effects of the ranges on each of s,d, and of slightly non-spherical particles were estimated by the measured variation in v_s. From (5-3)

$$\frac{\delta v_s}{v_s} \simeq \frac{1}{2}\left(\frac{\delta d}{d} + \frac{\delta s}{s-1} + \frac{\delta C_D}{C_D}\right).$$

Maximum $\frac{\delta d}{d}$ due to the range already given is 10.6%; for $\frac{\delta s}{s-1}$ the maximum is $\frac{1.011 - 1.007}{1.007}$, 57%, so the maximum error expected in v_s from these two causes is nearly 34%. The effect of shape remains to be determined.

The measured results from two samples of 50 particles each are given in the following table.

Table 5-1.

Polystyrene fall speeds and drag coefficients.

s	$\bar{v}_s$	Standard deviation	$r_1^{(1)}$	$r_2^{(1)}$	$Re_{pt}^{(2)}$	$C_D^{(3)}$	$C_D^{(4)}$
1.022-1.029	.054	.007	26	39	30	2.16	2.0-2.2
1.007-1.015	.033	.008	48	72	18	3.11	2.9-3.1

(1) 95% (r_1) or 99% (r_2) of the approximately normal population of which the measured v_s are a sample are within $\pm$ r_1% or $\pm$ r_2% of the mean.

(2) Based on $\bar{v}_s$, d = 0.073 inches, n = 1.1 x 10^{-5} $ft^2 sec.^{-1}$ at test temperature.

(3) From (5-3) using $\bar{v}_s$, d = 0.073 inches, s = 1.025,1.011.

(4) From a standard C_D-Re_p curve, Figure 2, Goldstein (1938).

The measured C_D based upon mean fall speed of the samples are seen to be very close to standard values. The range on v_s for the more dense group of particles is in the order expected from the known ranges on s and d, but the range on the lighter particles is about twice that expected. This is probably due to a greater variation in shape, but the effect on drag coefficient averaged over 50 particles is clearly small.

CHAPTER SIX.

6. EXPERIMENTAL RESULTS AND DISCUSSION.

6.1 Introduction.

The results of experiments to establish the water velocity and turbulence parameters within the diffuser are given in 6.2 and 6.3. The effect that the experimental lighting system (5.5)has on particle sighting distributions and hence on calaulated drag coefficients, is explained in 6.4 and the calculated drag coefficients are given in 6.5. The results are analysed statistically in 6.51 and compared in 6.53 with a similar analysis (6.52) applied to a series of measurements made by Torobin and Gauvin (1961c).

6.2 Diffuser water velocity.

Figure 6-1 shows the static pressure variation with downstream position, x, in the diffuser, length L_d, for the driving flow static pressure used in the main tests, Hm = 20 p.s.i.g., and for two higher values. The separation of the total head tube face and static pressure tapping was 0.75 inches, or $\frac{x}{L_d} = 0.066$, and the correction made necessary by this separation (see 5.3) was always less than 0.15 feet of water. The error in calculating this correction from Figure 6-1 for the flow rate corresponding to Hm = 20 p.s.i.g. would be less than $\pm$ 0.02 feet and the lowest static pressure in the diffuser is 2.3 feet above the static

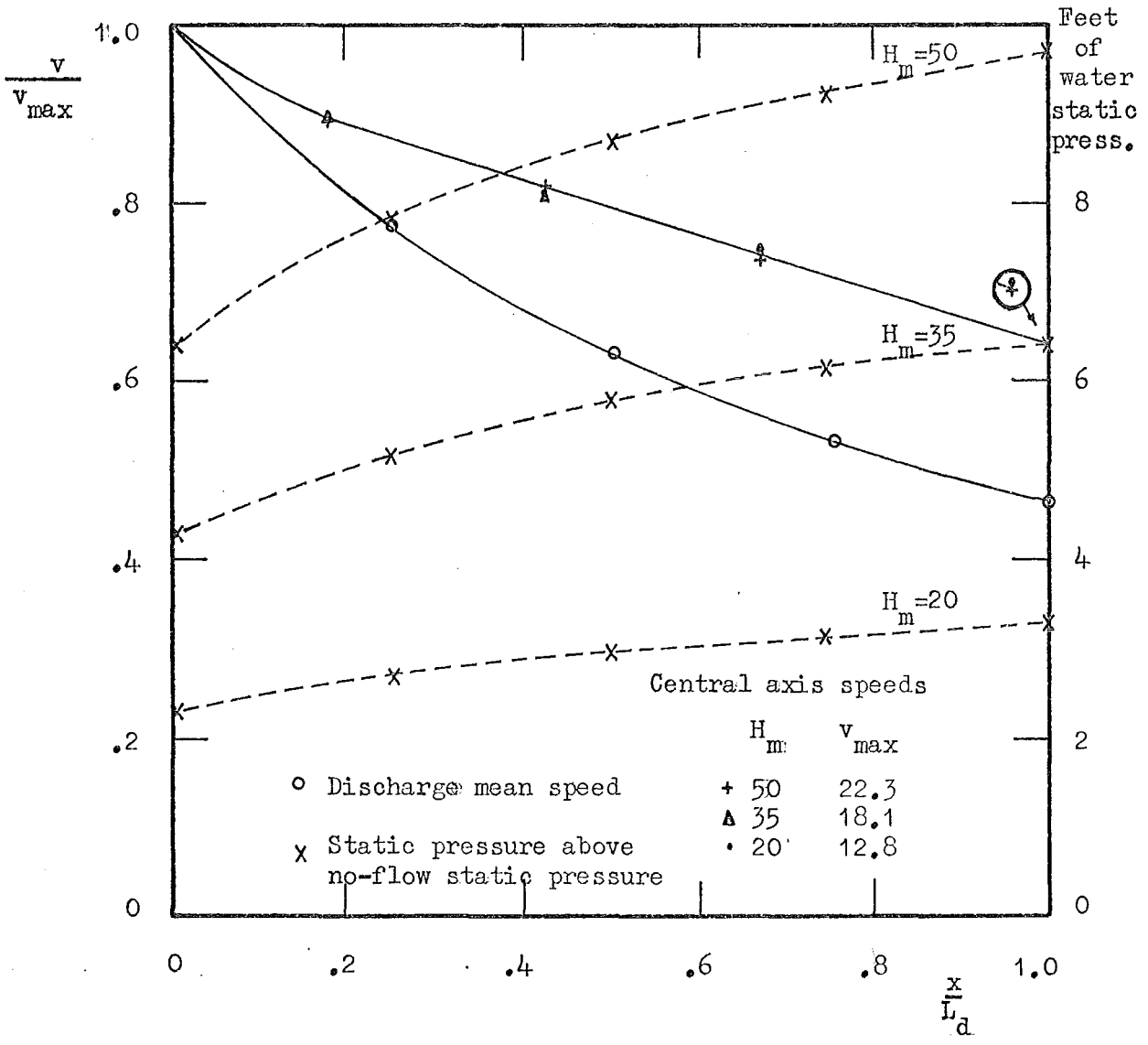

Figure 6-1. Static pressure and water speed variation through the diffuser.

pressure at zero flow, about 5 feet of water. The resulting maximum error in calculating speed would be $\pm$ 0.5 $(\frac{0.02}{7.3})$, $\pm$ 0.14%, which is negligible. The variation of measured speed in the streamwise direction through the diffuser is also shown in Figure 6-1.

The complete set of horizontal and vertical velocity profiles at five positions (upstream of, three stations in, and downstream of the diffuser) for the same three circuit flow rates as in Figure 6-1 are presented in dimensionless form in Figure 6-2. The dimensionless profiles were independent of flow rate for the range of Reynolds number (based on v_m and y_m or z_m, see Figure 6-2) 7.5×10^4 to 1.9×10^5, but dependent upon downstream position. The horizontal and vertical profiles at $\frac{x}{L_d} = 0$ show the symmetry at entry to the diffuser, thereafter the effect of the diffuser is evident. Horizontal profiles are more affected than vertical profiles by the diffuser, as would be expected, there being no change in the vertical dimension. The two horizontal profiles at $\frac{x}{L_d} = 0.68, 1.0$ show points of inflexion just over half-way to each wall, but all profiles are quite symmetrical and have approximately uniform curvatures near the centreline (see 4.2). Each curve on Figure 6-2 is the average of those for three flow rates; all points from the three flow rates fell within 2% of the average curve. The use of the measured profiles to estimate

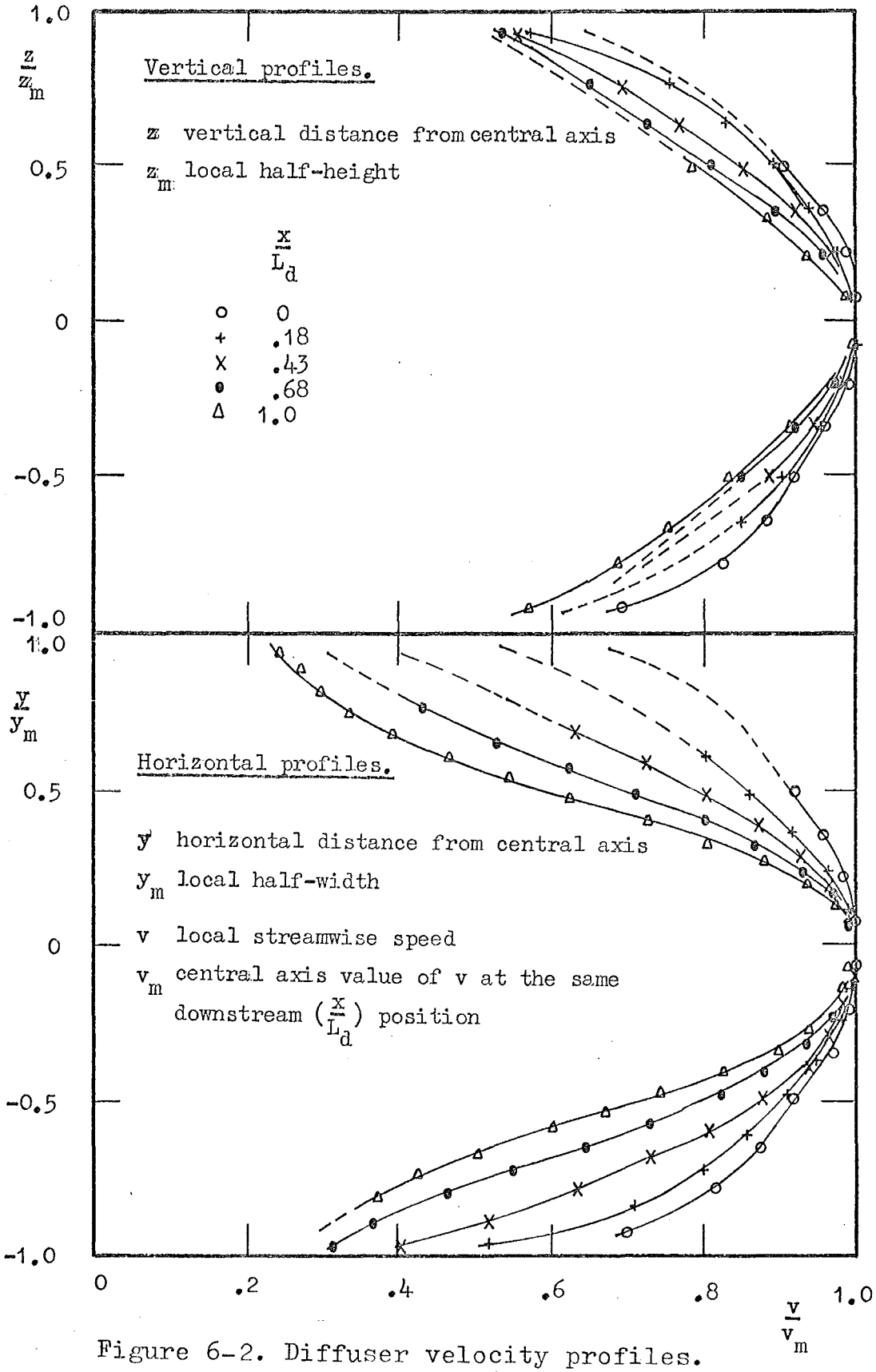

Figure 6-2. Diffuser velocity profiles.

values off the central planes and to compute mean water speeds for each grid position, (X,Y,Z) in Figures 4-2 and 5-16, is described in 4.5. The results are given in Table 6-1. Values at $\frac{x}{L_d} = 0$ and $\frac{x}{L_d} = 1.0$ were actually measured 1.875 inches upstream and 1.0 inches downstream of the diffuser.

Table 6-1.

Diffuser water speed map - see Figure 5-16.

(All speeds in ft.sec.$^{-1}$)

1. $\frac{x}{L_d} = 0$, core mean = 11.88, wall mean = 8.28, section mean = 9.57.

Z	Y = 1	2	3	4	5
1	6.58	8.62	9.05	8.62	6.58
2	8.77	11.49	12.06	11.49	8.77
3	9.23	12.09	12.69	12.09	9.23
4	8.77	11.49	12.06	11.49	8.77
5	6.58	8.62	9.05	8.62	6.58

2. $\frac{x}{L_d} = 0.18$, core mean = 10.42, wall mean = 6.66, section mean = 8.01.

Z	Y = 1	2	3	4	5
1	4.99	6.97	7.31	6.97	4.99
2	7.15	9.99	10.49	9.99	7.15
3	7.71	10.77	11.30	10.77	7.71
4	7.15	9.99	10.49	9.99	7.15
5	4.99	6.97	7.31	6.97	4.99

3. $\frac{x}{L_d}$ = 0.43, core mean = 8.99, wall mean = 4.93, section mean = 6.39.

Z	Y = 1	2	3	4	5
1	3.32	5.48	5.98	5.48	3.32
2	5.11	8.44	9.21	8.44	5.11
3	5.63	9.29	10.15	9.29	5.63
4	5.11	8.44	9.21	8.44	5.11
5	3.32	5.48	5.98	5.48	3.32

4. $\frac{x}{L_d}$ = 0.68, core mean = 7.84, wall mean = 3.88, section mean = 5.31.

Z	Y = 1	2	3	4	5
1	2.41	4.60	5.22	4.60	2.41
2	3.77	7.19	8.15	7.19	3.77
3	4.27	8.15	9.24	8.15	4.27
4	3.77	7.19	8.15	7.19	3.77
5	2.41	4.60	5.22	4.60	2.41

5. $\frac{x}{L_d}$ = 1.0, core mean = 6.79, wall mean = 2.80, section mean = 4.31.

Z	Y = 1	2	3	4	5
1	1.54	3.90	5.31	3.90	1.54
2	2.30	5.84	7.94	5.84	2.30
3	2.31	6.51	8.85	6.51	2.31
4	2.30	5.84	7.94	5.84	2.30
5	1.54	3.90	5.31	3.90	1.54

"Core" values are the means of speeds in the 9 grid areas which have no contact with a wall, i.e. (Y,Z), Y = 2,3,4, Z = 2,3,4. "Wall" values are the means of speeds in 16 grid areas, which are each in contact with at least one wall, i.e. (Y,Z), Y = 1,2,3,4,5 when Z = 1 or 5; Z = 2,3,4 when Y = 1 or 5. "Section" values are the discharge means for the entire flow section.

6.3 Turbulence results.

Table 6-2 lists measured values of the longitudinal turbulence intensity, I, based on local mean water speed, v. Values shown as I_1 were determined using the sum of values from (5-1) while (4-14) was used to calculate the I_2 values. The latter are generally higher since they include frequencies above 5 Hz while the former include only frequencies above 20 Hz (see 5.4). In view of the symmetry of the mean velocity profiles about the central axis, Figure 6-2, the difference in values derived at $\frac{y}{y_m} = 0.5$ and $\frac{y}{y_m} = -0.5$ was unexpected. It was almost certainly caused by probe blockage (5.4). Both (4-14) and (5-1) contain the expression $\frac{\bar{e}}{\bar{e}^2 - \bar{e}_o^2}$ which decreases as the blockage effect causes the mean local speed, and therefore $\bar{e}$, to increase. For the values measured 3 feet upstream of the diffuser (shown as $\frac{x}{L_d} = 0$) the probe entered from the $\frac{y}{y_m} = -1$ side and I_2 at $\frac{y}{y_m} = -0.5$ is higher than that at

$\frac{y}{y_m}$ = 0.5 by 23%; at the remaining three positions the probe entered from the $\frac{y}{y_m}$ = 1 side and the values at $\frac{y}{y_m}$ = 0.5 markedly exceed those at $\frac{y}{y_m}$ = -0.5 (by as much as 40% of the $\frac{y}{y_m}$ = 0.5 value). Assuming that values differ more from undisturbed values as the probe projects further into the flow, $\frac{y}{y_m}$ = 0.5 values will be the best approximations to undisturbed values at the three positions within the diffuser (-0.5 upstream of the diffuser), centreline values will be low and $\frac{y}{y_m}$ = -0.5 values even lower. I_3 in Table 6-2 gives the centreline I_2 values and the most reliable of the other I_2 values.

Anomalous values of 5.1 for I_1 and 6.7 for I_2 occurred where gaps have been left in the table; the hypothesis that $\frac{y}{y_m}$ = 0.5, -0.5 values differ due to probe blockage would have them lower than their $\frac{y}{y_m}$ = 0.5 counterparts. A check made on the I_2 value only (without the full procedure, 5.4) gave 3.2% at $\frac{x}{L_d}$ = 0.21 $\frac{y}{y_m}$ = -0.5 while values at two other positions verified the values shown to within 4%, two more to within 30%. This probably indicates that an error occurred in obtaining the omitted values and does not detract from the probe blockage hypothesis.

Table 6-2.

Turbulence intensity, %.

$\frac{x}{L_d}$	$\frac{y}{y_m}$	I_1	I_2	I_3
0	0.5	1.4	2.0	2.6
0	0	0.9	1.2	1.2
0	-0.5	1.8	2.6	2.6
0.21	0.5	3.8	4.8	4.8
0.21	0	2.7	2.9	2.9
0.21	-0.5	-	-	4.8
0.46	0.5	6.3	7.5	7.5
0.46	0	3.5	4.4	4.4
0.46	-0.5	4.5	5.1	7.5
0.72	0.5	11.2	15.0	15.0
0.72	0	3.9	5.0	5.0
0.72	-0.5	6.0	9.0	15.0

I_1 is measured from the spectrographs, the sum of (5-1), lower frequency limit 20 Hz.

I_2 is measured directly from the anemometer, using (4-14), lower frequency limit 5 Hz.

I_3 is the intensity used to calculate Ir (see the reasons for its choice in the text).

The increase in intensity through the diffuser was expected; it may be compared with its opposite effect, the use of contractions in wind tunnels to damp the longitudinal component. Likewise it is known that the lateral distribution of I has a minimum at the central axis (see Laufer (1950)) in pipe or channel flow; the value of $I\frac{v}{v_m}$ at $\frac{y}{y_m} = 0.5$, $\frac{x}{L_d} = 0$ is 2.02 times the central axis value (Reynolds number $\frac{v_m\, y_m}{n} = 73{,}000$), 1.74 times in Laufer's results (Reynolds number 61,600, but two-dimensional flow of air in a 5 feet by 5 inches flow section channel). The ratio increases through the diffuser, from 2.02 at $\frac{x}{L_d} = 0$ to 2.4 at $\frac{x}{L_d} = 0.72$.

Two of the measured spectrographs from which values for (5-2) were noted are shown in Figure B-1 of Appendix B and the energy spectra derived from the four spectrographs at $\frac{y}{y_m} = 0$ and four values of $\frac{x}{L_d}$ are shown in Figure 6-3. All spectra were of similar shape and conformed approximately to the $-\frac{5}{3}$ inertial subrange at frequencies near 100 Hz (see page 189, Hinze (1959)). Laufer's result from the channel referred to above has the same general shape and is included in Figure 6-3 for comparison. The off-centreline spectra closely approximated the centreline spectrum at the same downstream position. It was noticeable that the $\frac{y}{y_m} = 0.5$ spectrum was of slightly different shape from the other two at $\frac{x}{L_d} = 0$, whereas the $\frac{y}{y_m} = -0.5$ spectra were the

Figure 6-3. Central axis turbulence spectra.

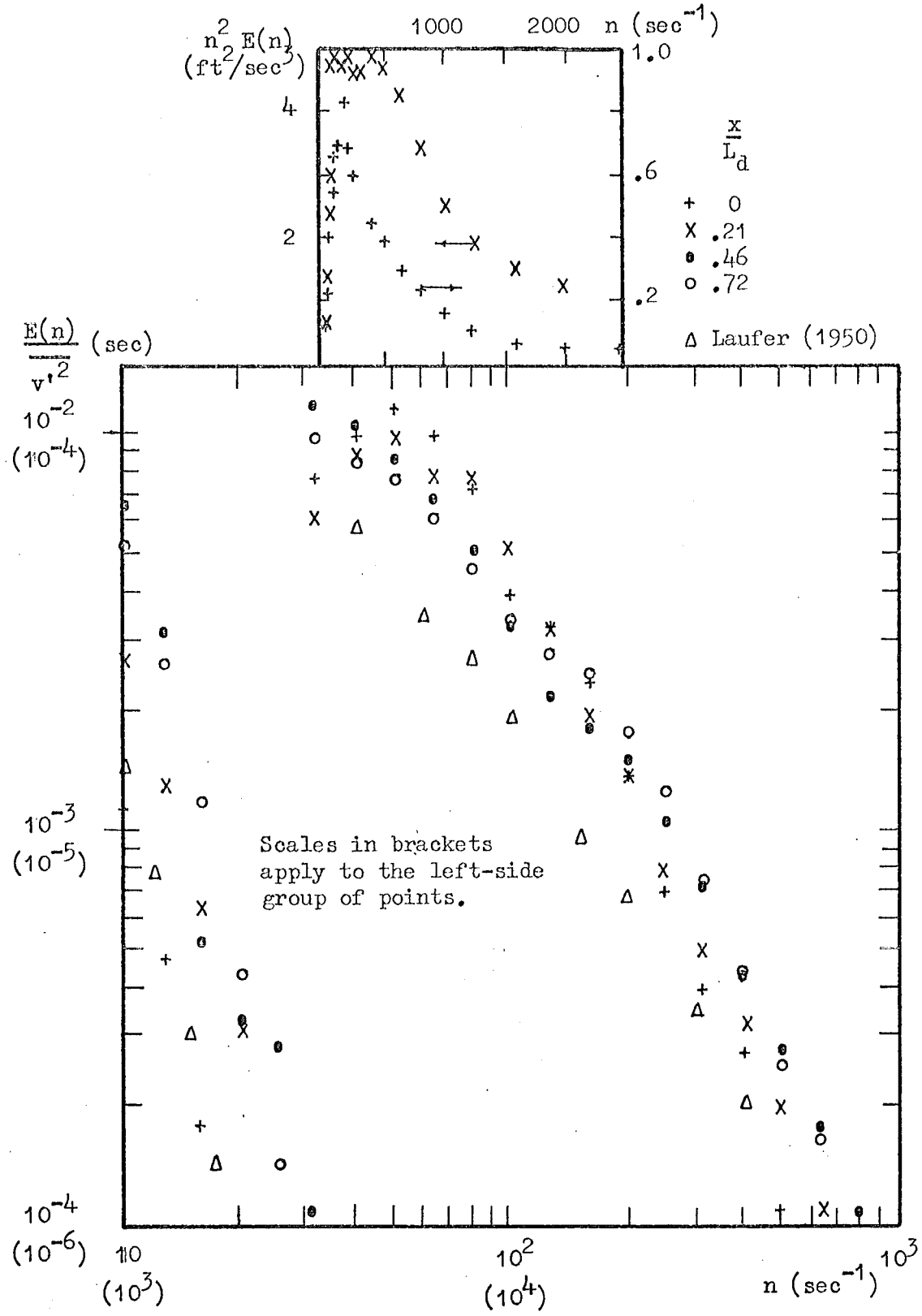

odd ones at $\frac{x}{L_d}$ = 0.21, 0.46. (The spectra at $\frac{x}{L_d}$ = 0.72 did not agree with this trend but scatter was higher at this position than at the other three). This variation again suggests the probe interference effect.

The variation in spectrum shape through the diffuser is clear from Figure 6-3; though slight it is systematic. E(n) decreases at lower frequencies and increases at higher frequencies as x (and the flow section area) increases.

Six of the twelve measured spectra showed peaks in the measured range of frequency (see 5.4) and five of these were either on the centreline or the side least affected by probe blockage (see note (1),Table 6-3). Using (4-18) to estimate Eulerian integral scale gives the five values shown in Table 6-3 as L_{e_1}. L_{e_2} in Table 6-3 represents those values of integral scale calculated from (4-19) which used measured values in the $-\frac{5}{3}$ ranges of the spectra. Solutions of (4-19) showed approximately constant values of L_{e_2} near the middle of the $-\frac{5}{3}$ ranges; higher values usually being obtained at both higher and lower frequencies.

The longitudinal correlation curves obtained by computing the Fourier transforms of the measured spectra, as described in 4.6, were of the shape expected at small separation distances but showed quite extensive negative correlation at greater separations. This makes measurement of area under the curve a little arbitrary; to provide a

comparison with the other methods the values shown as L_{e_3} in Table 6-3 were computed using (4-17), and taking as upper limit of x' that value where f first became zero. The four centre-line curves are shown in Figure 6-4; the $\frac{y}{y_m} = \pm 0.5$ curves were of similar shape.

Table 6-3.

Longitudinal Eulerian integral scale (inches).

$\frac{x}{L_d}$	$\frac{y}{y_m}$ (1)	L_{e_1}	L_{e_2}	L_{e_3}
0	$\pm$0.5	0.4	0.5	0.21
0	0	0.4	0.4	0.22
0.21	$\pm$0.5	0.3	.5-.6	0.19
0.21	0	0.3	.2-.3	0.19
0.46	$\pm$0.5	0.4	0.2	0.12
0.46	0	-	.3-.5	0.17
0.72	$\pm$0.5	-	0.5	0.16
0.72	0	-	0.2	0.13

L_{e_1} is the scale from von Karman's formula, (4-18);
L_{e_2} is the scale from Liepmann and Laufer's formula, (4-19);
L_{e_3} is the scale from correlation curves, by (4-17).

(1) The probe blockage effect explained in connection with turbulent intensities, Table 6-2, is known to have affected spectrum measurements. The $\frac{y}{y_m} = \pm 0.5$ values are

from $\frac{y}{y_m} = -0.5$ at $\frac{x}{L_d} = 0$, $\frac{y}{y_m} = 0.5$ elsewhere (see the first paragraph of 6.3).

L_{e_3} values were expected to be low; the low-frequency cut-off prevented contributions from frequencies below 20 Hz being included in the Fourier integral, (4-16). L_{e_1} and L_{e_2} are unaffected by the low frequency limit. Integral scale is therefore in the range 0.2 to 0.6 inches (approximately, 0.2 to 0.6 of the half-height) and shows tendencies to be greater upstream than downstream, and greater halfway horizontally to the diverging walls than on the centreline. None of the methods gives clearly accurate estimates of integral scale.

The area beneath curves of $(n^2 E(n), n)$ to linear scales was used to estimate microscale, using (4-21). The insert on Figure 6-3 shows two of the centreline curves and illustrates the main problem of the method, the difficulty in determining the area under the tail of the curve. A planimeter was used on large-scale graphs like those in the insert, extrapolating the curves to $n^2 E(n) = 0$ at approximately the same slope as that of the last recorded values. These calculated values of microscale, λ_1, are given in Table 6-4. Microscale was also calculated from correlation curves including those in Figure 6-4, using (4-20) and a separation of 0.01 inches; these are the λ_2 values. λ_3 values in Table 6-4 were measured using the

zero-counting technique and calculated from (4-22). The Λ_3 column is incomplete as some results were clearly incorrect (those from an unamplified signal, see 5.4).

Microscale, like integral scale, shows tendencies to decrease through the diffuser and to have values higher at $\frac{y}{y_m} = \pm 0.5$ than at $\frac{y}{y_m} = 0$. It is in the order of 10% (extremes of 7-35%) of the half-height; the corresponding figure from Laufer's (1950) results is 3% at $\frac{y}{y_m} = 0$, 9% at $\frac{y}{y_m} = \pm 0.5$. Raichlen (1967), in open channel flow of water, found Λ to be 7-13% of the depth. The agreement among values found by the different methods is better than for integral scale, Table 6-3, and it is considered that the values of Λ_2 are the most reliable of all the scale measurements.

The frequencies of circuit vibrations in longitudinal (streamwise) and vertical directions (5.4) were predominately 150 Hz and 250 Hz near the diffuser. Large-scale graphs like the insert on Figure 6-4 showed some obvious changes in curve shape (usually a marked decrease, as for the curves shown) at frequencies 100-150 Hz and 250 Hz. However, the effect is less noticeable on $(\frac{E(n)}{v'^2}, n)$ curves, Figure 6-3, and no correction was made.

Table 6-4.

Longitudinal microscale (inches).

$\frac{x}{L_d}$	$\frac{y}{y_m}$ (1)	$\mathcal{L}_1$	$\mathcal{L}_2$	$\mathcal{L}_3$
0	0.5	.31	.22	.22
0	0	.25	.13	.16
0	-0.5	.22	.16	-
0.21	0.5	.15	.11	-
0.21	0	.13	.13	.07
0.21	-0.5	.22	.19	.10
0.46	0.5	.11	.09	-
0.46	0	.11	.09	-
0.46	-0.5	.12	.10	-
0.72	0.5	.13	.10	-
0.72	0	.10	.08	-
0.72	-0.5	.10	.06	-

$\mathcal{L}_1$ is microscale from the measured spectra, using (4-21);

$\mathcal{L}_2$ is microscale from the correlation curves, using (4-20);

$\mathcal{L}_3$ is microscale from zero-counting, using (4-22).

(1) The probe interference effect will effect $\mathcal{L}_1$, $\mathcal{L}_2$, values, but not $\mathcal{L}_3$ values.

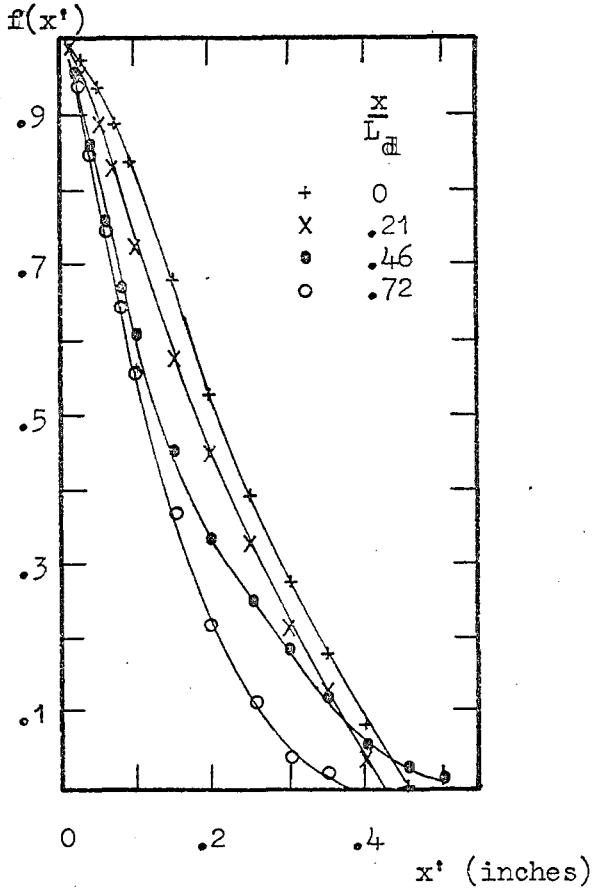

Figure 6-4. Central axis longitudinal correlation.

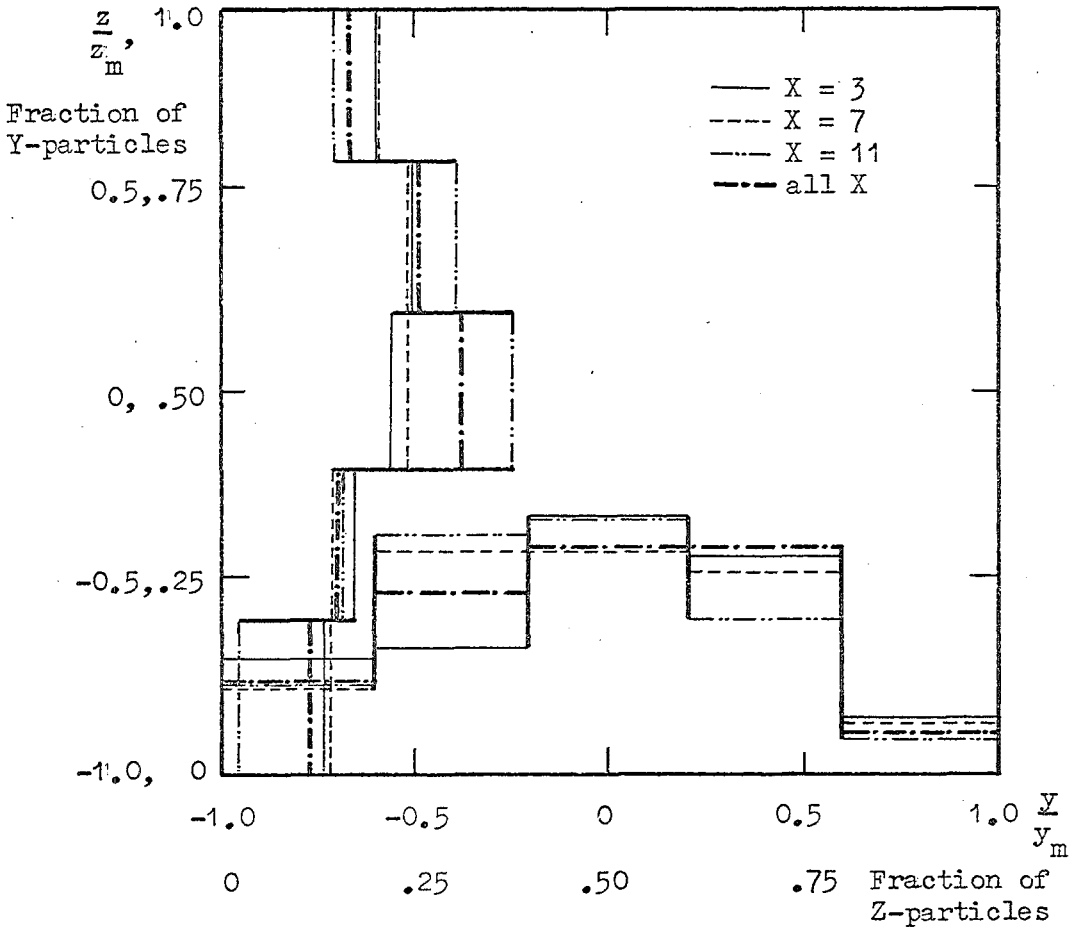

Figure 6-5. Typical particle sighting distributions.

6.4 Particle sighting distributions; entry conditions.

A neutrally buoyant particle suspended in turbulent flow in a uniform, horizontal conduit has been shown to wander across the flow section so that its mean forward speed after a sufficient length of travel differs from the fluid mean speed only because it neglects that range of speeds in the region close to the walls from which its finite size excludes it. Particles with relative density slightly greater or less than unity sample more of the slower speeds near the bottom or top of the conduit, respectively, and have lower mean speeds than their neutrally buoyant counterparts; smaller particles will be more affected than larger particles by the latter effect as they are excluded from less of the lower speed region near the walls. (See Barnard and Binnie (1963) and references therein).

The particles used for these experiments could be expected to have paths whose probability distributions have peaks in the vertical (z) direction just below the mid-height due to their slightly greater than unity relative density, and distributions in the horizontal (y) direction showing their tendency to resist the influence of curved streamlines i.e. their inertial tendency to stay nearer the diffuser centre. The particle sighting distributions depended both upon the true probability distributions and

the effectiveness of the photographic system used to record them; some regions were better lit than others. Some actual sighting distributions are shown in Figure 6-5.

An uneven sighting distribution could unfairly bias a calculated average; e.g. if in a core average (see 6.2) lighting is such that more Y,Z = 3,3 particles (the fastest-moving) than any other are sighted, a straightforward mean including all particles in the 9 core grid volumes would be high. The mean should be obtained by finding individual means in the 9 grid volumes and calculating their average. Figure 6-5 shows the variation between grid volumes but not within grid volumes. Assuming the particles are not stratified in any way the sighting distribution within grid volumes may be inferred from a smooth curve drawn through the histogram mid-ordinates. Such a curve showed that in an extreme case there could have been 50% more particles sighted in 0.1 of a grid volume nearer the distribution peak than in 0.1 of a grid volume more remote from the peak. As particle speeds in general increased towards the diffuser central axis a high value for the grid volume mean would result. With small sample sizes the effect contributes to a variation in means between adjacent grid volumes.

Another local effect was the poor sighting against the pressure tappings, Figures 5-9,14; this reduced the number

of central axis sightings and gave a low particle mean at the Y,Z = 3,3 grid volumes. The main effect of the sighting distributions in these experiments was to give higher mean speeds than the true grid volume average in general, and thus lower drag coefficients than would be obtained if such averaging was made unnecessary by a much larger number of measurements. The form of the dependence of drag coefficient upon its parameters will not be altered, however, and so the uneven sighting distributions do not affect the main purpose of the experiments.

6.5 Drag coefficients in non-steady, turbulent flow.

The particle motion data obtained by analysing negatives (see 5.51) was processed at the University of Canterbury computing centre on an IBM 360/44 computer. The set of results for each grid volume is given in Appendix C. For the reasons given in 4.4 and 6.4 the sample sizes at individual grid volumes are too small and averaging over several grid volumes proved necessary. Six grouping were considered (see Figures 4-2, 5-16):

(i) The four volumes at the corners of the 9 core volumes at each downstream position:

(ii) The three core volumes at Y = 2:

(iii) The three core volumes at Y = 4:

(iv) The three core volumes at Z = 2:

(v) The three core volumes at Z = 4:

Table 6-5.

Average drag coefficients and parameters.

Set (i), s = 1.025.

$\frac{x}{L_d}$	C_{DA}	$Re_p^{(1)}$	2Ac	Ir
.200	2.84	253	2.09	2.02
.225	2.30	300	1.64	1.75
.250	2.06	310	1.46	1.76
.275	1.78	333	1.24	1.71
.300	1.55	345	1.07	1.68
.325	1.11	379	.74	1.59
.350	.933	414	.60	1.50
.375	.756	448	.48	1.41
.400	.906	425	.58	1.54
.425	.774	460	.49	1.46
.450	.619	505	.38	1.36
.475	.601	530	.37	1.36
.500	.604	550	.37	1.35
.525	.579	550	.35	1.41
.550	.496	574	.30	1.41
.575	.460	587	.27	1.46
.600	.416	610	.24	1.46

Set (i), s = 1.011.

.250	12.25	150	9.00	3.66
.275	8.46	219	6.09	2.61
.300	7.06	300	5.09	1.94
.325	5.05	391	3.60	1.54
.350	2.60	550	1.82	1.13
.375	1.95	632	1.34	1.01
.400	1.27	700	.86	.93
.425	.53	780	.31	.86
.450	.26	840	.13	.82

Table 6-5 (continued).

	$\frac{x}{L_d}$	C_{DA}	Re_p	2Ac	Ir
Set (ii)					
	.200	9.63	129	7.28	3.96
	.225	5.02	164	3.70	3.18
	.250	6.92	152	5.12	3.59
	.275	5.04	210	3.64	2.70
	.300	4.72	210	3.36	2.76
	.325	3.32	246	2.33	2.45
	.350	2.71	257	1.88	2.42
	.375	1.62	316	1.08	2.01
	.400	1.66	316	1.11	2.07
	.425	1.42	328	.91	2.05
	.450	.982	375	.61	1.85
	.475	1.02	351	.64	2.06
	.500	.903	364	.54	2.06
	.525	.806	364	.48	2.15
	.550	.645	364	.37	2.24
Set (iii)					
	.200	9.63	129	7.28	3.96
	.225	5.02	164	3.70	3.18
	.250	8.80	199	6.40	2.74
	.275	5.91	270	4.24	2.12
	.300	4.90	305	3.50	1.91
	.325	3.65	351	2.59	1.72
	.350	3.35	410	2.35	1.52
	.375	2.14	528	1.48	1.21
	.400	2.26	586	1.58	1.12
	.425	1.37	690	.93	.98
	.450	.784	772	.51	.90
	.475	.531	809	.33	.89
	.500	.335	820	.18	.91
	.525	.139	820	.039	.95
	.550	.100	831	.016	.98

Table 6-5 (continued).

	$\frac{x}{L_d}$	C_{DA}	Re_p	2Ac	Ir
Set (iv)					
	.275	1.24	128	.98	4.43
	.300	9.11	128	6.80	4.50
	.325	8.92	176	6.50	3.43
	.350	7.59	245	5.50	2.54
	.375	6.84	292	4.95	2.18
	.400	3.13	433	2.21	1.51
	.425	1.82	490	1.24	1.37
	.450	1.03	561	.67	1.23
	.475	.545	584	.32	1.23
	.500	.184	572	.06	.97
Set (v)					
	.225	.365	421	.15	1.24
	.250	.588	421	.32	1.30
	.275	.605	434	.33	1.32
	.300	.705	445	.42	1.31
	.325	.623	468	.36	1.29
	.350	.966	480	.62	1.30
	.375	1.04	502	.67	1.26
	.400	1.10	550	.72	1.19
	.425	1.02	561	.66	1.20
	.450	.846	620	.55	1.12
	.475	.545	679	.33	1.06
	.500	.284	690	.14	1.08

Table 6-5 (continued).

Set (vi)

$\frac{x}{L_d}$	C_{DA}	$Re_p^{(1)}$	2Ac	Ir
.225	7.86	72	6.97	7.08
.250	33.0	72	28.0	7.40
.275	20.6	119	15.4	4.61
.300	10.1	191	7.31	2.93
.325	6.23	226	4.50	2.57
.350	4.77	250	3.40	2.40
.375	2.98	334	2.10	1.83
.400	1.86	381	1.26	1.66
.425	1.21	393	.78	1.65
.450	1.01	405	.64	1.65
.475	.686	465	.41	1.50
.500	.577	476	.33	1.51
.525	.460	489	.25	1.54

(1) Kinematic viscosity, $n = 1.2 \times 10^{-5}$ $ft^2 sec.^{-1}$

(vi) All nine core volumes.

Table 6-5 lists average results in each of the above six sets for each $\frac{x}{L_d}$ value considered. A simple (unweighted) average of the mean speeds in the relevant grid volumes was used to calculated the spatial means (see 6.4).

A sufficient number of particle sightings was obtained in sets (i) and (vi) to allow the two particle density fractions to be considered separately and this was done for set (i). In sets (ii) to (vi) a relative density of s = 1.015 was used (see 5.6).

The variation of mean particle speeds with distance through the diffuser is shown in Figure 6-6 compared with the appropriate mean water speed calculated for the grid volumes considered from the values in Table 6-1. The limited distance over which the curves of $\frac{v_p}{v_{max}}$ can be drawn is caused by the interference due to the diffuser flanges (see 5.5) and by the fewer sightings in downstream parts of the diffuser, where illumination was weaker.

The curves of Figure 6-6, together with particle relative density and diameter, enable C_{DA} and Ac to be calculated from (4-6,7) respectively and $Re_p = \frac{2a(v_p - v)}{n}$ to be evaluated. The values of $\frac{dv}{dx}$ used in (4-6,7) were found by differentiating a quadratic fitted to the measured $(\frac{v}{v_{max}}, \frac{x}{L_d})$ curve. $\frac{dv}{dx}$ is then $\frac{v_{max}}{L_d}$ multiplied by the slope of the curve. At each $\frac{x}{L_d}$ position the slope of

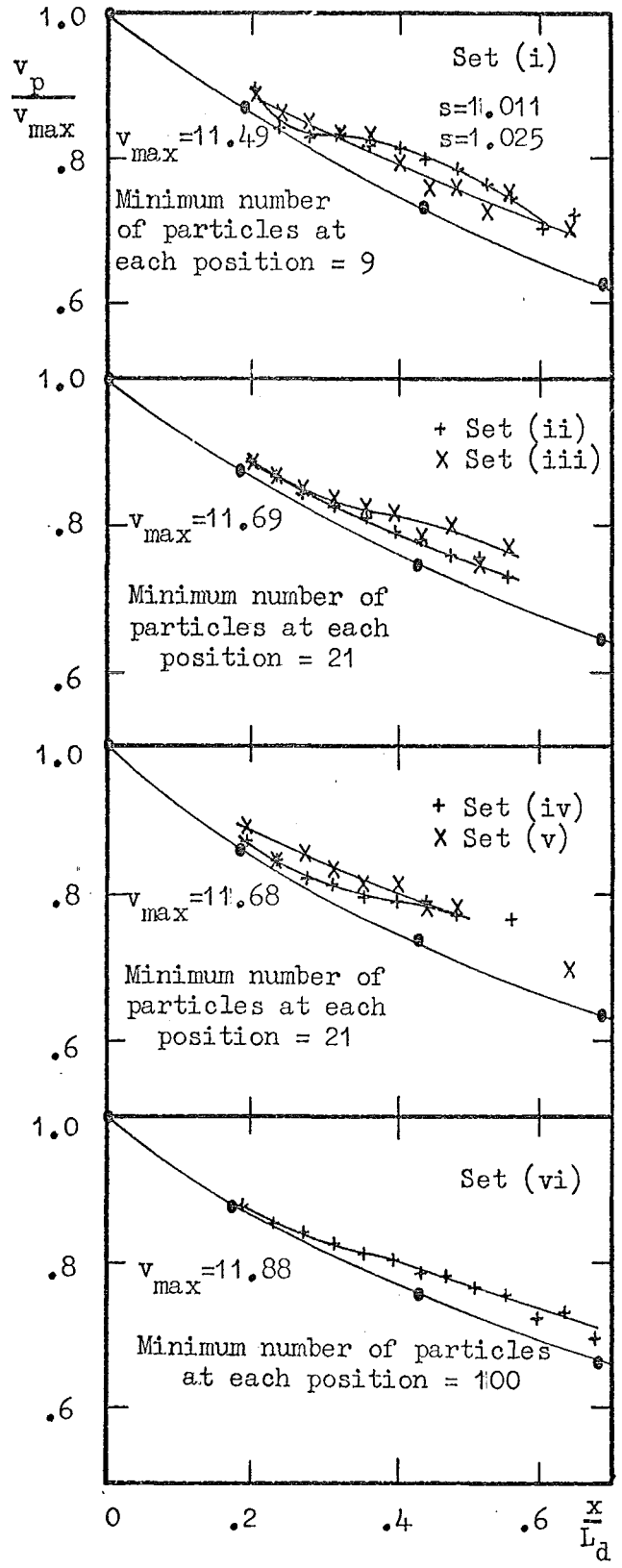

v_{max} is that central axis value of mean water speed, v, at $\frac{x}{L_d}$=0 which is appropriate to the grid volumes in each set.

• Water speed averaged over the same grid volumes as particle speed.

Figure 6-6. Mean particle speeds.

the $\frac{v_p}{v_{max}}$ curve was measured by carefully drawing a tangent. Multiplying this slope by the factor $\frac{v_{max}}{L_d}$ gives $\frac{dv_p}{dx}$. The values of Ac calculated from (4-7) are shown doubled in Table 6-5 as it is more usual to use diameter as the typical length in such a dimensionless group.

Values of particle relative turbulence intensity, Ir, appropriate to sets (i) to (vi) inclusive above were estimated from the values of turbulence intensity, I_3, in Table 6-2. Values of I at $\frac{x}{L_d}$ = 0.2 to 0.6 were estimated for $\frac{y}{y_m}$ = 0 and $\pm$ 0.5 by smooth curves drawn through plots of the I_3, $\frac{x}{L_d}$ values in Tables 6-2. Using interpolated local values of mean water speed at the same $\frac{x}{L_d}$ values the root-mean-square fluctuation energies per unit mass, $Iv = \sqrt{v'^2}$, were calculated for these values of I. The values of Iv at $\frac{y}{y_m} = \pm$ 0.5, when divided by the local slip speed, v_p-v, (like v, interpolated from Figure 6-6) gave the estimates of Ir for the spatial averages of C_{DA} which involved grid volumes midway between diffuser central axis and boundaries, sets (i) to (v) above. Values of Iv halfway from the central axis to top or bottom boundaries (sets (iv), (v)) or halfway to the corners (set(i)) are thus assumed to approximate values of Iv halfway from the central axis to the side walls. Such an assumption is necessary as only the $\frac{y}{y_m} = \pm$ 0.5 and 0, $\frac{z}{z_m}$ = 0 values were measured. Set (vi) involves eight grid volumes halfway to

boundaries and the central grid volume; for this set of results Ir was estimated from

$$Ir^2 = \frac{(Iv)_o^2 + 8(Iv)_{o.5}^2}{9(v_p - v)^2},$$

where the subscripts refer to the value of $\frac{y}{y_m}$. Values of Ir for set (vi) thus take the lower values of I near the central axis into account.

The variation of turbulence scale in the area of interest is slight, Tables 6-3,4. As a much wider range of scale values would be needed to detect their expected small contribution to C_{DA} values (see 3.45) scale is not included in the subsequent analysis, except to specify the approximate values for these experiments.

The arguments presented in Chapter 3 suggested that C_{DA} would depend upon Re_p, Ac, Ir, and to a lesser extent upon s and the relative turbulence scale. As it was experimentally impracticable to fix the values of four of the parameters while examining the influence of the fifth upon C_{DA} the 91 values in Table 6-5 do not show the influence of the four included parameters directly. It is evident from the table that the low slip speeds in these experiments give very high values of the particle relative turbulence intensity. C_{DA} values range from an order of magnitude larger than steady drag values at the same particle Reynolds number when this is about 100, to an

order of magnitude smaller when Re_p is about 1000. Also, a general pattern of C_{DA} decreasing with increasing Re_p or Ir and increasing with increasing Ac is apparent. A log-log plot of C_{DA}-Re_p was made with the values of Ac, Ir noted against each point. This suggested that sharp changes in direction of (C_{DA},Re_p) curves for constant Ac,Ir would not occur - the Reynolds number range of 70-850 is apparently below values where minimums occur for the ranges on the other parameters in these results. It also showed that these curves would have negative slope and be approximately linear on a log-log plot so that a multiple linear regression technique using logarithms of the experimental parameters as modified variables is an appropriate way of examining the results.

6.51 Statistical analysis of the drag coefficient results.

The fit of the data to

$$C_{DA} = B\ Re_p^{\,h}\ Ac^{i}\ Ir^{j}\ s^{k} \qquad (6\text{-}1)$$

was investigated by transforming to modified variables:

$$\ln C_{DA} = \ln B + h \ln Re_p + i \ln Ac + j \ln Ir + k \ln s,$$

$$L_C = L_b + h\,L_r + i\,L_a + j\,L_i + k\,L_s, \quad \text{say.} \qquad (6\text{-}2)$$

Then L_b is the intercept and h,i,j,k are the partial regression coefficients found by standard regression techniques (see, for instance, Volk (1958), Williams (1959)).

Modification of (6-1) to (6-2) means that the regression minimises the sum of squares of the deviations of observed

L_c from predicted L_c, rather than observed C_{DA} from predicted C_{DA}. The "logarithmic transposal discrepancy error" means that undue emphasis is placed on fitting the power equation to small values of C_{DA}. (Note, for instance, that observed C_{DA} deviations; 12 - 8 = 4, and 0.15 - 0.1 = .05 both give the same L_c deviation, 0.4055). Data points will appear evenly spread about the regression hyperplane using log-log coordinates, but to linear coordinates the hyperplane may appear to ignore some larger values of C_{DA}. Using (6-2) is of no serious disadvantage here as the functional form is of more importance than exactness of fit.

The regression was performed on an IBM 360/44 by a standard program (REGR) from a Scientific Subroutine package, IBM (1968). Table 6-6 is a summary of the relevant results.

The variance ratios in Table 6-6 may be compared with tables of Fisher's F (e.g. Fisher and Yates (1963)), and are seen to be all highly significant; there is much less than a one in one thousand probability that any of the correlations could have occurred by chance. The high correlations between "independent" variables shown in the last three rows of Table 6-6 does not detract from the significance of the other correlations, but does make it more difficult to separate the individual effects of variables. That Ac alone explains 99% of the variation in

Table 6-6.

Multiple regression; C_{DA} upon combinations of Re_p, Ac, Ir, and s.

Included parameters	L_b (1)	h	i	j	k	Correlation (2)	Sums of squares (3) ATR	DFR	Degrees of freedom (4)	Variance ratio
C_{DA} : Re_p,Ac,Ir,s	11.980	-.220	.824	-.117	-9.939	.996	123.756	.925	4,86	2875
C_{DA} : Re_p,Ac,Ir	11.910	-.233	.836	-.150	-	.996	123.609	1.073	3,87	3341
C_{DA} : Re_p,Ac	1.045	-.101	.840	-	-	.996	123.595	1.086	2,88	5007
C_{DA} : Re_p,Ir	20.484	-3.227	-	1.756	-	.840	88.051	36.630	2,88	105.8
C_{DA} : Ac,Ir	.402	-	.849	.090	-	.995	123.566	1.115	2,88	4876
C_{DA} : Ac	.451	-	.874	-	-	.995	123.503	1.178	1,89	9329
C_{DA} : Re_p	10.883	-1.764	-	-	-	-.829	85.739	38.943	1,89	195.9
C_{DA} : Ir	-.616	-	-	1.972	-	.787	77.215	47.467	1,89	144.8
Re_p : Ac						-.817	18.410	9.141	1,89	179.3
Ir : Ac						.776	11.972	7.887	1,89	135.1
Ir : Re_p						-.981	19.109	.750	1,89	2266

(1) L_b is the natural logarithm of B, (6-1).
(2) The first five values in the table are multiple correlation coefficients, the positive value of a square root; the last six are simple correlation coefficients.
(3) ATR, attributable to the regression; DFR, deviations from the regression.
(4) For 91 sets of C_{DA} and its parameters the number of degrees of freedom attributable to the regression, n, equals the number of independent variables included; the number of degrees of freedom for deviation from the regression is 91 - n - 1.

C_{DA} (0.995^2, line 6 of Table 6-6) is the most striking result immediately provided by the regression analysis. The significance of contributions by the other variables may be assessed by a variance analysis (e.g. page 272, Volk (1958)). A comparison between the regression of C_{DA} upon Ac and C_{DA} upon Re_p, Ac is worked out to show the method; as the method is the same in each case only the results will be quoted for the other cases, in Table 6-7. Values marked (+) come from Table 6-6.

Sum of squares of deviation removed by the regression of C_{DA} upon Re_p, Ac $= 123.595^{(+)}$

Sum of squares of deviation removed by the regression of C_{DA} upon Ac $= 123.503^{(+)}$

Difference caused by including Re_p with 1 degree of freedom $= 0.092$

Residual sum of squares of deviation, C_{DA} upon Re_p, Ac with 88 degrees of freedom $= 1.086^{(+)}$

Variance ratio for comparison with Fisher's F

$$= \frac{88 \times 0.092}{1.086}$$

$$\simeq 7.5$$

Fisher's F with 1,88 degrees of freedom at 1% probability, $F_{.01,1,88} \simeq 6.97$

The same at 0.1% probability,

$F_{.001,1,88} \simeq 11.68$

The F values show that there is a one in one thousand probability that the apparent improvement due to considering Re_p as well as Ac could have come about by chance, but not a one in one hundred possibility. This is usually expressed by saying that the improvement is significant at 1% but not at 0.1%. Thus, in Table 6-7, if the significance of the improvement is "at 5%, not at 1%", one can say that the included variable is significant allowing one chance in twenty of being wrong, but is not significant if only one chance in one hundred of being wrong is allowed. Smaller percentages therefore indicate the most significant results.

Table 6-7.

Significance of the parameters of C_{DA}.

Parameters compared.	Significance of the improvement.
1. C_{DA}:Ac with C_{DA}:Re_p,Ac	At 1%, not at 0.1%
2. C_{DA}:Ac with C_{DA}:Ac,Ir	At 5%, not at 1%
3. C_{DA}:Re_p,Ac with C_{DA}:Re_p,Ac,Ir	Not at 20%
4. C_{DA}:Ac,Ir with C_{DA}:Re_p,Ac,Ir	At 10%, not at 5%
5. C_{DA}:Re_p with C_{DA}:Re_p,Ac	At << 0.1%
6. C_{DA}:Re_p with C_{DA}:Re_p,Ir	At 5%, not at 1%
7. C_{DA}:Re_p,Ir with C_{DA}:Re_p,Ac,Ir	At << 0.1%
8. C_{DA}:Re_p,Ac,Ir with C_{DA}:Re_p,Ac,Ir,s	At 0.1%

The distinction between correlation and causation has been often pointed out but is also often disregarded. The statistical analysis must be interpreted with a knowledge of the physical situation, keeping the limitations of the analysis in mind. For instance, statistically, inclusion of s as a parameter (Table 6-7, line 8) significantly improves the correlation between C_{DA} and Re_p, Ac, Ir, and the contribution s makes is large (k, Table 6-6). But it is known that only 3 values of s were used in the experimental results, each representing a range of s values (5.6) and the significance of s as a causative agent cannot be regarded as proved. Inclusion of Re_p along with Ac causes a significant improvement (line 1 of Table 6-7) as would be expected from the physical argument. There is high (negative) correlation between Ir and Re_p; Re_p is directly proportional to slip speed as only one diameter was used, and as the variation in Iv is quite small Ir is nearly inversely proportional to slip speed. Because of this high correlation it is difficult to show whether or not Ir is causing some of the variation in C_{DA}. Significant improvements are given by Ac, Ir or Re_p, Ir over Ac alone or Re_p alone, respectively (lines 2,6 of Table 6-7) but Ir does not add significantly to the correlation already provided by Re_p, Ac (line 3 of Table 6-7).

To summarise the results of Table 6-7, the statistical

analysis shows that addition of either Re_p or Ir improves the initial correlation between C_{DA} and Ac, Re_p giving a slightly greater improvement than Ir. Further addition, e.g. of Ir to Re_p, Ac, is not significant statistically, but of course the analysis does not show such improvement to be impossible, just that these particular results do not show it to be significant. With the physical arguments of Chapter 3 in mind, one may suggest that, for the ranges of s and relative turbulence scale in these experiments, C_{DA} is a function at least of Ac and either or both of Re_p, Ir.

The contribution of Ir is similar to that of Re_p (h, j, Table 6-6), increase in either being correlated with, and probably causing, a decrease in C_{DA}, as Torobin, Gauvin and Clamen found. Torobin and Gauvin (1960b, 1961b,c) and Clamen and Gauvin (1969) did not, however, detect a contribution from Ac. The experimental results of Torobin and Gauvin (1961c) are reinterpreted in the following sub-section.

6.52 Statistical analysis of Torobin and Gauvin's drag coefficient results.

Torobin and Gauvin used solid particles fired vertically into a surrounding steady, turbulent, vertical air stream at speeds below that of the air. Table 1 of their 1961c paper includes C_{DA}, Re_p and Ir values and the information necessary to calculate Ac from (see the first equation

in 4.3)

$$Ac = \frac{a\,\frac{dv_p}{dt}}{(v_p - v)^2} \quad , \quad \text{as } \frac{dv}{dt} = 0.$$

The density ratio was in all cases very high so that fluctuating motion of the particles did not generally occur and s has not been included as a parameter in this analysis. There are about a dozen sets of C_{DA}, Re_p, Ac, Ir in each of 32 firings; 5 different particle diameters were used. Ac was calculated by the present writer for 158 sets drawn from 14 firings, including at least two with each particle diameter. Torobin and Gauvin's $C_{DA} = F(Re_p, Ir)$ results exhibit minimums at Reynold's numbers above the critical Reynold's number. Only sets in which the Reynold's number was below the suggested values where minimums occur were included in the 158, so that multiple linear regression of the modified variables as in (6-2) is appropriate. Exactly the same procedure as described in 6.51 was applied to these data. Tables 6-8 and 6-9 summarise the results.

Comparison of the variance ratios with Fisher's F, as before, shows that the correlation between C_{DA} and Ir could well have occurred by chance (the probability is much greater than 20%), that there is only a one in a hundred probability of the correlation between Re_p and Ir occurring by chance and for all other cases the probability is less than one in one thousand. Although the multiple correlations are not as high as in Table 6-6 the simple

Table 6-8.

Multiple regression : C_{DA} upon combinations of Re_p, Ac, and Ir (Torobin & Gauvin's results).

Included parameters	L_b (1)	h	i	j	Correlation (1)	Sums of squares (1) ATR	DFR	Degrees of freedom (1)	Variance ratio
C_{DA} : Re_p,Ac,Ir	5.954	-.896	.139	-.440	.858	12.551	4.485	3,154	143.6
C_{DA} : Re_p,Ac	6.118	-.837	.102	-	.800	10.891	6.145	2,155	137.4
C_{DA} : Re_p,Ir	6.383	-1.079	-	-.270	.772	10.149	6.887	2,155	114.2
C_{DA} : Re_p	6.416	-1.005	-	-	-.745	9.452	7.585	1,156	194.4
C_{DA} : Ac	.608	-	.180	-	.560	5.350	11.686	1,156	71.4
C_{DA} : Ir	-1.088	-	-	-.001	-.001	.00002	17.036	1,156	.00019
Ac : Re_p					-.394	25.584	139.574	1,156	28.6
Ac : Ir					.387	24.783	140.375	1,156	27.5
Re_p : Ir					-.261	.637	8.721	1,156	11.4

(1) See the explanatory notes following Table 6-6.

correlations among the "independent" variables are lower, so that it is easier to separate the effects of different variables. Table 6-9 is derived in exactly the same way as Table 6-7; Re_p explains most of the C_{DA} variation, about 55% in terms of sum of squares of deviations.

Table 6-9.

Significance of the parameters of C_{DA} (Torobin and Gauvin's results).

Parameters compared.	Significance of the Improvement.
C_{DA}: Re_p with C_{DA}: Re_p,Ac.	At << 0.1%
C_{DA}: Re_p with C_{DA}: Re_p,Ir.	At << 0.1%
C_{DA}: Re_p,Ac with C_{DA}: Re_p,Ac,Ir.	At << 0.1%
C_{DA}: Re_p,Ir with C_{DA}: Re_p,Ac,Ir.	At << 0.1%

Statistically, there is little doubt that both Ac and Ir improve the initial correlation afforded by Re_p. In the absence of other variables to which Re_p, Ac, Ir are correlated which would cause the variation in C_{DA} it is safe to suggest that for the range of s and relative turbulence scale in Torobin and Gauvin's experiments, C_{DA} is a function of Re_p, Ac, Ir at least. Although Ac has been shown to make a significant contribution, the magnitude of the contribution is much smaller than in the results of Table 6-6 (see i in Table 6-8).

6.53 Comparison of the results in 6.51, 6.52.

6.53 Comparison of the results in 6.51, 6.52.

As it has not been possible to assess the effects, if any, of s and relative turbulence scale upon C_{DA} from either set of experimental results a comparison is drawn between the dependence of C_{DA} upon Re_p, Ac, Ir for each set. Using (6-1) and L_b, h, i, j from the appropriate rows of Tables 6-6, 6-8, the power laws which best express the fit of the data considered are:

$$C_{DA} = 7.25\ Re_p^{-.233}\ Ac^{.836}\ Ir^{-.150} \quad \text{(present results, 6.51)}, \qquad (6\text{-}3)$$

$$C_{DA} = 385\ Re_p^{-.896}\ Ac^{.139}\ Ir^{-.440} \quad \text{(Torobin and Gauvin's results, 6.52)} \qquad (6\text{-}4)$$

Figures 6-7,8 illustrate (6-3,4) graphically. From either the equations or graphs it is clear that although the functional form is qualitatively the same for the two sets of experimental results it is quantitatively different. At the very low values of Ac in Torobin and Gauvin's results ($10^{-6} < Ac < 10^{-4}$) this parameter makes a much smaller contribution than in the results from the present study ($10^{-2} < Ac < 10^{2}$). The contributions of Re_p and Ir are both less for the present results, where the particle relative turbulent intensities are higher ($0.8 < Ir < 7.5$ c.f. $0.1 < Ir < 0.4$ in Torobin and Gauvin's experiments) and the Reynolds number range is lower ($70 < Re_p < 850$ c.f. $350 < Re_p < 2500$). Figures 6-7,8,9 also show the approximate

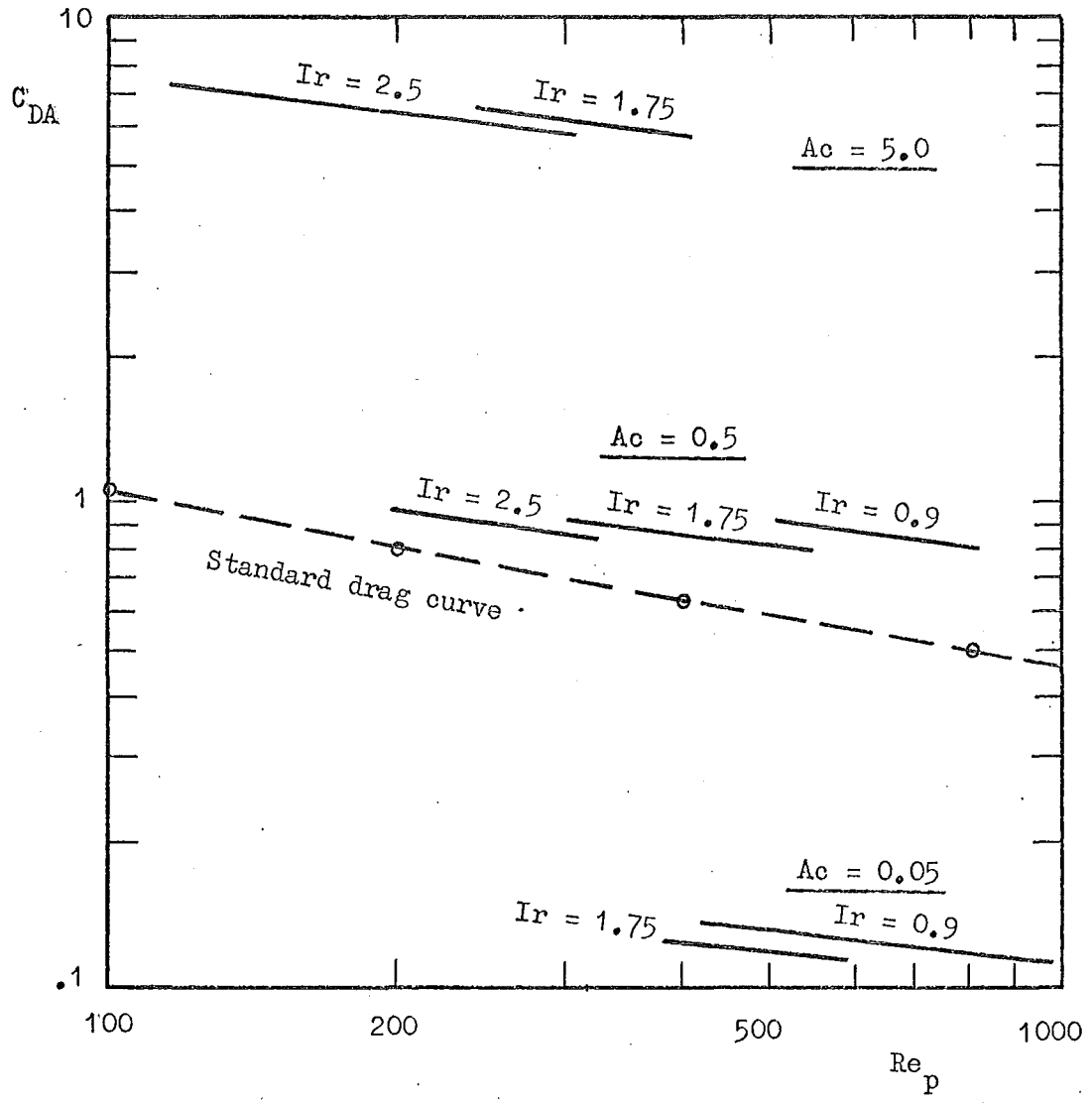

The full lines have been placed approximately in areas where comparable experimental points occurred.

Figure 6-7. Illustration of the regression equation (6-3). (Experimental results from this study).

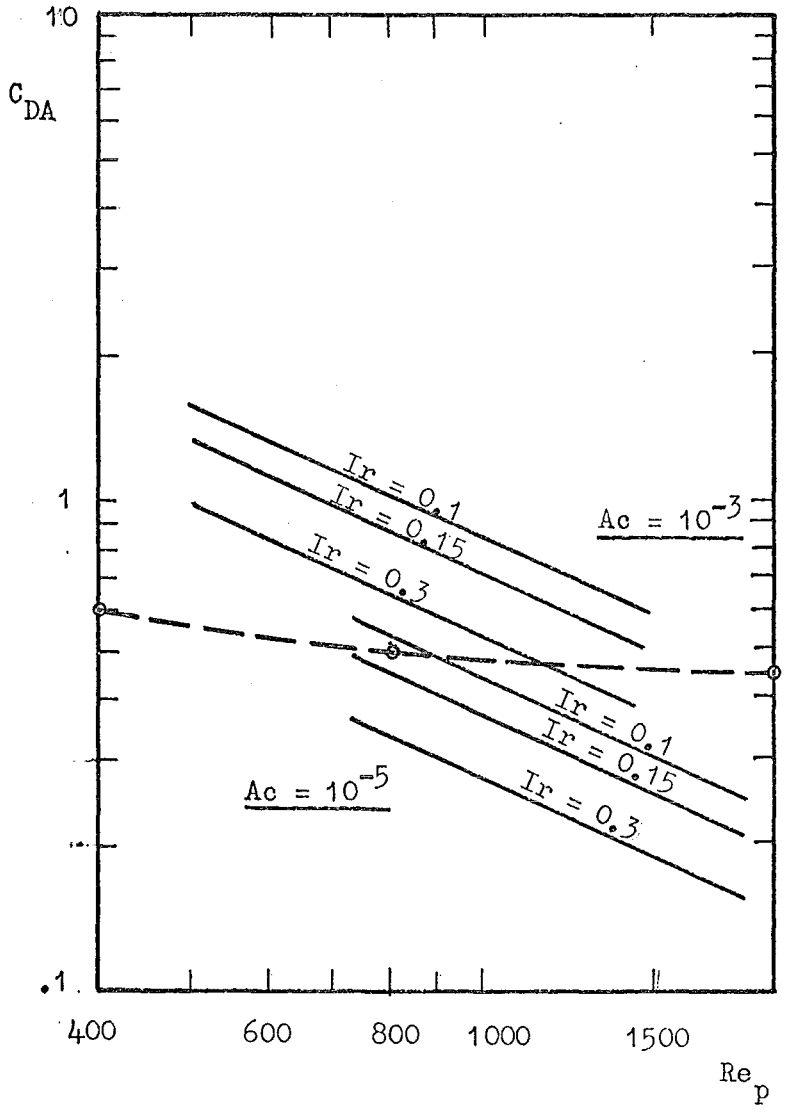

Figure 6-8. Illustration of the regression equation (6-4). (Experimental results from Torobin and Gauvin (1961c)).

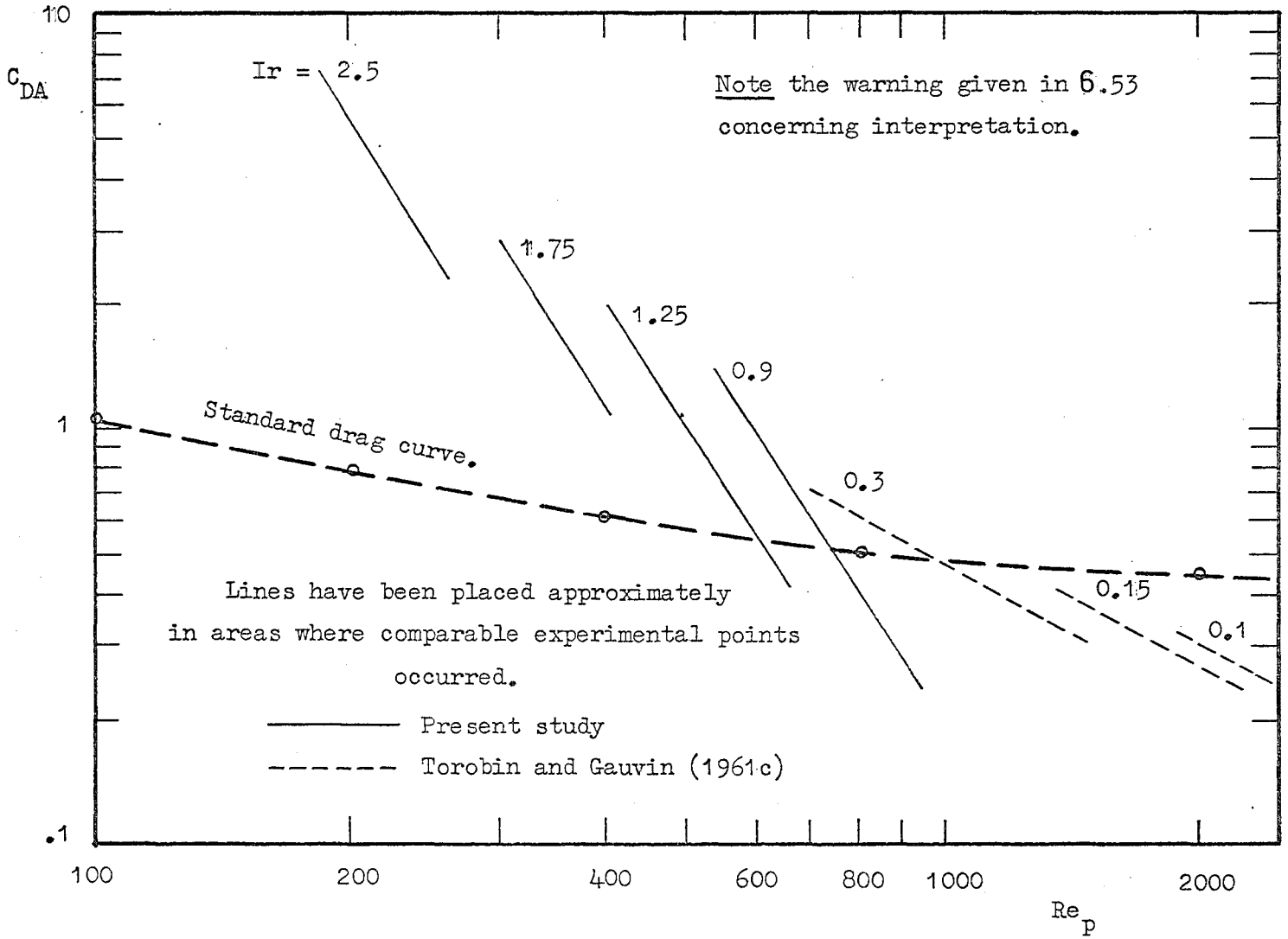

Figure 6-9. Illustration of regression equations ignoring Ac.

position of the standard steady-state drag curve for comparison.

Figure 6-7,8 also show why ignoring Ac makes comparatively little difference to the curves obtained from Torobin and Gauvin's results, but a large difference in the present case. The slope of a line drawn as an average through data represented by curves of the same Ir in Figure 6-8 is of slope near to those already present; but the same procedure applied to Figure 6-7 would give a line of quite different appearance. This is illustrated in Figure 6-9 where the regression equation

$$C_{DA} = B\ Re_p^{\ h}\ Ir^j$$

has been fitted to both sets of experimental results using values of L_b, h, j from Tables 6-6,6-8. It should be emphasized that the writer believes this to be an incorrect representation, almost meaningless for the present results, but approximately true for Torobin and Gauvin's, where Ac has less importance.

Torobin and Gauvin (1961c) analysed their results in a slightly different way; having detected no influence of acceleration the dependence of C_{DA} on Re_p for different Ir could be plotted as in their papers (see Figure 3-2). However, Dr. Gauvin and his colleagues "have long suspected that acceleration or deceleration should have an effect on the coefficient of drag" and have carried out further work

at much higher rates of deceleration which "indicates clearly the presence of an acceleration effect" (personal communication from W.H. Gauvin, August 1969).

The apparent qualitative agreement between the drag coefficient results from the solids-gas system with steady air velocity used by Torobin, Gauvin and Clamen, and the solids-liquid system with convectively non-steady liquid velocity used in the present study is perhaps the most important result of this thesis.

CHAPTER SEVEN.

7. SUMMARY OF RESULTS AND CONCLUSIONS.

7.1 Comments upon the experimental method.

1. The new method gives experimental values of the drag coefficient which are comparable with those of other methods.

2. It is capable of use with much wider ranges of the experimental variables than reported in this study. This will be necessary, especially to establish the importance of relative turbulence scales and density ratio.

3. It is readily adaptable to measure drag coefficients from slip speeds in a combined gravitational and inertial field.

4. The ways in which measurements (of turbulence parameters and local mean slip speeds in particular) may be refined have been indicated.

5. The method would be much improved by a less tedious means of interpreting photographic measurements.

7.2 Non-steady, turbulent drag coefficients.

1. Using the low particle Reynolds number drag solution of Chapter 2 as a basis, and further physical argument in Chapter 3 for higher particle Reynolds numbers and turbulent ambient fluid, it was predicted that the parameters upon which C_{DA} might depend are : Re_p, Ac, Ir, $\frac{L_e}{a}$, $\frac{\ell}{a}$ and s.

2. The ranges of these experimental variables in this study were:

Non-steady, turbulent drag coefficient;	$0.1 < C_{DA} < 35$
Particle Reynolds number;	$70 < Re_p < 850$
Particle relative acceleration number;	$10^{-2} < 2Ac < 10^{2}$
Particle relative turbulence intensity;	$0.8 < Ir < 7.5$
Relative integral scale of turbulence;	$5 < \frac{L_e}{a} < 18$
Relative microscale of turbulence;	$1.5 < \frac{\ell}{a} < 6.6$
Particle relative density;	$1.011 < s < 1.025$
Particle diameter, inches;	$0.066 < d < 0.081$

3. Within these ranges C_{DA} was found to be a function of Ac, and either or both of Re_p and Ir. Although these results alone were insufficient to determine which of the alternatives is correct, taken in conjunction with other results they show the case including Ac, Re_p, and Ir to be most likely. C_{DA} decreased with increasing Re_p at fixed Ac, Ir; increasing with increasing Ac at fixed Re_p, Ir; decreasing with increasing Ir at fixed Re_p, Ac. The first and last of these tendencies is in agreement with results previously observed; dependence upon Ac has not been observed by those few workers who have measured turbulence parameters but is similar to the dependence found by other workers in non-turbulent flow.

4. Application of the method of analysis of this thesis to the results of Torobin and Gauvin (1961c) shows

that the quite different experimental method employed by them gives drag coefficients which depend upon Re_p, Ac, Ir in qualitatively the same way as the drag coefficients of the present study, although Torobin and Gauvin did not report dependence upon Ac.

5. 2Ac makes a large contribution to the value of C_{DA} in these experiments, where its values are between 10^{-2} and 10^{2}; it makes a small contribution in the experiments of Torobin and Gauvin, where its values are between 10^{-4} and 10^{-6}.

6. The dangers in comparing values of C_{DA} obtained by differing methods, including this one, have been pointed out (in 4.4 and 6.4).

REFERENCES.

Abramowitz, M. & I.A. Stegun (1965) "Handbook of Mathematical Functions." Dover, N.Y.

Barnard, . & A.M. Binnie (1963) "The Vertical Diffusivity and Mean Velocity of Particles in a Horizontal Pipe." J. Fl. Mech., V 15, p 35.

Basset, A.B. (1888) Phil. Trans., p 43.

_____ (1910) "On the Descent of a Sphere in a Viscous Fluid." Quart. J. Pure & App. Maths, V41, p369-381.

Batchelor, G.K.(1966) "The Motion of Small Particles in Turbulent Flow." Proc. 2nd Australasian Conference on Hydraulics and Fluid Mechanics, p O 19.

_____ (1967) "An Introduction to Fluid Dynamics." C.U.P.

Boggio, T. (1907) Rendiconti della Reale Accademia dei Lincei, V 16, Series 5, November.

Bonnington, S.T. (1956) "Jet Pumps." B.H.R.A., S.P. 529.

_____ & D. Watts (1964) "The State of the Art of Jet Pump Design." B.H.R.A., T.N. 830.

Boussinesq, J. (1885a) Comptes rendus de l'Academie des Sciences, C, p 935.

_____ (1885b) "Application des Potentiels a l'Etude de l'Equilibre et du Mouvement des Solides Elastiques." p 278. (referred to in Boussinesq (1885a)).

Brush, L.M., Hau-wong Ho and Ben-chie Yen (1964) "Accelerated Motion of a Sphere in a Viscous Fluid." Proc. A.S.C.E., V 90, HY 1, p149.

Clamen, A. & W.H. Gauvin (1969) "Effects of Turbulence on the Drag Coefficients of Spheres in a Supercritical Flow Regime." A.I.Ch.E., V 15, No.2, p 184.

Corrsin, S. & J. Lumley (1956) "On the Equation of Motion for a Particle in a Turbulent Fluid." App. Sci. Res., V 6A, p 114.

DISA (1966) 1. "DISA Instruction Manual for 55 A 01 Constant Temperature Anemometer." Reg. No. 9150 A 0213. 2. "General Description." DISA Elecktronik A/S, Herlev, Denmark.

Dryden, H.L. (1935) J.Washington Acad. Sci., 25, p 101.

_____ (1931) N.A.C.A., T.R. 392.

_____ & E.Kuethe (1929) N.A.C.A., T.R. 342.

_____ , G.B. Schubauer, W.L. Mock & H.K. Skramstad (1937) N.A.C.A., T.R. 581

Fisher, Sir R.A. & F. Yates (1963) "Statistical Tables..." 6th Edition, Oliver and Boyd, London.

Goldstein, S. (1929) Proc. Roy. Soc., A, V 123, p 225.

_____ (1938) "Modern Developments in Fluid Mechanics." Clarendon Press, Oxford.

Graf, W.H. (1967) "A Modified Venturimeter for Measuring Two-phase Flow OR Particle Dynamics and the Venturimeter." I.A.H.R., J., V 5, No 3, p 162.

Hinze, J.O. (1959) "Turbulence." McGraw-Hill.

Hjelmfelt, A.T. & L.F. Mockros (1966) "Motion of Discrete Particles in a Turbulent Fluid." App. Sci. Res., V 16, No.2, p 149.

_____ & _____ (1967) "Stokes Flow Behaviour of an Accelerating Sphere." Proc. A.S.C.E. V 93, E.M.6, p 87.

Hughes, W.F. & W. Gaylord (1964) "Basic Equations of Engineering Science." Schaum, N.Y.

I.B.M. (1968) "System 360 Scientific Subroutine Package." 360A - CM - 03X Version III, H 20 - 0205 - 3, 4th Edition.

Iverson, H.W. & R. Balent (1951) "A Correlating Modulus for Fluid Resistance in Accelerated Motion." J. App. Phys. V 22, No 3, p 324.

Keim, S.R. (1956) "Fluid Resistance to Cylinders in Accelerated Motion." Proc. A.S.C.E., V 82, HY6.

Kline, S.J. (1959) "On the Nature of Stall." A.S.M.E. Trans., V 81, D, p 305.

_____ , D.E. Abbott & R.W. Fox (1959) "The Optimum Design of St. Walled Diffusers." A.S.M.E. Trans, V 81, D, p 321.

Laufer, J (1950) "Some Recent Measurements in a Two-dimensional Turbulent Channel." J. Aero. Sci., V 17, No.5, p 277.

Liu, V.Cheng (1956) "Turbulent Dispersion of Dynamic particles." J. Meteorology, 3, p 399.

Lumley, J. (1947) "Some Problems Connected with the Motion of Small Particles in Turbulent Fluid." (Thesis) John Hopkins University, U.S.A.

Lunnon, R.G. (1924) "The Resistance of Air to Falling spheres." Phil. Mag., V 47, p 173.

_____ (1926) "Fluid Resistance to Moving Spheres." Proc. Roy. Soc., A, V 110, p 302.

Milne-Thompson, L.M. (1955) "Theoretical Hydrodynamics." 3rd Edition, MacMillan, London.

Mueller, N.H.G. (1964) "Water Jet Pump." Proc. A.S. C.E., V 90, HY3, p 83.

Navier, C.L. (1823) Memoires de l'Academie Royale des Sciences, 6, p 389.

Odar, F. & W.S. Hamilton (1964) "Forces on a Sphere Accelerating in a Viscous Fluid." J. Fl. Mech., V 18, Pt.2, p 302.

Oseen, C.W. (1927) "Hydrodynamik." Leipzig

Pearcey, T & G.W. Hill (1956) Australian J. Phys, 9, p 18.

Picciati, (1907a,b,c,d) Rendiconti della Reale Accademia dei Lincei, V 16, Series 5; May, June, July and August.

Raichlen, F. (1967) "Some Turbulence Measurements in Water." Proc. A.S.C.E., V 93, EM2, p 73.

Rayleigh, Lord (1892) "On the Question of the Stability of the Flow of Fluids." Phil. Mag. (5), V 34, p 59.

_____ (1899) "Investigations in Capillarity..." Phil. Mag., V 48, p 321.

_____ (1904) Note to a Paper by Professor Zahm, "Fluid Friction on Even Surfaces." Phil. Mag.(6)V 8, p 66.

_____ (1909) "Note as to the Application of the Principle of Dynamical Similarity." Report, Adv. Comm. Aero. No.15.

_____ (1911) "On the Motion of Solid Bodies Through Viscous Liquid." Phil. Mag., V 21, p 697 OR Scientific Papers, V 6, p 29, C.U.P., 1920.

Reneau, L.R., J.P. Johnston & S.J. Kline (1967) "Performance and Design of Straight, Two-dimensional

Diffusers." A.S.M.E. Trans. V 89 D, No.1, p 141.

Rouse, H (Editor) (1959) "Advanced Mechanics of Fluids." Wiley N.Y.

Schlichting, H (1960) "Boundary Layer Theory." 4th Edition, McGraw-Hill.

Shaw, R. (1959) "The Measurement of Static Pressure." Aeronautical Research Council, 20, 829.

Silvester, R. (1961) "Characteristics and Applications of the Water Jet Pump." La Houille Blanche, v 16, p 451.

Soo, S.L. (1967) "Fluid Mechanics of Multiphase Systems." Blaisdell.

Stepanoff, A.J. (1955) "Centrifugal and Axial Flow Pumps." 2nd Edition, Wiley, N.Y.

Stokes, Sir G.G. (1845) Trans. Camb. Phil. Soc., 8, p 287.

Stokes, Sir G.G. (1851) Trans. Camb. Phil. Soc., 8.

Taylor, Sir G.I. (1935) "Statistical Theory of Turbulence:" I-IV." Proc. Roy. Soc., A, V 151, p 421.

_____ (1936) "Statistical Theory of Turbulence -V" Proc. Roy. Soc., A, V 156, p 307.

_____ (1938) "The Spectrum of Turbulence." Proc. Roy. Soc., A, V 174, p 476.

Tchen, C.M. (1947) "Mean Value and Correlation Problems..." (Thesis) Martinus Nijhoff, The Hague.

_____ & G.B. Schubauer (1959) "Turbulent Flows and Heat Transfer." V 5 of "High Speed Aerodynamics and Jet Propulsion." Princeton University Press.

_____ & _____ (1961) "Turbulent Flow." P.U.P.

Tikhonov, A.N. & A.A. Samarskii (1964) "Partial Differential Equations of Mathematical Physics." V 1. Holden-Day, San Francisco.

Torobin, L.B. & W.H. Gauvin (1959a,b,c) "Fundamental Aspects of Solids-gas Flow." Can. J. Chem. Eng. V 37, p 129, p 167, p 224.

_____ & _____ (1960a,b) ibid. V 38, p 142, p 182.

_____ & _____ (1961a) ibid. V 39, p 113.

_____ & _____ (1961b) "Turbulent Flow Ballistics Facility for Particle Momentum Transfer Studies." A.I.Ch.E. V 7, No.3, p 406.

_____ & _____ (1961c) "The Drag Coefficients of Single Spheres Moving in Steady and Accelerated Motion in a Turbulent Fluid." A.I.Ch.E., V 7, No.4, p 615.

Townsend, A.A. (1956) "The Structure of Turbulent Shear Flow." C.U.P.

Vanoni, V. & N. Brooks (1955) "A study of Turbulence and Diffusion Using Tracers in a Water Tunnel." C.I.T. Hyd. Lab. Report E-46.

Villat, H. (1943) "Lecons sur les Fluides Visqueux." Gauthier-Villars, Paris.

Volk, W. (1958) "Applied Statistics for Engineers." McGraw-Hill.

Williams, E.J. (1959) "Regression Analysis." John Wiley, N.Y.

APPENDIX A.

CERTAIN DERIVATIONS REQUIRED IN 2.5.

$\left(\frac{d^2f}{dr^2}\right)_{r=a}$ and $\left(\frac{d^3f}{dr^3}\right)_{r=a}$ are required, and both involve $\left[\frac{dh}{dr}\right]_{r=a}$.

From (2-48)

$$\frac{df}{dr} = -\frac{a^3 v_r'}{2r^2} + h - \frac{1}{r^2}\int_a^r r\,h(r,t)\,dr,$$

$$\frac{d^2f}{dr^2} = \frac{a^3 v_r'}{r^3} + \frac{dh}{dr} - \frac{h}{r} + \frac{2}{r^3}\int_a^r r\,h(r,t)\,dr,$$

$$\frac{d^3f}{dr^3} = -\frac{3a^3 v_r'}{r^4} + \frac{d^2h}{dr^2} - \frac{1}{r}\frac{dh}{dr} + \frac{3h}{r^2} - \frac{6}{r^4}\int_a^r r\,h(r,t)\,dr,$$

so that

$$\left(\frac{d^2f}{dr^2}\right)_{r=a} = v_r' + \left(\frac{dh}{dr} - \frac{h}{r}\right)_{r=a},$$

$$\left(\frac{d^3f}{dr^3}\right)_{r=a} = -\frac{3v_r'}{a} + \left(\frac{d^2h}{dr^2} - \frac{1}{r}\frac{dh}{dr} + \frac{3h}{r^2}\right)_{r=a},$$

and, using (2-36)

$$\left(\frac{d^3f}{dr^3}\right)_{r=a} = -\frac{3v_r'}{a} + \left(\frac{3h}{r^2} - \frac{1}{r}\frac{dh}{dr} + \frac{1}{n}\frac{dh}{dt}\right)_{r=a}.$$

(2-45) shows that

$$\frac{dh(a,t)}{dt} = \frac{3a}{2}\frac{dv_r'}{dt}, \qquad \frac{h(a,t)}{a} = \frac{3}{2}v_r'(t)$$

whence

$$\left(\frac{d^2f}{dr^2}\right)_{r=a} = \left(\frac{dh}{dr}\right)_{r=a} - \frac{v_r'(t)}{2}, \tag{A-1}$$

$$\left(\frac{d^3f}{dr^3}\right)_{r=a} = \frac{3v_r'(t)}{2a} + \frac{3a}{2n}\frac{dv_r'}{dt} - \frac{1}{a}\left(\frac{dh}{dr}\right)_{r=a}. \tag{A-2}$$

$(\frac{dh}{dr})_{r=a}$ must be obtained from (2-47); write (2-47) as

$$2\sqrt{\pi n}\, h(r,t) = \int_a^\infty b(r')\, f_1\, dr' - 3an \int_o^t v_r'(t')\, \frac{df_2}{dr}\, dt' \qquad (A-3)$$

where

$$f_1(r,r',t) = \frac{1}{\sqrt{t}} \left[e^{-\frac{(r-r')^2}{4nt}} - e^{-\frac{(r-2a+r')^2}{4nt}} \right], \qquad (A-4)$$

$$f_2(r,t,t') = \frac{1}{\sqrt{t-t'}}\, e^{-\frac{(r-a)^2}{4n\,(t-t')}}, \qquad (A-5)$$

so that

$$\frac{df_2}{dr} = -\frac{(r-a)}{2n\sqrt{(t-t')^3}}\, e^{-\frac{(r-a)^2}{4n\,(t-t')}}. \qquad (A-6)$$

Note that

$$\frac{d^2 f_2}{dr^2} = -\frac{1}{n}\frac{df_2}{dt'}. \qquad (A-7)$$

Differentiating (A-3) with respect to r

$$2\sqrt{\pi n}\,\frac{dh}{dr} = \int_a^\infty b(r')\,\frac{df_1}{dr}\,dr' - 3an\int_o^t v_r'(t')\,\frac{d^2 f_2}{dr^2}\,dt',$$

$$= I_1 - 3an\, I_2, \text{ say.} \qquad (A-8)$$

Using (A-7)

$$I_2 = -\frac{1}{n}\int_o^t v_r'(t')\,\frac{df_2}{dt'}\,dt',$$

$$= - \frac{1}{n} \left[v_r'(t') \, f_2 \right]_o^t + \frac{1}{n} \int_o^t f_2 \frac{dv_r'}{dt'} \, dt' \, . \qquad (A-9)$$

From (A-5), $f_2(r,t,t)$ is zero (for $r \neq a$), and as r tends to a as closely as desired $f_2(a,t,0)$ tends to $\frac{1}{\sqrt{t}}$ and $f_2(a,t,t')$ tends to $\frac{1}{\sqrt{t-t'}}$ so (A-9) becomes

$$I_2 = \frac{1}{n} \frac{v_r'(0)}{\sqrt{t}} + \frac{1}{n} \int_o^t \frac{1}{\sqrt{t-t'}} \frac{dv_r'}{dt'} \, dt' \, . \qquad (A-10)$$

From (A-4)

$$\frac{df_1}{dr} = \frac{1}{2nt^{\frac{3}{2}}} \left[(r-2a+r') \, e^{-\frac{(r-2a+r')^2}{4nt}} - (r-r') \, e^{-\frac{(r-r')^2}{4nt}} \right] ,$$

$$\left(\frac{df_1}{dr} \right)_{r=a} = \frac{1}{n\sqrt{t^3}} (r'-a) \, e^{-\frac{(r'-a)^2}{4nt}} \, . \qquad (A-11)$$

From (A-6,11)

$$\left(\frac{df_1}{dr} \right)_{r=a} = - 2 \left(\frac{df_2}{dr} \right)_{r=r',t'=0} \, . \qquad (A-12)$$

(A-12) and the form of f_2 given by (A-7) enable the integration by parts of I_1 to be performed; from (A-8)

$$I_1 = - 2 \int_a^\infty b(r') \left(\frac{df_2}{dr} \right)_{r=r',t'=0} dr'$$

$$= 2 \int_a^\infty \frac{db(r')}{dr'} f_2(r',t,0)\, dr'$$

$$- 2 \left[b(r')\, f_2(r',t,0) \right]_a^\infty . \qquad \text{(A-13)}$$

From (A-5)

$$f_2(r',t,0) = \frac{1}{\sqrt{t}} e^{-\frac{(r'-a)^2}{4nt}} ,$$

$$f_2(a,t,0) = \frac{1}{\sqrt{t}} ,$$

and f_2 tends to zero as r' becomes very large.

From (2-45,46)

$$b(a) = \frac{3av_r'(0)}{2} .$$

Substituted into (A-13) these results show

$$I_1 = \frac{2}{\sqrt{t}} \int_a^\infty \frac{db(r')}{dr'} e^{-\frac{(r'-a)^2}{4nt}} dr' + \frac{3av_r'(0)}{\sqrt{t}} . \qquad \text{(A-14)}$$

Combining (A-8,10,14) the desired result is

$$2\sqrt{\pi n} \left(\frac{dh}{dr}\right)_{r=a} = \frac{2}{\sqrt{t}} \int_a^\infty \frac{db(r')}{dr'} e^{-\frac{(r'-a)^2}{4nt}} dr'$$

$$- 3a \int_o^t \frac{1}{\sqrt{t-t'}} \frac{dv_r'}{dt'} dt' . \qquad \text{(A-15)}$$

APPENDIX B.

TURBULENCE SPECTROGRAPHS.

Figure B-1 on the following page shows measured turbulence spectra; see sections 5.4 and 6.3.

Top and centre: 2 spectrographs recorded at the same conditions and position (on the centreline, upstream of the diffuser).

Bottom: The curve fitted to the 2 recorded spectrographs (by eye) from which f' measurements were made; see equation (5-1).

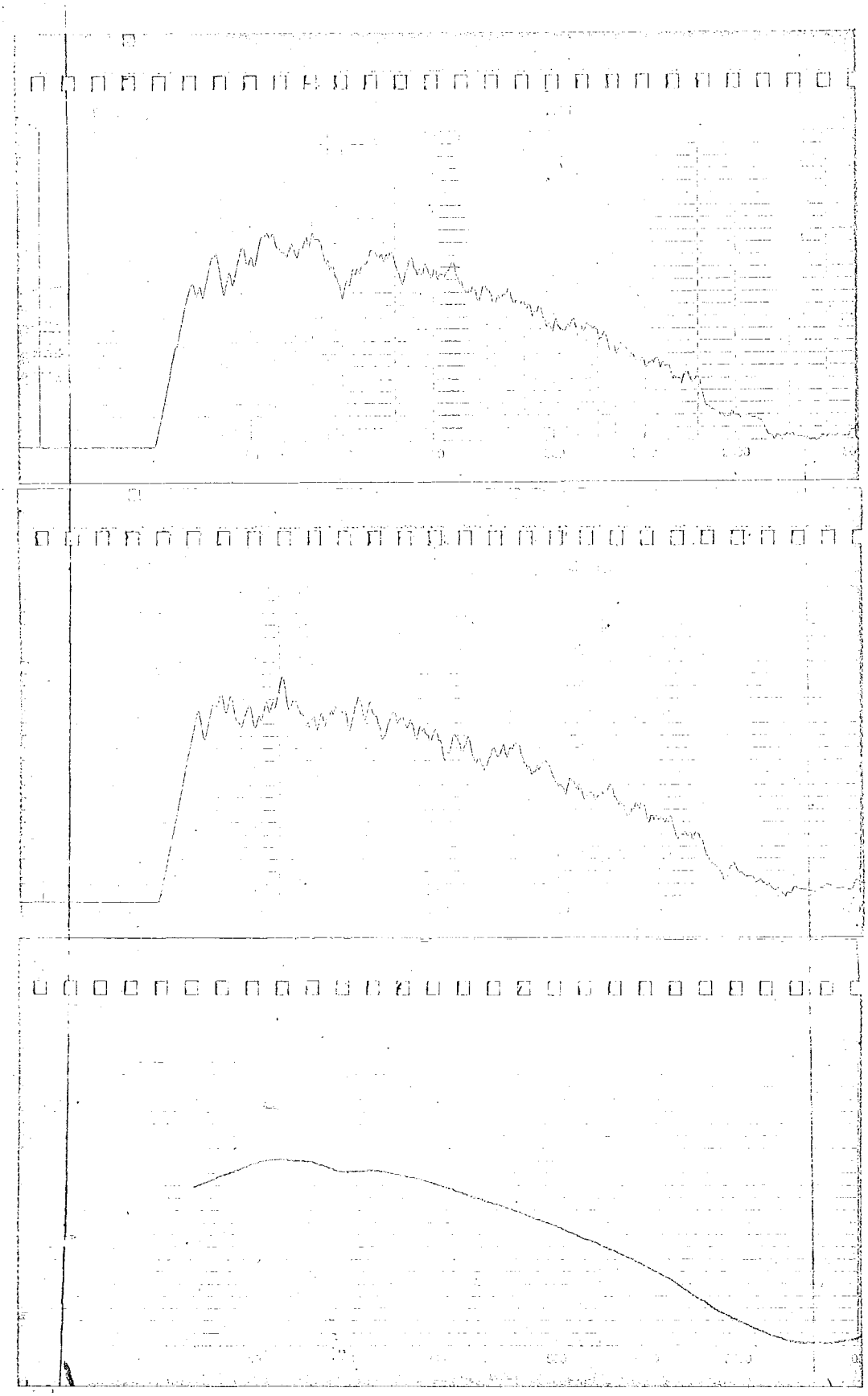

APPENDIX C.

The two tables following show the measured mean particle speeds at individual grid volumes for two different density ratios.

X, Y, Z	grid positions, see Figure 5-16
v_p	mean particle speed
S.D.	standard deviation on v_p
C.V.	coefficient of variation, $\frac{100\ S.D.}{v_p}$
No.	the number of measurements of individual particle speeds used to calculate the mean

Table C-1.

Measured particle speeds, s = 1.011.

X	Y	Z	v_p	S.D.	C.V.	No.
3	3	3	11.32	0.74	6.56	14
4	3	3	10.91	1.02	9.35	17
5	3	3	10.79	0.97	9.01	18
6	3	3	10.55	0.87	8.27	18
7	3	3	10.27	0.96	9.30	17
8	3	3	10.44	0.69	6.63	19
9	3	3	10.07	0.67	6.69	17
10	3	3	9.89	0.93	9.35	24
11	3	3	9.96	0.56	5.58	15
12	3	3	9.52	1.02	10.67	13
13	3	3	9.39	0.92	9.84	14
14	3	3	9.30	0.63	6.74	14
15	3	3	9.39	0.91	9.69	16
16	3	3	8.91	0.59	6.58	5
3	2	3	10.51	1.09	10.34	8
4	2	3	10.32	1.17	11.36	10
5	2	3	9.95	0.95	9.57	15
6	2	3	10.52	1.54	14.63	6
7	2	3	9.55	1.05	11.01	14
8	2	3	9.20	0.98	10.66	12
9	2	3	9.38	1.24	13.19	10
10	2	3	8.80	0.87	9.86	8
11	2	3	9.25	1.03	11.12	8
12	2	3	9.14	1.06	11.61	6
13	2	3	8.83	0.69	7.86	5
14	2	3	8.77	0.54	6.14	5
15	2	3	8.90	0.55	6.18	2
16	2	3	7.81	0.95	12.21	4
3	3	2	10.45	0.90	8.66	13
4	3	2	10.08	0.89	8.84	6
5	3	2	10.15	0.81	7.98	14
6	3	2	9.12	1.03	11.26	5
7	3	2	9.51	0.89	9.35	11
8	3	2	9.07	0.76	8.39	4
9	3	2	9.77	0.52	5.37	7
10	3	2	8.45	0.92	10.91	5

X	Y	Z	v_p	S.D.	C.V.	No.
11	3	2	8.96	0.94	10.53	5
12	3	2	9.70	0.24	2.47	2
13	3	2	9.45	0.47	5.02	4
14	3	2	9.07	0.54	5.90	4
15	3	2	9.40	0.55	5.85	2
16	3	2	7.54	0.0	0.0	1
3	3	4	11.03	0.55	5.03	8
4	3	4	9.73	1.13	11.58	9
5	3	4	10.07	1.11	11.04	10
6	3	4	10.20	0.60	5.88	5
7	3	4	9.76	0.95	9.78	8
8	3	4	9.66	0.63	6.52	3
9	3	4	9.17	0.95	10.34	8
10	3	4	9.36	0.83	8.82	5
11	3	4	9.29	0.79	8.54	8
12	3	4	9.22	1.08	11.71	2
13	3	4	8.40	0.94	11.22	4
14	3	4	8.29	1.22	14.73	5
15	3	4	7.78	1.18	15.11	7
16	3	4	7.34	0.95	12.96	3
3	4	3	10.52	0.79	7.49	6
4	4	3	10.64	1.19	11.14	8
5	4	3	10.25	0.76	7.39	9
6	4	3	9.82	1.13	11.54	8
7	4	3	9.80	0.78	7.92	6
8	4	3	9.97	0.90	9.06	9
9	4	3	9.27	0.98	10.53	7
10	4	3	9.60	1.34	13.94	10
11	4	3	9.48	0.90	9.46	6
12	4	3	9.47	1.00	10.57	9
13	4	3	8.90	0.66	7.39	4
14	4	3	8.93	1.29	14.47	6
15	4	3	8.78	1.52	17.35	7
16	4	3	8.41	1.13	13.44	4
3	2	2	10.16	1.39	13.63	3
4	2	2	9.19	0.74	8.07	5
5	2	2	9.55	0.91	9.50	5
6	2	2	9.13	1.18	12.90	4
7	2	2	9.42	1.14	12.12	5
8	2	2	9.10	1.14	12.50	6
9	2	2	9.64	0.80	8.26	3
10	2	2	9.13	0.77	8.43	7

X	Y	Z	v_p	S.D.	C.V.	No.
11	2	2	9.29	0.62	6.63	4
12	2	2	7.85	0.42	5.35	2
13	2	2	8.27	0.0	0.0	1
14	2	2	8.41	0.23	2.72	3
15	2	2	7.57	1.12	14.80	2
16	2	2	7.76	1.06	13.69	3
3	2	4	10.46	0.82	7.82	6
4	2	4	10.11	1.34	13.25	7
5	2	4	9.91	1.01	10.16	13
6	2	4	9.50	1.06	11.16	9
7	2	4	9.22	0.86	9.32	14
8	2	4	9.19	0.56	6.14	9
9	2	4	8.90	0.86	9.63	8
10	2	4	8.57	0.70	8.14	11
11	2	4	8.79	0.75	8.58	9
12	2	4	8.79	0.75	8.58	9
13	2	4	8.20	0.89	10.90	4
14	2	4	7.90	0.99	12.52	6
15	2	4	7.40	0.98	13.29	5
16	2	4	7.99	1.38	17.26	6
3	4	2	10.48	0.63	5.99	8
4	4	2	10.26	1.10	10.74	10
5	4	2	9.74	1.31	13.46	7
6	4	2	9.74	1.14	11.68	17
7	4	2	9.51	1.13	11.90	9
8	4	2	9.64	0.56	5.83	9
9	4	2	9.55	1.22	12.73	4
10	4	2	9.44	0.99	10.49	7
11	4	2	8.38	0.13	1.55	2
12	4	2	9.06	1.13	12.47	6
13	4	2	8.41	0.28	3.33	2
14	4	2	9.53	0.56	5.88	2
15	4	2	8.48	0.21	2.48	2
16	4	2	8.69	0.86	9.93	3
3	4	4	10.33	1.23	11.88	14
4	4	4	9.29	1.0	10.76	12
5	4	4	9.78	1.15	11.74	18
6	4	4	9.46	1.08	11.39	15

X	Y	Z	v_p	S.D.	C.V.	No.
7	4	4	9.54	0.80	8.35	10
8	4	4	9.50	0.92	9.72	15
9	4	4	9.34	0.86	9.16	9
10	4	4	9.12	0.68	7.44	15
11	4	4	8.49	0.71	8.36	6
12	4	4	8.43	1.08	12.80	6
13	4	4	7.85	0.60	7.67	4
14	4	4	8.37	0.27	3.21	4
15	4	4	7.88	0.74	9.36	5
16	4	4	7.57	0.71	9.43	3

Table C-2.

Measured particle speeds, s = 1.025.

X	Y	Z	v_p	S.D.	C.V.	No.
3	3	3	12.04	0.30	2.49	2
4	3	3	10.73	0.68	6.32	13
5	3	3	11.26	0.60	5.29	3
6	3	3	10.45	0.49	4.72	11
7	3	3	10.32	0.88	8.56	7
8	3	3	10.47	0.41	3.96	7
9	3	3	10.31	0.55	5.30	12
10	3	3	10.16	0.39	3.84	5
11	3	3	9.91	0.72	7.26	7
12	3	3	8.81	0.85	9.65	5
13	3	3	9.85	0.57	5.74	3
14	3	3	9.23	0.49	5.32	6
15	3	3	9.29	0.69	7.48	5
16	3	3	9.28	0.42	4.53	2
3	2	3	10.90	0.35	3.24	3
4	2	3	10.58	0.20	1.93	3
5	2	3	10.54	0.66	6.24	6
6	2	3	9.62	0.60	6.26	6
7	2	3	10.72	0.06	0.56	2
8	2	3	10.00	1.23	12.29	6
9	2	3	9.46	1.36	14.38	4
10	2	3	9.44	1.16	12.31	5
11	2	3	9.29	0.79	8.51	5
12	2	3	9.58	0.60	6.26	2
13	2	3				0
14	2	3	9.05	0.0	0.0	1
15	2	3	8.55	0.10	1.17	2
16	2	3	8.80	0.18	2.05	2
3	3	2	10.16	0.59	5.86	5
4	3	2	11.26	0.0	0.0	1
5	3	2	9.22	0.93	10.14	3
6	3	2	10.06	1.20	11.93	6
7	3	2	9.28	0.30	3.23	2
8	3	2	10.42	0.0	0.0	1
9	3	2	9.89	0.85	8.56	5
10	3	2	9.43	0.68	7.22	4

X	Y	Z	v_p	S.D.	C.V.	No.
11	3	2	9.66	0.54	5.59	3
12	3	2	9.34	0.66	7.10	4
13	3	2	8.25	0.30	3.64	2
14	3	2	9.95	0.10	1.0	2
15	3	2	8.60	0.95	11.05	2
16	3	2	8.14	0.0	0.0	1
3	3	4	10.30	0.63	6.08	5
4	3	4	10.26	0.84	8.18	9
5	3	4	9.78	0.24	2.42	6
6	3	4	10.10	0.70	6.93	10
7	3	4	9.16	0.84	9.19	4
8	3	4	10.02	0.92	9.19	6
9	3	4	9.64	1.26	13.11	6
10	3	4	10.14	0.48	4.77	3
11	3	4	9.27	0.87	9.39	5
12	3	4				0
13	3	4	9.15	0.60	6.56	2
14	3	4	9.05	0.70	7.73	2
15	3	4				0
16	3	4	8.68	0.42	4.84	2
3	4	3	10.45	0.31	2.97	4
4	4	3	11.17	0.18	1.59	4
5	4	3	10.42	0.63	6.09	6
6	4	3	10.14	0.59	5.78	6
7	4	3	9.94	0.65	6.52	5
8	4	3	9.42	1.02	10.78	10
9	4	3	9.56	0.59	6.22	5
10	4	3	10.13	0.93	9.13	5
11	4	3	9.24	0.53	5.74	7
12	4	3	8.54	0.76	8.91	3
13	4	3	9.12	0.78	8.61	3
14	4	3	8.45	0.80	9.52	3
15	4	3	8.48	0.86	10.11	3
16	4	3	9.22	0.36	3.90	2
3	2	2	9.55	0.78	8.16	2
4	2	2	9.74	0.56	5.76	5
5	2	2	8.69	0.27	3.07	3
6	2	2	9.35	0.68	7.29	5
7	2	2	8.94	0.81	9.05	4
8	2	2	8.17	0.25	3.00	3
9	2	2	8.67	0.82	9.41	5
10	2	2	8.38	0.70	8.30	3

X	Y	Z	v_p	S.D.	C.V.	No.
11	2	2	7.99	0.91	11.44	4
12	2	2	8.49	0.89	10.46	5
13	2	2	8.27	0.0	0.0	1
14	2	2	9.11	0.28	3.07	2
15	2	2	6.87	0.0	0.0	1
16	2	2				0
3	2	4	10.45	0.69	6.61	11
4	2	4	10.55	0.81	7.68	3
5	2	4	10.06	0.82	8.14	11
6	2	4	9.81	0.55	5.65	10
7	2	4	10.09	0.71	7.04	7
8	2	4	9.63	0.30	3.13	9
9	2	4	9.08	1.14	12.53	6
10	2	4	8.97	0.50	5.57	8
11	2	4	8.62	0.54	6.28	5
12	2	4	7.15	0.0	0.0	1
13	2	4	8.22	1.22	14.86	3
14	2	4	8.08	1.49	18.46	3
15	2	4	6.31	0.0	0.0	1
16	2	4	7.62	1.02	13.45	3
3	4	2	10.22	0.54	5.33	7
4	4	2	9.91	0.85	8.62	4
5	4	2	9.48	0.39	4.12	5
6	4	2	9.50	0.61	6.45	7
7	4	2	8.95	0.32	3.62	3
8	4	2	9.42	0.84	8.88	7
9	4	2	8.32	0.74	8.94	4
10	4	2	8.38	0.0	0.0	2
11	4	2				0
12	4	2	9.25	0.42	4.54	2
13	4	2	6.45	0.0	0.0	1
14	4	2	8.34	1.33	15.95	2
15	4	2	8.76	0.49	5.59	2
16	4	2				0
3	4	2	10.06	1.11	11.00	7
4	4	4	9.65	0.75	7.82	4
5	4	4	9.97	0.98	9.79	9
6	4	4	9.46	0.94	9.94	8
7	4	4	9.76	0.72	7.35	6
8	4	4	8.70	1.13	12.97	5
9	4	4	8.79	1.11	12.60	7
10	4	4	8.73	1.26	14.45	6

X	Y	Z	v_p	S.D.	C.V.	No.
11	4	4	8.38	0.52	6.20	2
12	4	4	9.04	0.35	3.87	2
13	4	4	6.45	0.0	0.0	1
14	4	4	7.08	1.05	14.83	2
15	4	4	7.29	0.0	0.0	1
16	4	4	6.59	0.0	0.0	1